THESIS

A CATCHMENT IS MORE THAN THE SUM OF ITS REACHES: POST-FIRE RESILIENCE AT MULTIPLE SPATIAL SCALES

Submitted by

Shayla P. Triantafillou

Department of Geosciences

In partial fulfillment of the requirements

For the Degree of Master of Science

Colorado State University

Fort Collins, Colorado

Summer 2024

Master's Committee:

Advisor: Ellen Wohl

Sara Rathburn
Ryan Morrison

ABSTRACT

A CATCHMENT IS MORE THAN THE SUM OF ITS REACHES: POST-FIRE RESILIENCE AT MULTIPLE SPATIAL SCALES

As wildfires are projected to increase in frequency and severity, there is a growing interest in understanding river resilience to the wildfire disturbance cascade. Numerous 3rd-order mountain catchments within the Cache la Poudre (Poudre) River basin in the Colorado Front Range, USA burned severely and extensively during the 2020 Cameron Peak fire. Many of these catchments experienced debris flows and flash floods triggered by convective storms after the fire. The downstream effects of the debris flow sediment varied along a continuum from attenuated and largely contained within the catchment, through contributing to a pre-existing debris fan at the catchment outlet, to releasing substantial volumes of water and sediment to the Poudre River. I conceptualize these catchments as exhibiting decreasing resilience to post-fire disturbance along the continuum described above based on the geomorphic evidence of relative sediment export. The characteristics affecting resilience and magnitude of response to disturbance span multiple spatial scales from the catchment to stream corridor reaches hundreds of meters in length. I conceptualize characteristics on different spatial scales as driving or resisting response to disturbance and therefore impacting the resilience outcome of the catchment. As the magnitude of resisting characteristics increases at the catchment, inter- and intra-reach scales, I hypothesize that a catchment will be more resilient to the wildfire disturbance cascade. At the catchment scale I consider geomorphic, burn, vegetation, and precipitation characteristics. I conducted longitudinally continuous surveys to measure reach-scale characteristics within each study catchment. I focus on the reach-scale geomorphic, vegetation, and burn characteristics, with a particular focus on elements that introduce inter- and intra-reach spatial heterogeneity including channel

planform, beaver-modified topography, the distribution of channel and floodplain logjam distribution density, and the floodplain width/channel width ratio for the population of reaches within each catchment. The floods observed at the study catchments illustrate fire lifting the elevation above which rainfall-induced flooding occurs due to the efficient conveyance of water from hillslopes to channels after wildfire. Results suggest that inter- and intra-reach spatial heterogeneity are better descriptors of resilience than catchment-scale characteristics: resilience is associated with greater longitudinal variations in floodplain/channel width and more reaches with wide floodplains, low channel gradients, beaver-modified topography, and multi-stem deciduous vegetation.

ACKNOWLEDGEMENTS

I would like to acknowledge and thank the many people and organizations who made this research possible. First, I would like to thank my advisor, Dr. Ellen Wohl, who has selflessly mentored and encouraged me to be a better scientist and for undoubtedly changing the trajectory of my career. From formulating this project to navigating the ups and downs of field-based research, Ellen struck the perfect balance of freedom and guidance.

I am grateful to the members of my thesis committee, Dr. Sara Rathburn and Dr. Ryan Morrison, for lending their time, expertise, and feedback. I thank the many people who generously spent their time in the field with me over many miles of unforgiving terrain: Sarah Dunn, Madeline Fergusen, Claire Pickerel, Maya Daurio, Connor Mertz, Brady Jones, Nate Fraser, Victoria Arnold, and Aaron Katz. To Celeste Wieting and Colin Barry, thank you for all the fun on the river. To Chelsey Heiden and others at Ayres, thank you for the field knowledge, photos, and connections. Thank you to Kayleigh Keller and Ann Hess for thoughtfully considering and advising me on numerous geomorphic datasets. For the most patient help with precipitation data, thank you to Phoebe White and Megan Sears. To everyone who helped me with coding, Danny White, Juli Scamardo, Pat Ronnau, and B Steele, my sincerest thanks for spending time problem solving with me even from afar. I am grateful to Francis Rengers for the many insightful conversations. Thank you to the fluvial geomorphology research group at CSU who have been instrumental collaborators, mentors, and friends. You have made this a more enjoyable and rewarding experience than I could have hoped for. Thank you to all my friends and family, especially my parents, who have in so many ways helped me pursue this path. I am so grateful for my family sharing in every bump in the road in addition to celebrating every success.

I extend my thanks to the private landowners, especially Maya Daurio, and to Arapahoe and Roosevelt National Forest for granting access to and knowledge of the land they steward. I also acknowledge, with respect, the Arapahoe, Cheyenne, and Ute Nations and peoples as the original inhabitants and stewards of this land and all the relatives within it.

Finally, I extend my thanks to the Colorado Water Center, American Water Resources Association, Colorado Riparian Association, Rocky Mountain Association of Geologists, Colorado State University and Warner College of Natural Resources for funding this project.

TABLE OF CONTENTS

LIST OF TABLES

LIST OF FIGURES

1. INTRODUCTION

Wildfire combusts surface and subsurface organic matter and alters hillslope soil properties. Less roughness on the hillslope and changes in soil chemistry decrease infiltration and increase runoff generation after wildfire (e.g., Benavides-Solorio & MacDonald, 2001; Moody & Martin, 2001a; Blount et al., 2020). Burned drainage basins, or catchments, typically have elevated sediment and water fluxes compared to unburned catchments, driving changes in river corridor form, function, and hazards (Rathburn et al., 2018). Resilience, or the capacity to absorb the impacts of disturbance while retaining the same structure and function, is one way to describe the range of responses after wildfire. In the context of post-fire fluxes, resilience is associated with attenuation through dissipating flow energy, promoting deposition, and decreasing erosion. Attenuation is influenced by increased lateral connectivity and decreased longitudinal connectivity in a river corridor. Even the temporary storage of disturbance-generated materials can be crucial to attenuating fluxes, particularly in a flood scenario. The disturbances that follow fire and the concept of resilience act at multiple spatial scales from the channel reach to the entire catchment. Attenuation via spatial heterogeneity to dissipate flow energy can be in the form of large wood (Sear et al., 2010), beaver-modified topography (Burchsted et al., 2010), and topography created by river dynamism over time (Naiman et al., 2005). A river segment may have the capacity to attenuate fluxes or convey fluxes downstream efficiently. The resilience of a catchment will therefore be influenced by the capacity for attenuation within the reaches that comprise the river network. Even though a theoretical catchment may possess characteristics that effectively attenuate fluxes, there is a certain magnitude of disturbance that will overwhelm the capacity of that system to absorb the impacts instead of conveying them downstream. In practice, the dynamics between catchment and reach-scale characteristics and the magnitude of disturbance inputs largely determines the fluvial response to disturbance.

Although previous studies have characterized the conditions necessary to trigger post-fire debris flows (e.g., Cannon & Reneau, 2000; Cannon, 2001; Parrett et al., 2004; Cannon et al., 2008), little research exists on how characteristics spanning multiple spatial scales, particularly elements of spatial heterogeneity, impact the range of fluvial responses in the context of resilience after wildfire. As wildfires become more frequent and severe in the American West, understanding the forms and processes that foster fluvial resilience to wildfire becomes increasingly important.

1.1 Background

As wildfires increase in frequency and severity, understanding the characteristics that promote catchment resilience post-fire is critical to protect our water resources. Walker et al. (2004) define resilience as the capability of a system to absorb disturbance while undergoing change so as to still retain essentially the same function, structure, identity, and feedbacks. Catchments exhibit differing resilience post-fire. Resilience varies within and between catchments in relation to biogeomorphic characteristics.

The characteristics affecting the magnitude of response to disturbance span multiple spatial scales from catchment to reach (Figure 1). Characteristics influencing erosional force, such as higher channel gradient, magnify the response whereas characteristics resisting erosion and geomorphic change, such as floodplain vegetation, reduce the response to disturbance. I conceptualize these characteristics as driving or resisting response to disturbance. Driving characteristics will contribute to a greater magnitude of response in the form of more efficient conveyance of fluxes, which result in lower resilience after disturbance. Resisting characteristics will promote attenuation of fluxes, resulting in greater resilience after disturbance. This conceptualization provides a framework for comparing characteristics amongst catchments that burned in the 2020 Cameron Peak Fire. Wohl et al. (2022) conceptualize reach-scale flux attenuation as increasing resilience on the catchment scale. Because total

channel length of first- to third-order streams is cumulatively dominant (Downing, 2012), reach-scale attenuation must greatly influence the magnitude of disturbance cascade initiated by wildfire. This suggests that catchment-scale resilience is greatly influenced by features that attenuate fluxes at the reach scale.

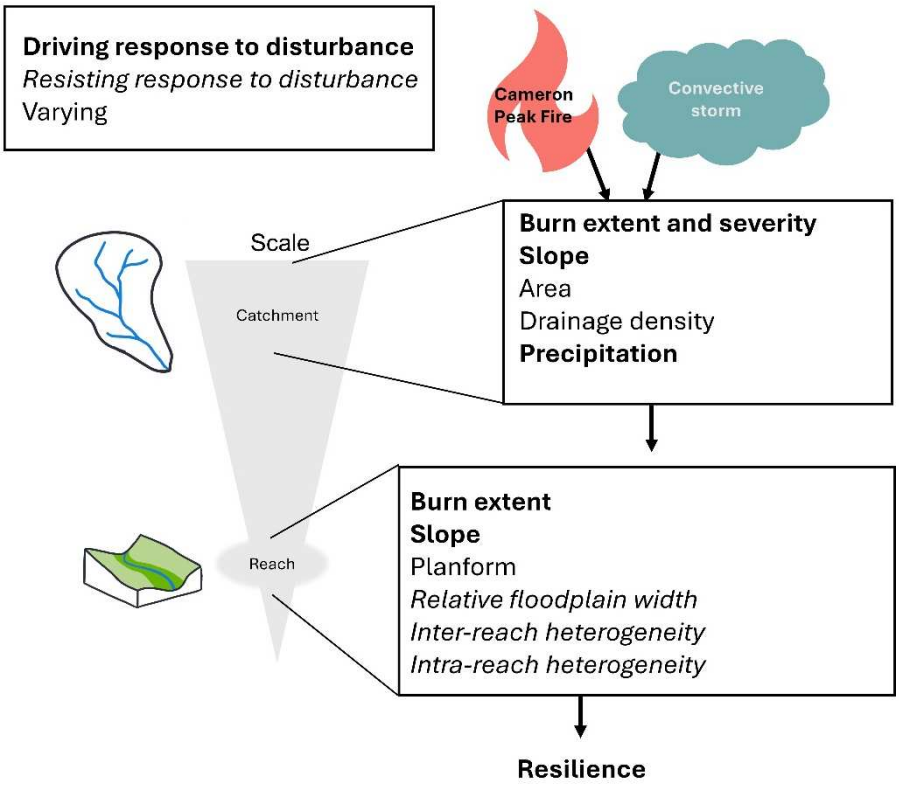

*Figure 1: Multi-scale characteristics influencing river corridor response to disturbance. Assuming an increase in the relative magnitude of the specified characteristic, each characteristic is categorized as either **driving** (bold), resisting (italic), or varying in response to disturbance. The inverse is also implied to be true.*

Reach-scale flux attenuation is primarily driven by valley geometry, spatial heterogeneity of the river corridor, vegetation, and 3D connectivity within the stream corridor (Wohl, 2016; Wohl et al., 2017, 2018). Reaches with less lateral confinement allow for more overbank flow, greater channel sinuosity, and formation of multithread channel planform, facilitating energy dissipation and associated sediment deposition (e.g., Pang, 1998; Entwistle et al., 2018), which lead to lateral channel migration

and diverse floodplain topography (Naiman et al., 2005). The presence of large wood (Sear et al., 2010) and beaver-modified terrain (Burchsted et al., 2010) contribute to greater spatial heterogeneity.

As landcover and climate change, wildfires will continue to increase in frequency and severity (Westerling et al., 2006; Bowman et al., 2009; Dennison et al., 2014). Consequently, understanding and fostering the characteristics that promote catchment resilience post-fire is critical for water resources and hazard mitigation in Colorado. Although we understand the general interactions described above, there has been little work to quantitatively compare catchments that are and are not resilient to wildfire, or to quantify the spatial distribution, types, and levels of heterogeneity that create resilience. These issues are of critical importance as communities in fire-prone regions strive to implement pre- and post-fire landscape management designed to enhance resilience to wildfire disturbances.

1.1.1 Wildfire disturbance cascade

Wildfires initiate a disturbance cascade (Figure 2). When fire burns a landscape, it affects the hillslopes and river corridors. The impacts of fire on the hillslope are transferred to the river corridor because of the connection between valley floor and adjacent hillslopes (Hynes, 1975; Davis, 1898). Because of this connection, wildfires affect hydrology, water quality, and geomorphology in river corridors (Tiedemann et al., 1979; Minshall et al., 1989; Mast & Clow, 2008). The energy that is released from burning organic matter during the fire is described as fire intensity (Keeley, 2009). Fire severity describes the effects of fire intensity on the plant communities in the area that has been burned, including above and belowground impacts (Keeley, 2009). High severity fires combust organic matter, reducing ground cover and changing hillslope roughness, evapotranspiration, and runoff generation

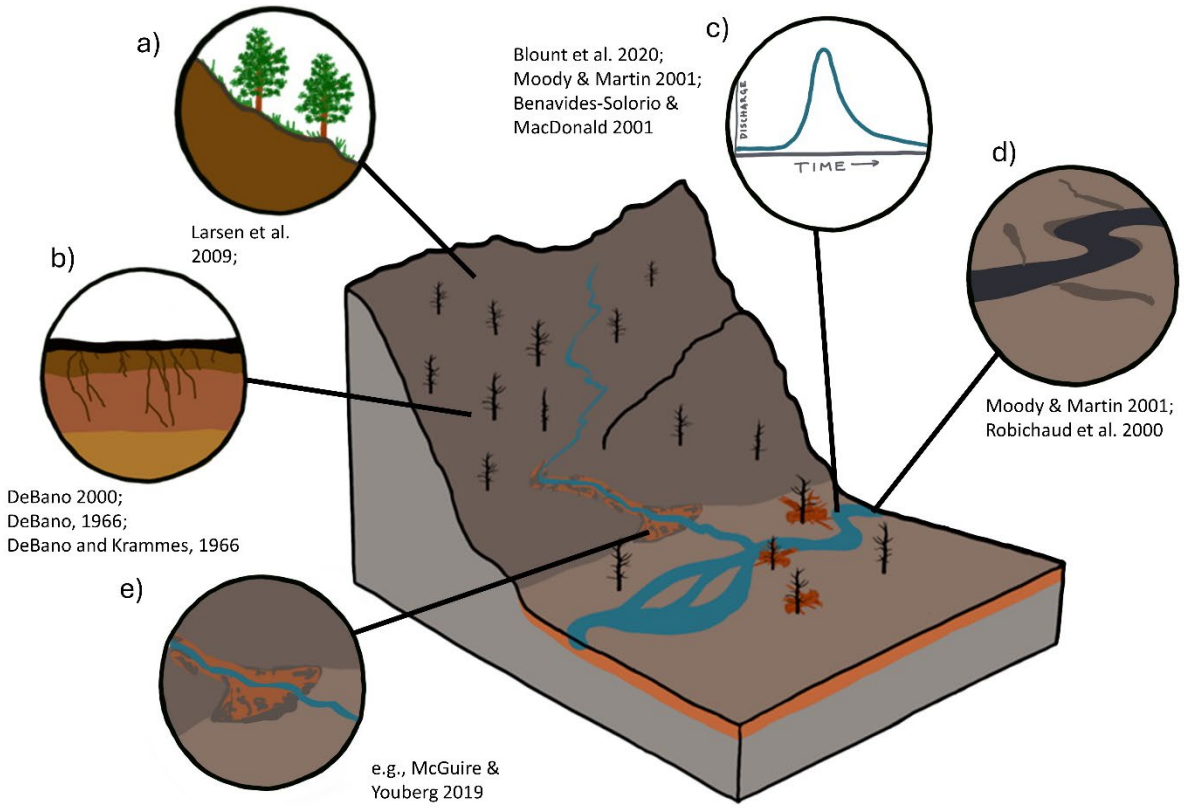

Figure 2: Wildfires initiate a cascade of disturbances across landscapes. Removal of vegetation and altering of soil structures (a & b) increase fluxes of water, sediment, and pollutant transport relative to precipitation (c & d) and decrease the precipitation threshold to trigger debris flows (e).

(Blount et al., 2020). High temperatures also alter soil structures, increasing water repellency and decreasing infiltration rates (DeBano, 2000). Across the landscape, burned hillslopes have lower erosion thresholds and therefore increased erosion (Moody & Martin, 2001a). Stand-killing wildfires result in heightened sediment and water fluxes throughout burned catchments (Benavides-Solorio & MacDonald, 2001), driving changes in river corridor characteristics on multiple spatial and temporal scales. Elevated erosion response typically persists for up to five years in the Colorado Front Range (Moody, 2001; Moody & Martin, 2001b; Ryan et al., 2024). Three years following wildfire, Moody & Martin (2001a) documented a 200-fold increase in erosion rates in catchments in the Colorado Front Range.

Because wildfire increases flow, sediment, and nutrient fluxes, water quality is impacted. Heightened levels of phosphate associated with sediment (Coombs & Melack, 2013; Emelko et al., 2016) and nitrate associated with lower microbial processing capacity (McDaniel, 2021) result from fire. Following the High Park fire in 2012, water entering the Fort Collins Water Treatment Facility had elevated levels of turbidity, nutrients, and dissolved organic matter, contributing to water quality impairment (Hohner et al., 2016).

Water quality impairment affects riparian biota. Elevated levels of suspended sediment can cause fish kill years after wildfire (Bozek & Young, 1994). Stream macroinvertebrates respond variably to wildfire, likely due to heterogeneity of the fire itself, post-fire precipitation events, and time since the fire (Gresswell, 1999; Cooper et al., 2015; Tuckett & Koetsier, 2018). On a short-term timescale of 1-5 years, greater concentrations of phosphorus after severe wildfire can be associated with elevated algal production and shifts towards greater invertebrate abundance and diversity (Silins et al., 2014). In the first year after fire, Preston et al. (2023) saw mortality of smaller trout, lower density of benthic macroinvertebrates, and lower fluxes of emerging aquatic insects. Ash can disrupt aquatic biota as an endocrine disruptor and may persist in streams (Gonzalez 2023). Vegetation in perennial shaded headwater reaches provides refuge for stream invertebrates and the loss of vegetation via combustion

affects stream invertebrate communities (Cooper et al. 2021). Stream invertebrate communities can recover after 10 years post-fire (Cooper et al., 2021). The interactions between fire, vegetation, and geomorphology influence in-channel biota in complex and dynamic ways.

Debris flows occur more frequently in burned catchments in the Intermountain West (e.g. Meyer & Wells, 1997; Parrett, 1987; Cannon, 2001; Parrett et al., 2004; Cannon & Gartner, 2005) because wildfire increases flow and sediment transport relative to precipitation intensity. Unlike debris flows started by landslides, post-fire debris flows are triggered by exceedance of a rainfall intensity-duration threshold. These events derive sediment from within the channel via lateral and vertical erosion (Santi et al., 2008). There is commonly no initiation point and these debris flows can occur with little antecedent moisture (Cannon et al., 2008). The storms that trigger these debris flows in Colorado are typically short in duration, triggering debris flows within minutes to hours of rainfall, and high in intensity. Intensities in southwestern Colorado recorded by rain gauges are 3 mm/h for 3 hours to trigger debris flows. In California, Cannon et al. (2008) documented intensities recorded by rain gauges of 25 mm/h for 10 minutes and 5 mm/h for 20 h that triggered debris flows in the first season following fire.

1.2.2 Resilience

Resilience thinking encompasses natural systems including physical systems, ecosystems, and societal systems. As humans change river systems, there are more pronounced and persistent stressors on river systems. This is changing the ways that rivers respond to disturbance, which are more commonly complex and unpredictable (Thoms et al., 2018). Thoms and Fuller (2023, p. xviii) see this as a call for "a mindset that seeks to understand the variability, heterogeneity, and complexity" of our river systems. Although land management policies still frequently align with a requirement of stability and equilibrium (Benson & Garmestani, 2011), publications, policies, programs, and communications are more often using resilience thinking (Parsons & Thoms, 2018).

Although there are different perspectives on resilience in the literature, I define resilient systems as able to absorb disturbance without large changes in process, structure, identity, and feedbacks. This view is guided by principles of disturbance, thresholds, and recovery in terms of equilibrium (Thorn & Welford, 1994). My concept of geomorphic resilience includes the capacity of a system to absorb disturbances, as is the emergent view recently (Thoms et al., 2018; Thoms et al., 2018; Fuller et al., 2019). In these ways, the concept of resilience is inherent in the assumptions and theories upon which fluvial geomorphology is built (Fuller et al., 2019). Fluvial landscapes are dynamic in nature, and dynamic systems have been described in association with resilience by the ball and cup model presented by Holling (1973). This conceptual model describes a system being held in a certain state by reinforcing processes and feedbacks, until a limit at the edge of that state over which those same feedbacks and processes will shift the system into a new state. In the context of absorbing disturbances, a more resilient system is made up of processes and feedbacks that hold a system in the same state as a response to disturbance. Systems that are less resilient under this definition are more prone to shifting to an alternative stable regime, either gradually or suddenly (Schumm, 1979).

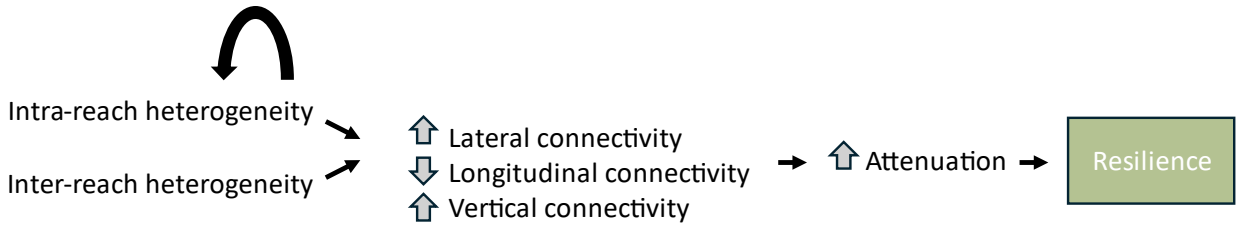

Figure 3: Spatial heterogeneity within river reaches and amongst reaches contributes to increasing lateral connectivity, decreasing longitudinal connectivity, and increasing vertical connectivity. Spatial heterogeneity also increases spatial heterogeneity in a positive feedback. These changes in connectivity increase attenuation of water, sediment, and pollutant fluxes, therefore creating a resilient system. Black arrows represent cause and effect. Grey arrows represent relative changes in process magnitudes.

Ecosystem heterogeneity contributes to resilience (Rahel, 2002), a concept that also applies to river systems (e.g., Thoms et al., 2017). Spatial heterogeneity in rivers contributes to resilience by attenuating downstream fluxes of water and sediment (Wohl, 2016). Attenuation of downstream fluxes

can be described as decreasing longitudinal connectivity to inhibit the downstream transport of water, sediment, and other fluxes (Figure 3). Features on local and river corridor scales that introduce spatial heterogeneity in river channels can reduce flow velocity in channels and floodplains by increasing lateral connectivity and decreasing longitudinal connectivity. Increasing lateral connectivity and hydraulic roughness promote attenuation, which contributes to resilience by reducing the magnitude of material fluxes and associated adjustments in river corridor form in downstream portions of a river network.

Spatial heterogeneity can occur longitudinally as sections of river alternate between wide, low gradient reaches and confined, high gradient reaches, which are commonly referred to as beads and strings, respectively (Stanford et al., 1996). Natural alternation of beads and strings can be caused by differences in lithology (Wohl et al., 1994), bedrock jointing, (Ehlen & Wohl, 2002), changes in relative base level (Duvall et al., 2004), or glaciation (Wohl, 2013a; Hauer et al., 2016). Humans alter rivers to create artificial strings where rivers are confined to narrow channels disconnected from the adjacent floodplain through channelization, flow regulation, and levees. Because of their lower gradient and less confined river corridors, beads are more strongly influenced by deposition compared to strings (Montgomery & Buffington, 1997) while the channel remains connected to the floodplain. Beads contain disproportionately high amounts of heterogeneity elements on a local scale and therefore resilience-promoting elements relative to their length in the river corridor (Wohl et al., 2018). For example, beads contain disproportionately high volumes of wood (Wohl, 2011), beaver modified topography (Westbrook et al., 2006), and channel-hyporheic connectivity (Ader et al., 2021).

On a local scale, spatial heterogeneity influences response to disturbance (Wohl et al., 2024b). Lateral connectivity within a river corridor, particularly between channel and floodplain, tends to reduce longitudinal connectivity and promote attenuation. Variations in substrate, bedforms, planform, channel-floodplain connectivity, beaver-modified topography, and logjams contribute to spatial heterogeneity, lateral connectivity, and attenuation in a river corridor by increasing hydraulic roughness

and trapping capacity within the river corridor. Water flowing at slower velocities promotes sedimentation (Jones & Smock, 1991) and trapping of organic matter (Marshall et al., 2021). Beavers within a fluvial system create structural and functional heterogeneity in river corridors that contributes to resilience when faced with disturbance (Polvi & Wohl, 2013; Fairfax & Whittle, 2020; Dunn, 2023). In-channel wood is associated with more overbank flow, multichannel planforms, and channel-floodplain lateral connectivity, all of which promote attenuation of fluxes (Wohl, 2011; Collins et al., 2012; Livers & Wohl, 2016).

Spatial heterogeneity and flux attenuation can create a positive feedback. One example starts with logjams attenuating flow. Flow attenuation then leads to overbank flow, which leads to channel avulsion and multithreaded channels that further increase spatial heterogeneity and attenuation (e.g., O'Connor et al., 2003; Collins et al., 2012; Livers et al., 2018). This positive feedback between heterogeneity and attenuation contributes to catchments remaining in a single, dynamic state rather than shifting to an alternative state when disturbed by reinforcing processes and feedbacks. Thus, the positive feedback of heterogeneity and attenuation contributes directly to resilience as defined by the ability to absorb response to disturbance without changing the identity of the system.

1.2.3 Cameron Peak Fire

2020 was a year of record-breaking fires in the Front Range of Colorado, most notably the Cameron Peak fire, which was the largest fire in Colorado history to date. It started on the east side of Cameron Peak, 65 km (40 miles) west of Fort Collins, on August 13, 2020, likely of human cause. Over almost 4 months, the fire burned 845 km^2 (208,913 acres) until it was 100% contained on December 2nd. From ignition at 3000 m (10,000 ft), warm and windy conditions contributed to the fire moving east rapidly in a series of runs up to 400 square km (100,000 acres) in a day during September and October (Johnson, 2021). The fire burned 469 structures. Within the burn scar, over 40% was classified as being burned at moderate to high severity (USDA Forest Service, 2020).

1.2.4 Storm and flood events

Following the Cameron Peak fire in 2020, there were a series of convective storms over the summers of 2021 and 2022 across the burn scar (Table 1). The USGS post-fire debris-flow hazard assessment model estimated a 15-minute intensity threshold for 50 percent likelihood of debris flow of 33.2 mm/h over the entire Cameron Peak Burn area (Kostelnik et al., 2022).

On 20 July 2021, there was a convective storm over much of the Cameron Peak burned area that caused flooding and multiple debris flows. Intense precipitation occurred over the study catchments between 22:00 Coordinated Universal Time (UTC) (4:00 PM Mountain Daylight Time (MDT)) on 20 July and 2:00 UTC on 21 July (8:00 PM MDT on 20 July). Rain gauges located near the center of intense precipitation recorded peak 15-minute rainfall intensities of 36.6 and 51.8 mm/h, respectively. These rates exceed the threshold of 33.2 mm/h modeled for the entire fire area (Kostelnik et al., 2022). The first reports of flooding in the area were at 00:00 UTC (6:00 PM MDT). Black Hollow and Sheep Creek had high flows that appear to have been generated by sediment entrainment through surface runoff rather than infiltration, which is common in unburned settings (Cannon & Gartner, 2005). This process, described by Meyer & Wells (1997) as 'progressive sediment bulking,' is caused by high volumes and rates of hillslope runoff converging in hollows and low order channels. Sediment in Black Hollow was entrained primarily from the valley floor rather than from adjacent uplands based on lack of observed hillslope mass movements, rills, and gullies in the Black Hollow catchment. The Black Hollow debris flow resulted in the destruction of private property, damage to the roadway and bridge, and four fatalities. The debris flow in Black Hollow followed the existing channel down to and along the mainstem Cache la Poudre (Poudre) River, resulting in fish kill, water quality issues throughout the catchment, and extensive sedimentation on an alluvial fan (Kostelnik et al., 2022). Although the 20 July 2021, storm event did not cause major geomorphic change in Little Beaver Creek, a convective storm on 15 July 2022, resulted in major flooding the following summer (Wohl et al., 2024a).

Table 1: Event-triggering storm dates and times at each of the study catchments.

Site	Date	Time (UTC)	Source
Little Beaver Creek Tributary A Jack's Gulch	July 15, 2022	22:30	Trail camera
Black Hollow	July 20, 2021	22:00	Kostelnik et al., 2022
Sheep Creek Sheep Gulch	July 20, 2021	22:00	Landowner communication
Fish Creek	July 15, 2022	22:30	Landowner communication, spatial proximity to LBC confirmed with visual assessment of radar.

1.2.5 Management challenges and significance of wildfires

Fire is a geomorphic and ecological disturbance to landscapes. Although biotic communities are adapted to fire in this region, the short-term impacts can alter ecosystem function. Long-term changes in fire regime are trending towards more severe and more frequent fires, which fire-adapted species may not be able to tolerate or recover from. Additionally, post-fire impacts to rivers can be harmful to humans and resources that we rely on. Multiple debris flows occurred during the convective storms following the Cameron Peak fire. The largest of these debris flows was in the Black Hollow catchment.

Increased sediment levels entering drinking water treatment facilities reduce the rates of water processing (Smith et al., 2011). Post-fire sediment can fill intake pipes and reservoirs more rapidly than pre-fire conditions (Bladon et al., 2014; Gannon et al., 2021). After the Cameron Peak fire, the City of Fort Collins shut off water intake from the Poudre River because of elevated levels of sediment and instead relied entirely on reservoirs to supply municipal water. The City of Fort Collins shuts down water intake from the Poudre when turbidity exceeds 100 Nephelometric Turbidity Units (NTU). After the convective storm event, the monitoring station downstream from Rustic documented turbidity exceeding 1000 NTU. Multiple strategies are commonly used to mediate the impacts of increased fluxes

of water and sediment after fire. Application of mulch and/or seeds to slow the movement of runoff downslope and promote revegetation is a common practice (Jonas et al., 2019). Although it is widely used, it is an expensive solution that has not been documented consistently as an effective treatment (Schmeer et al., 2018; Maiolo-Heath, 2021). As with mulching, aerial seeding and hand planting saplings are expensive, difficult to implement on a large scale, and not always effective mitigation strategies (Robichaud et al., 2000). Individual structures implemented on hillslopes include wattles, contour felling, and erosion barriers installed to dissipate flow and sediment fluxes (Robichaud et al., 2008, 2020; De Girolamo et al., 2022)

Individual structures in river channels are another common way to minimize the impacts of fire. In-channel structures include replanted riparian vegetation, especially willow (*Salix* spp.), check dams, log jams, and beaver mimicry structures to retain sediment after wildfire (Graham, 2003; Pollock et al., 2007).

The ten largest fires in Colorado history have happened since 2002 (Colorado State Forest Service, 2024). Climate change and a history of fire suppression in the Intermountain West are causing fires to occur with increasing frequency and severity. Climate change creates compounding disturbances that limit vegetation recovery when fire coincides with drought, heatwaves, and insect outbreaks (Nolan et al., 2021). As anthropogenic influences change fire regimes to be more frequent and severe, population centers are expanding the intersection of urban and wild spaces and recreational uses of forest lands are increasing, causing more risk of fire impacts on populated areas (Higuera et al., 2023).

There remains a knowledge gap of the features that reduce fire impacts and promote resilience on a burned landscape at the catchment to the local scale. The Poudre River catchment, much of which burned in the 2020 Cameron Peak fire, is a source of drinking water to over 350,000 residents in the

Colorado Front Range (Smith et al., 2011). Understanding how catchments respond to fire is important to protect and manage our landscapes and water resources.

1.2 Research objectives and hypotheses

Recent large-scale wildfires in the western United States highlight the need to understand resilience to disturbance in fire-prone regions. The Cameron Peak fire provides an opportunity to investigate the different responses to wildfire across multiple river catchments. This study evaluates the factors that influence how river corridors across multiple catchments attenuate the fluxes of water and sediment due to wildfire. I ranked seven catchments that burned in the Cameron Peak fire on a resilience scale and measured characteristics on the catchment scale and the river reach scale to improve understanding of the contexts that promote resilience or drive response to disturbance following wildfire. At the catchment scale, I described variables across the entire drainage basin. The reach scale consisted of the active channel(s) and the entire width of the floodplain in short longitudinal segments of river corridor up to 1 km in length. Understanding how characteristics within catchments and river corridors drive or resist disturbance will help managers efficiently implement post-fire mitigation strategies. I present two research objectives and their rationales below.

1.1.1 Research objective 1

Evaluate the influence of catchment-scale characteristics on catchment resilience to the wildfire disturbance cascade.

1.1.2 Rationale for research objective 1

Wildfires can burn entire landscapes, and wildfires make the basins vulnerable to the compounding effects that follow fire. As a result of the link between valleys and rivers, studies have quantified an increase in hillslope sediment entering rivers after fire (e.g., Benevides-Solorio and MacDonald, 2005). Hillslope runoff increases when a catchment is burned, commonly resulting in higher peak flows over

shorter durations compared to unburned catchment (Shakesby & Doerr, 2006). Local scale measurements likely do not reflect larger scale processes that impact responses on the catchment scale. Slope and drainage area can dominate the morphology and processes in a drainage network to act as source, transport, and response sections, where slope and drainage area are the determinant characteristics (Montgomery & Buffington, 1997).

Catchment geomorphology that reflects the drainage area, relief-ratio, and slope within the context of lithology and biome influences water and sediment yields throughout catchments (Wohl, 2018). Fire and subsequent precipitation patterns are highly spatially heterogeneous and may affect neighboring catchments differently. Temporal context across a catchment may also affect the geomorphic response within a catchment. For example, if a large fire or flood has occurred recently, there may not be fuel or sediment available for transport even if all other conditions remain constant (e.g., Harvey, 1984; Cenderelli & Wohl, 2003). In the context of wildfire disturbance, the geomorphic, vegetation, and burn characteristics of a catchment may influence the overall resilience of that catchment.

1.1.3 Hypothesis 1

More resilient catchments will have more characteristics that resist disturbance and less resilient catchments will have more characteristics that drive disturbance on the catchment scale.

Although I seek to quantify characteristics that resist and enhance disturbance, the sample size at the catchment scale limits statistical comparisons across sites. I describe below how I assess relative catchment-scale resilience, but 'more characteristics' in the hypothesis above can refer to greater magnitude of a single characteristic or greater magnitude of multiple characteristics.

1.1.4 Research objective 2

Evaluate the influence of reach-scale characteristics on catchment resilience to the wildfire disturbance cascade.

1.1.5 Rationale for research objective 2

Physical complexity in fluvial systems, such as multithread channels, logjams, and beaver-modified topography, contribute to resilience after disturbance (Rathburn et al., 2018). These features occur and interact on a smaller spatial scale than the catchment. There are longitudinal trends in river characteristics that include downstream trends in stream power (Knighton, 1999), fining of channel-bed sediment (Frings, 2008), and large wood (e.g., Gurnell et al., 2002). Even so, these trends that may be described on the catchment scale are dependent not only on regional and catchment context, but also on relative spatial positioning of the many elements that affect form and process.

The local scale, or the reach scale, reflects processes and forms, resilience, and trajectories of change (Brierley et al., 2008; Fryirs et al., 2012). Channel geometry reflects the processes occurring in the context of sediment supply, energy available as flow, and vegetation, large wood, and geomorphic units (Brierley et al., 2008). On the local scale, geomorphic units influence hyporheic exchange (Elliott & Brooks, 1997; Boulton, 2007), invertebrate and fish distribution (Downes & Hindell, 2000; Pusey et al., 2000), and organic matter deposition (Hoover et al., 2006). In the context of sediment delivery, local features affect the way that sediment is delivered from source to sink of a catchment by temporary or long-term storage (Fryirs et al., 2007). In the context of wildfire disturbance where elevated levels of water and sediment are moving through a catchment, features that promote this attenuation should contribute to the overall resilience of the catchment.

1.1.6 Hypothesis 2

More resilient catchments will have greater heterogeneity at the inter-reach scale and more heterogeneity elements at the intra-reach scale.

Because each catchment includes multiple reaches, sample size for quantifiable heterogeneity variables facilitates statistical analyses at the inter- and intra-reach scales.

1.3 Study Area

The study site is in the Southern Rocky Mountains in the Front Range of Colorado, USA. The seven catchments within the study area are third-order tributaries in the Poudre River catchment (Figure 4). These catchments burned in the Cameron Peak fire in 2020 and had subsequent flood and debris flow events triggered by convective storms in the summers of 2021 and 2022.

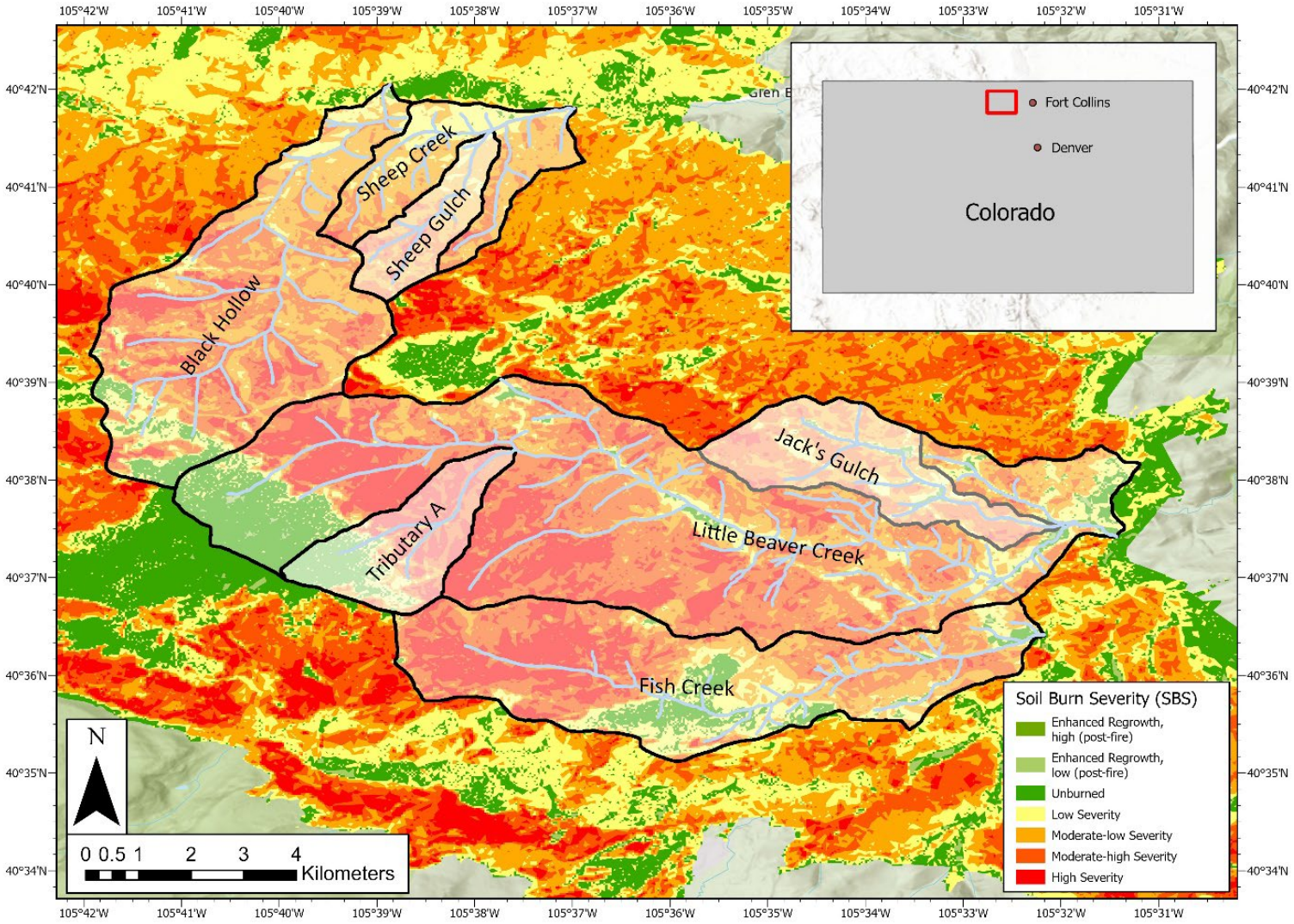

Figure 4: Map of seven study catchments and their location within Colorado. The study area on the inset map is shown in red. All study catchments were within the burn scar of the 2020 Cameron Peak fire. The dNBR-derived soil burn severity of the study catchments is also depicted (Woodward & Voorster, 2022). Little Beaver Creek Tributary A and Jack's Gulch are within the Little Beaver Creek catchment. Sheep Gulch is within the Sheep Creek catchment.

1.3.1 Geology

The study areas are in the northern Front Range, which was modified in the Laramide Orogeny (ca. 70-45 million years ago). This region of the high Colorado Rocky Mountains is underlain primarily by Precambrian- and Proterozoic-aged granitoids and gneisses (Green, 1992; Horton, 2017). Bedrock weathers to surficial deposits of gravel to sand made up of feldspar, quartz, and mica (Birkeland et al., 2003). Loess caps of silt and clay sediments are present but far less abundant. The study sites were below the glacial maximum and were therefore not glacially modified during the Pleistocene (Madole et al., 1998).

1.3.2 Climate and hydrology

Elevation is a control on many climate variables in the Rocky Mountains of Colorado (Doesken et al., 2003). Temperature decreases as elevation increases. Wind is controlled by topography in mountainous regions and there are typically mountain-valley circulations with diurnally shifting wind patterns. Elevation is also a control, with increasing precipitation at higher elevations. In the winter, this affects the snowpack and subsequent runoff. In the Poudre River catchment, this means that stream discharge increases with elevation across intermittently snow-covered areas, which tend to be mid-elevation catchments similar to those in this study (Harrison et al., 2021). In the summer, mountainous parts of Colorado have frequent thunderstorms (Jarrett, 1993) that cause flooding in some locations. Flood-causing thunderstorms typically occur below 2300 m (7500 ft) (Hansen et al., 1978; Jarrett, 1990).

The study sites are ungauged tributaries, but the U.S. Geological Survey maintains a stream gage at Rustic in the Poudre River catchment that indicates that annual peak runoff occurs during late spring snowmelt (Figure 5). This trend remains the same between pre- and post-fire years, but the highest flow during the 2021 water year on the mainstem Poudre was a convective summer storm on 20 July 2021. Gauge data from the first year after the fire at Little Beaver Creek show the same trend of peak runoff during spring snowmelt, but indicate that convective summer storms also cause high, peaked flows

(Figure 5c) (White et al., 2022; Wohl et al., 2022). Although the floods initiated by convective storms do not comprise a seasonally recurrent part of the hydrograph, they cause flashy and spatially discontinuous flooding, initiate mass movements, and erode sediment from the hillslopes and carry it through channels (Figure 5c). Convective storms have the capacity to initiate substantial geomorphic change within burned tributary catchments, and the impacts of these local events have been observed outside of these catchments in downstream river corridors (Grimm et al., 1995).

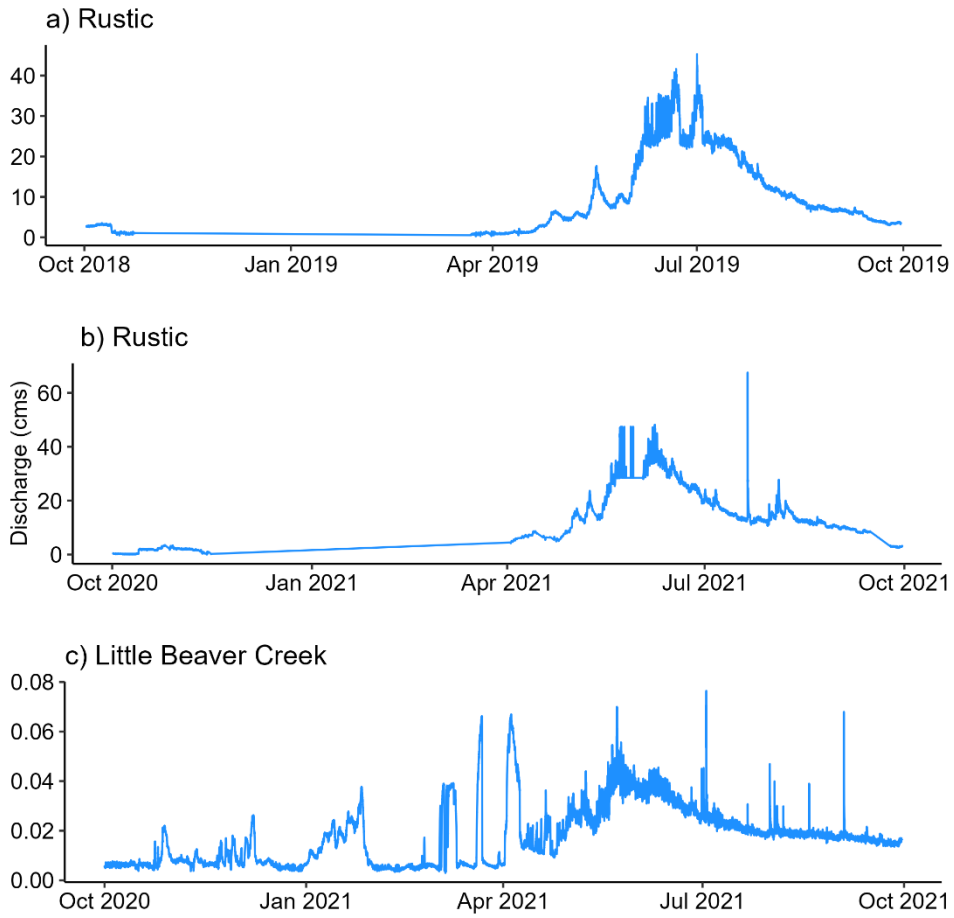

Figure 5: Hydrographs showing the discharge over a water year at a) the Rustic gauge on the mainstem Cache la Poudre in 2019 before the Cameron Peak fire b) the Rustic gauge in 2021 the first year after the Cameron Peak fire and c) Little Beaver Creek, a third order tributary, in 2021 the first year after the Cameron Peak fire. Spring snowmelt comprises the major peak of the hydrograph at all sites. At both sites after the Cameron Peak fire there are flashy peaks over the summer that occurred after summer convective storms. The highest peak on b) is the July 20, 2021, storm that triggered many debris flows within the Cameron Peak fire perimeter.

1.3.4 Ecology

The study region is composed of coniferous, montane forests at mid-elevations between 2100 and 2750 m (7000 to 9000 ft) and subalpine forests between 2600 and 3650 m (8500 to 12000 ft) (Chapman et al., 2006). In the mid-elevation zone, vegetation communities are an overstory dominated by ponderosa pine (*Pinus ponderosa*) and Douglas-fir (*Pseudotsuga menziesii*) with pockets of aspen (*Populus tremuloides*). Shrubs, grasses, and herbaceous species make up the understory. At the higher elevations within the study area, the forests are dominated by lodgepole pine (*Pinus contorta*), Engelmann spruce (*Picea engelmannii*), and subalpine fir (*Abies lasiocarpa*).

River corridors and wetlands in the study region are composed of riparian shrubland species including a variety of willow species (*Salix* spp.), thinleaf alder (*Alnus incana*), and river birch (*Betula occidentalis*) (Malone et al., 2019). Up to 2438 m (8000 feet), the lowest elevation extents of the study region support narrowleaf cottonwoods (*Populus angustifolia*).

Although fire, blowdown, insect outbreaks, and avalanches are natural disturbances that have affected vegetation communities in the Rocky Mountain region over millennia, vegetation communities have remained relatively stable in composition over the last 8000 years (Minckley et al., 2012). Despite these disturbances occurring naturally, increased rates of forest disturbance and disturbance frequency are likely to significantly alter vegetation communities (Overpeck et al., 1990). Decades of fire suppression in the western US have also changed the vegetation communities, resulting in more vegetation in the understory and denser, evenly aged forests (Veblen & Lorenz, 1986; Veblen & Donnegan, 2005).

Today, the single largest driver of forest loss in the northern Front Range is wildfire (Rodman et al., 2019). Historically, land use changes have influenced the regional vegetation communities. The removal of Native American communities led to changes associated with their land-use practices, and

likely to a change in vegetation communities (Veblen et al., 2000). Logging, mining, and ranching increased during this time from the mid-1800s and early 1900s across the Front Range (Veblen & Lorenz, 1986; Veblen & Donnegan, 2005; Dethier et al., 2018). These practices have affected forests in the region in complex ways, initially by reducing forest cover (Rodman et al., 2019).

1.3.5 Regional fire regime

A fire regime is a way of describing how fire affects an ecosystem through the combination of factors in a location over a period of time (Krebs et al., 2010). Parameters included in describing a fire regime can include the conditions of individual fires, temporal and spatial distribution, and the effects of fire on a landscape. Montane ecosystems made up of ponderosa pine in Colorado have a fire history mostly of low-severity, high-frequency fires (Goldblum & Veblen, 1992; Brown & Shepperd, 2001; Donnegan et al., 2001; Gartner et al., 2012). High-frequency, low-severity in this setting typically refers to a fire regime with a mean fire interval of 30 years or less (Sherriff & Veblen, 2006; Sherriff et al., 2014). These frequent fires were not commonly stand-killing fires, which created a forest of diverse stand age and species composition (Veblen & Donnegan, 2005). Within the fires that burn montane forests in the Front Range, there is a high degree of spatial variability in burn severity (McKinney, 2019). These mixed-severity fires indicate a combination of regional factors and local factors such as elevation, aspect, and species population dynamics, influencing burn severity spatially (Brown & Wu, 2005).

Historically, fires have burned in this region in the late summer to fall. Precipitation records paired with fire scars indicate that fires most commonly occurred in dry years that follow two to three wet years in the region. At a smaller spatial scale, the mean fire return interval, or average number of years between successive fires in a location over a given period, is correlated with elevation. More frequent fires have historically occurred at lower elevations of ponderosa pine ecosystems. Within the Arapahoe-Roosevelt National Forest where the study catchments are located, Sherriff & Veblen (2007) modeled the historical fire regime of the montane zone to be 20% high-frequency, low-severity.

The removal of Native American communities and associated land-use practices led to a decline in intentional burning (Veblen et al., 2000). Deforestation and widespread human-caused fires occurred between 1860 and the 1920s (Wohl, 2001). Decades of intentional fire suppression began in the 1920s when roads were constructed (Veblen & Lorenz, 1986; Veblen & Donnegan, 2005). As this development has become expansive since the 1940s, wildfire suppression has become more aggressive while the risk of human-started fires has increased (Platt et al., 2011).

2. METHODS

This study included field-based and remote data collection (Table 2). I collected field data during the summer of 2023 through longitudinal surveys of the seven catchments. I completed geospatial and statistical data analysis using R Studio (R Core Team, 2022), ArcGIS Pro (ESRI, 2023), Python in Jupyter Notebook, and Google Earth Engine.

Table 2: Summary of methods, data products, and purpose.

Methods	Data Product(s) and Purpose

Field survey	• Relative resilience of each catchment
	• Reach boundaries
	• Geomorphic characteristics
	  ○ Channel width
	  ○ Floodplain width
	  ○ Planform
	  ○ Presence of beaver modified topography
	• Vegetation
	  ○ Categorical floodplain vegetation type
	  ○ Basal area
	  ○ Channel jam density
	  ○ Floodplain jam density
	• Burn characteristics
	  ○ Burn status

Geospatial analyses	• Geomorphic catchment characteristics
	  ○ Area
	  ○ Mean catchment slope
	  ○ Elongation ratio
	  ○ Relief ratio
	  ○ Drainage density
	  ○ Concavity index
	• Vegetation catchment characteristics
	  ○ NDVI
	• Burn characteristics
	  ○ Burn extent
	  ○ Burn severity
	• Precipitation
	  ○ 15-minute precipitation intensity

Statistical analyses	• Hypothesis testing • Descriptive regression models
Sensitivity analyses	• Geomorphic change during events

2.1 Site Selection and Description

The catchments selected for this study are all 3rd order tributaries in the Poudre River drainage basin that burned during the Cameron Peak fire in 2020. Prior to the Cameron Peak fire, selected sites had not burned for more than a century (National Interagency Fire Center, 2022). Sites were selected to have comparable burn characteristics, elevations, bedrock geology, glacial history, and known convective storms following the Cameron Peak fire. Of sites with these characteristics in common, I selected sites with i) permission to access the land whether public or private and ii) physical access to the catchment via either trail or road. Where possible, I selected sites with a drop-off location accessible by road to access the ridge at the headwaters of the basin and the confluence with the mainstem Poudre or South Fork Poudre.

2.2 Resilience ranking

After visiting each site and before analyzing data, I assigned a relative resilience ranking to each catchment *a priori* based on qualitative assessment of geomorphic indicators relating to their sediment export during summer convective storms. A catchment with a large debris or alluvial fan at the confluence with a larger channel was ranked as having the greatest sediment export and therefore the least relative resilience. A catchment that had no evidence of scour and deposition resulting from a large flood was ranked as the least impacted by wildfire and convective storms and therefore the most resilient. Where data availability allowed, I quantitatively constrained the amount of sediment export from the catchment.

2.3 Field survey

I conducted a longitudinal reach survey within each study catchment. The survey started at the drainage divide, moving downhill to find the first evidence of channelization and follow it to the stream head. I followed the river downstream, defining the boundaries between reaches by field-observed relative valley and channel geometry using a Garmin GPSMAP 66st and a Garmin eTrex10 with 3-m

horizontal accuracy. Within each reach I documented burn status, vegetation type, basal area, channel planform, channel bedform, bankfull width, floodplain width, number of channel and floodplain jams, and number of beaver berms. Burn status was documented categorically in the field as burned, unburned, or mixed. Vegetation type was noted categorically as conifer, willow, aspen, or herbaceous based on the species present, where herbaceous denoted a lack of trees rather than implying that there was no herbaceous vegetation where other species were present. Basal area of the river corridor forest was measured with a Panama Angle Gauge at approximately one channel width away from bankfull. All standing trees (living and dead) were included. Channel planform and channel bedform were determined categorically. Bankfull channel and floodplain widths were measured using a Laser Technology TruPulse 360B laser range finder and high-water marks indicative of high flows from the most recent spring snowmelt flows. Logjams were designated as at least three pieces of wood in contact, with each piece of wood at least 1 m in length and 10 cm in diameter. Jams within the bankfull channel were tallied as channel jams and jams outside of the bankfull channel but within the bounds of high-water marks were tallied as floodplain jams. The presence of beaver berms was tallied within each reach where clearly defined individual berms existed. Where there were complex beaver meadows, beaver modified terrain was noted as “beaver meadow,” indicating many berms that were not distinct throughout the length of the reach.

2.4 Remote methods

Catchment-scale characteristics and reach-scale characteristics that utilized spatial datasets to quantify elevation, burn characteristics, and vegetation characteristics were evaluated using remote data and methods. These metrics were categorized as geomorphic, burn, vegetation, and precipitation characteristics. I used repeat lidar to calculate a DEM of difference within the river corridor to quantify sediment export from Black Hollow where the data were available and spatially aligned.

2.4.1 Geomorphic characteristics

Elongation ratio was calculated as the ratio between the diameter of a circle encompassing the area of each basin and the maximum basin length (Schumm, 1956):

$$R_e = \frac{D_c}{L_b}$$

$$where\ D_c = diameter\ of\ the\ circle\ with\ the\ same\ area\ as\ that\ of\ the\ basin\ and\ L_b = maximum\ basin\ length$$

I calculated relief ratio as the difference between the highest and lowest points of each basin divided by the length of the longest NHD flowpath (USACE Hydrologic Engineering Center, 2023):

$$R_h = \frac{H}{L}$$

$$where\ H = basin\ relief\ and\ L = length\ of\ longest\ flow\ path$$

I calculated drainage density as the total NHD flowpath length in each catchment divided by the basin area (R. E. Horton, 1932):

$$D_d = \frac{\Sigma L}{A_{basin}}$$

$$where\ \Sigma L = total\ length\ of\ flowpaths\ and\ A_{basin} = basin\ area$$

I calculated the elevation of each reach boundary using the field-determined reach boundaries and the USGS DEM with 1/3 arc second (10 m) resolution derived from 3DEP LiDAR data. I extracted the elevation value from each reach boundary in ArcGIS Pro using the Add Surface Information tool. At locations where the point deviated from the flowline, I snapped the points to the National Hydrography Dataset (NHD) flowline and extracted the elevation from the snapped point using the same method. When both the field measured point and point snapped to the NHD flowline deviated from the apparent

river location, I selected the lowest elevation pixel within a valley cross section perpendicular to the channel and the field-measured point.

The channel gradient of each reach was calculated using the elevation derived from the 1/3 arc second resolution 3DEP DEM and the NHD stream distance between each reach boundary.

To represent each reach's location within the catchment, the distance downstream of each reach boundary was determined using a modified workflow from Peek (2021). I used R to import National Hydrography Dataset (NHD) flowlines using the nhdplusTools (Blodgett & Johnson, 2023) and sf (Pebesma, 2018; Pebesma & Bivand, 2023) packages, merged the flowline elements within each catchment, snapped the field-measured reach boundary points to the flowlines, and split the NHD flowlines into segments using the lwgeom package (Pebesma, 2023). I then imported the split flowlines into ArcGIS Pro, where I used the Calculate Geometry tool within the attribute table to calculate the geodesic length of each flowline segment corresponding to the length of each reach.

To calculate a concavity index for each site, I used the distance downstream (x) and the elevation of each reach boundary (y). I normalized the elevations of each reach boundary by the elevation at the lowest point within each catchment to ensure the lowest point was zero and the upstream points were relative to zero. I then calculated the area under the normalized longitudinal profile. I calculated the area under the straight-line distance from the highest to the lowest point on the normalized elevation profile of each site. I calculated the concavity index as the ratio between the area under the normalized longitudinal profile to the area under the normalized straight-line distance (Figure 6).

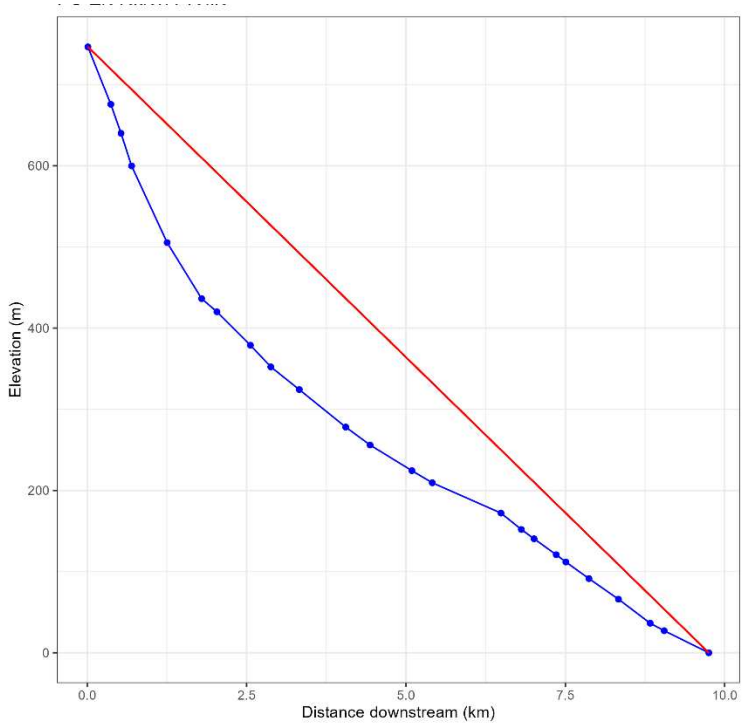

Figure 6: Example of an elevation profile used to calculate concavity index. The two lines represent the profiles necessary to calculate a concavity index where the elevation of each point is relative to the elevation at the lowest point, or the outlet of the catchment. The blue line is a longitudinal profile of a river. The red line is the straight-line profile of the river. The concavity index is calculated as the ratio between the area under the blue line and the area under the red line.

2.4.2 Burn characteristics

Burn characteristics of each catchment were calculated using a Soil Burn Severity dataset (Woodward & Vorster, 2022). These data were calculated using the delta normalized burn ratio (dNBR) and a similar imagery acquisition method used in Vorster et al. (2024) to calculate relativized burn ratio (RBR; Parks et al., 2015) and quantify burn severity across the Cameron Peak fire. Scaled dNBR values range from -500 to 700, and these values were classified into 7 categories based on the severity levels proposed by the U.S. Geological Survey (U.S. Geological Survey, 2022).

To capture burn characteristics of each catchment and reach, I calculated the total proportion burned at any severity (burn extent) and the percentage of each area burned at moderate-high and high severities (burn severity moderate-high, burn severity high) as classified by dNBR. I calculated these metrics for each catchment's total area and for each reach. To calculate the reach-scale burn metrics, I created a 50-m buffer around each stream segment and calculated the same metrics over each reach area. To compare these results to publicly available data, I calculated the same metrics using the Burned Area Emergency Response fire severity dataset calculated using normalized burn ratio (NBR) on the catchment scale (USDA Forest Service, 2020).

2.4.3 Precipitation

I identified the biggest storm events or the storm events that were responsible for the greatest amount of geomorphic change using a variety of methods, summarized in Table 1. I quantified and visualized precipitation over the study catchments using Multiple Radar/Multiple Sensor (MRMS) data from the National Oceanic and Atmospheric Administration (NOAA). The MRMS system uses data from multiple radar sensors, satellites, surface observations, upper air observations, lightning reports, rain gauges, and numerical weather prediction models to produce quantitative precipitation estimate (QPE) products that cover the continental United States and southern Canada (Zhang et al., 2016). The radar inputs to MRMS are 146 S-band dual-polarization radars and 30 C-band single polarization radars.

Hydrometeorological Automated Data System rain gauges are input into MRMS from 7,000 locations. The model data inputs are from High-Resolution Rapid Refresh. Climatology inputs into the system are from the Parameter-Elevation Regressions on Independent Slopes Model (PRISM; Daly et al., 1994, 2008; www.prism.oregonstate.edu).

MRMS QPE products have 1-km spatial resolution and two-minute temporal resolution. I followed the methods presented in White et al. (2023) to apply the MRMS correction to precipitation rate data. I used the radar-based QPE and the gauge-and-precipitation-and climatology-merged QPE products.

2.4.4 Vegetation

I used Google Earth Engine to calculate the Normalized Difference Vegetation Index (NDVI), which quantifies "greenness" across all catchments in the three years leading up to the Cameron Peak fire (2017, 2018, 2019) and post-fire (2021, 2022, 2023) to quantify vegetation. NDVI is calculated as the normalized difference between the near infrared (NIR) and red bands:

$$NDVI = \frac{NIR - Red}{NIR + Red}$$

Where NIR is the near infrared band. I used bands 5 and 4 from Landsat 8 to calculate NDVI values for the years 2017 to 2023, where each pixel of the final image is a median of the cloud-free pixel values over the growing season from June 1st to September 30th. In Google Earth Engine (Appendix III), I calculated summary statistics and vegetation recovery ratios for NDVI values using the terra and tidyterra packages in R (Hernangómez, 2023; Hijmans, 2023). To calculate the recovery ratio, I found the mean NDVI value of each pixel of the mosaic raster images from 2017 to 2019 to establish a baseline NDVI value pre-fire. The recovery ratio is the ratio of the NDVI value of each pixel in any post-fire year (2021 to 2023) over the pre-fire mean value:

$$Vegetation\ Recovery\ Ratio = \frac{NDVI_{post}}{\overline{NDVI}_{pre}}$$

Where $NDVI_{post} = NDVI\ pixel\ value\ in\ any\ post - fire\ year$ and

$\overline{NDVI}_{pre} = mean\ NDVI\ value\ of\ a\ pixel\ over\ pre - fire\ years$

I calculated recovery ratios within each study catchment and over each reach, where the reach area is a polygon buffering the flowline by 50 m on each side.

Normalized burn ratio (NBR) is the normalized difference between NIR and shortwave infrared (SWIR):

$$NBR = \frac{NIR - SWIR}{NIR + SWIR}$$

NBR values range between -1 and 1 where values closer to 1 indicate healthy vegetation and values near and below zero indicate burned or otherwise not productive vegetation (Hislop et al., 2018). Normalized burn ratio is a metric of "wetness." Wetness indices have been found to take longer to recover to pre-fire values than metrics of greenness (Hislop et al., 2018).

2.6 Analytical methods

I calculated the correlation between numerical variables when applicable and used these correlations to inform regression model analyses (Kassambara, 2023). Variables with correlations greater than or equal to 0.8 or less than or equal to -0.8 were considered highly correlated. I limited the inclusion of highly correlated variables to one in each statistical model created to ensure that the model was not overfit and that the regression coefficients were accurate.

2.6.1 Hypothesis testing

Statistical analyses were tested at the $\alpha = 0.05$ level. When testing for equality of variance, I used Levene's test in the car package in R (Fox & Weisberg, 2019). Where assumptions of normality and variance were met, I used an analysis of variance (ANOVA) to test the difference between groups in a population. When the assumption of normality was not met, I performed a logarithmic transformation on the response variable. If the data then met the assumptions of normality and variance, I tested the difference between groups in a population with an ANOVA. When the ANOVA suggested that there was a difference between groups, I generated pairwise comparisons using the emmeans package and a Tukey Honest Significant Difference method (Searle et al., 1980; Lenth, 2023). Where the assumptions of normality and variance were not met after transforming the data, I used a non-parametric Kruskal-Wallis Rank Sum test on the untransformed data to test the difference between groups in a population. I then used a Dunn's test (O. J. Dunn, 1964) to perform pairwise comparisons if the results of the Kruskal-Wallis test suggested a difference between groups.

2.6.2 Regression models

I created two models to describe the number of channel jams and floodplain jams surveyed in the field. I fit six Poisson regression models with the number of jams in each reach as the outcome and site as the predictor variable with an offset of the bankfull channel area, and different combinations of additional predictor variables that describe the geomorphic, vegetation, and fire characteristics. I calculated the Akaike information criterion (AIC) as an assessment of model quality for each of the six models and selected the best model as the model with the lowest AIC value. The statistical significance of Poisson regression models was assessed at the $\alpha = 0.05$ level using a likelihood ratio test.

3. RESULTS

Based on geomorphic indicators of relative sediment export, Black Hollow was the least resilient and Jack's Gulch was the most resilient catchment (Figure 7). A debris-fan 100-m wide formed at the junction of Black Hollow and the Poudre. Boulders and large wood were transported and deposited at the outlet of the catchment, destroying property, and resulting in a channel shift. Sediment from the event caused fish kill from the upper Poudre Canyon for almost 100 stream kilometers downstream (Battige, 2022). There was over 100,000 m^3 of net sediment erosion from the channel at Black Hollow. Sheep Creek and Tributary A within Little Beaver Creek had moderate debris fans at their outlets. There was evidence throughout the river corridors at these sites of erosion and incision indicating that the material deposited at the outlet was derived from the channel and floodplain. Fish Creek, Little Beaver Creek and Sheep Gulch were ranked as having a large flood and no fan at their outlets. There was evidence of flooding and erosion within the catchments, but there was no depositional fan at the outlet, indicating that the impacts of the flood were absorbed within the catchments. The most resilient site was Jack's Gulch. Jack's Gulch had no geomorphic evidence of sediment export at its confluence with the mainstem of Little Beaver Creek. Throughout the catchment, there was no evidence of major sediment redistribution, supporting the placement of Jack's Gulch at the more resilient end of the resilience scale. In reporting results related to these resilience rankings, I will refer to Black Hollow, Sheep Creek, and Little Beaver Creek Tributary A as less resilient sites and Fish Creek, Little Beaver Creek, Sheep Gulch, and Jack's Gulch as more resilient sites.

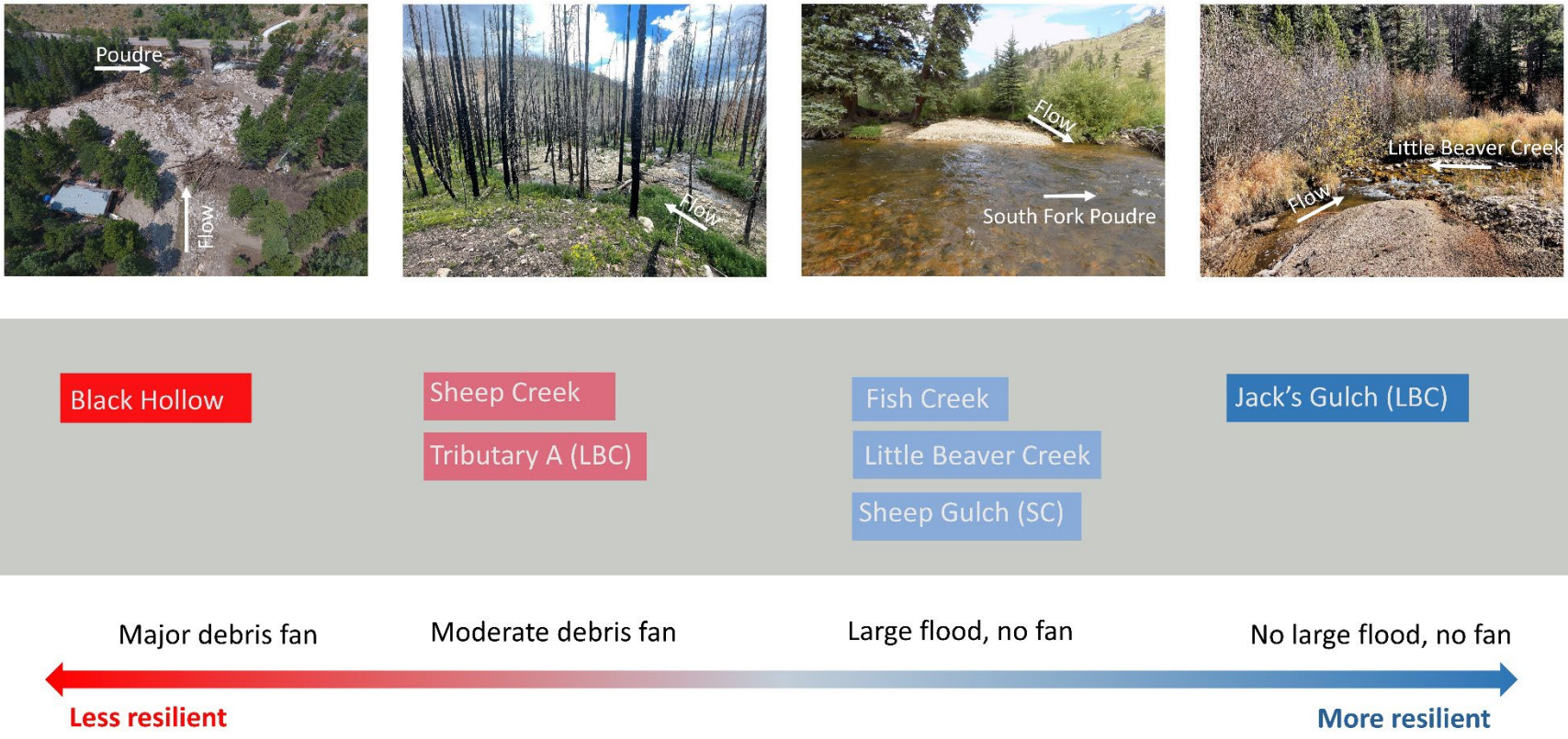

Figure 7: Results of a priori ranking of seven study catchments on a scale of less resilient to more resilient. Sites were ranked by post-event indicators of relative sediment export during storms and associated floods. The least resilient catchment, Black Hollow had a large fan at the outlet, representing a large amount of sediment export, and was categorized as a "Major debris fan". The least geomorphic impact at the outlet of a catchment was Jack's Gulch within the Little Beaver Creek catchment. There was no evidence of sediment scour or deposition at the outlet, so Jack's Gulch was categorized as having "No large flood". The images taken in the field illustrate the impacts visible at the catchment outlets that were the basis for ranking. Image credit from left to right: U.S. Geological Survey, S. Triantafillou, Ellen Wohl, S. Triantafillou

3.3 Catchment scale

3.2.1 Geomorphic characteristics

Among the seven study catchments, the smallest catchment was Sheep Gulch (2.8 km^2) and the largest was Little Beaver Creek (37 km^2) (Table 3, Figure 8). The mean catchment slopes ranged from 9.7% at Jack's Gulch to 40% at Sheep Gulch. Sheep Gulch was the smallest and steepest catchment. Little Beaver Creek had the greatest total stream length at almost 72 km and the greatest length of longest flow path at almost 15 km. Little Beaver Creek had the lowest relief ratio of 76 and Little Beaver Creek Tributary A had the highest relief ratio of 400. Drainage density ranged from 1.03 to 2.49 at Little Beaver Creek Tributary A and Sheep Creek, respectively. The concavity index ranged from 0.13 at Sheep Creek to 1.11 at Jack's Gulch. The elongation ratio ranged from 0.50 at Jack's Gulch and Fish Creek to 0.68 at Sheep Creek. Of the catchment scale characteristics, the elongation ratio was the only one to display a trend when plotted against resilience ranking: elongation ratio decreases with resilience among the seven study catchments. All four catchments ranked as "Large Flood" or "No Flood" have lower elongation ratios than the three catchments ranked as having a "Major Fan" or "Moderate Fan."

Table 3: Geomorphic characteristics of study catchments.

Site	Resilience	Area (km^2)	R_e	Mean basin slope (%)	Total stream length (km)	Drainage density	Relief ratio	Proportion with multi-channel	Concavity Index
Jack's Gulch	No Flood	5.96	0.50	21.00	4.60	0.77	115.53	0.31	1.11
Fish Creek	Large Flood	17.16	0.50	10.30	9.20	0.54	105.02	0.38	0.72
Little Beaver Creek	Large Flood	37.61	0.55	9.70	27.20	0.72	76.44	0.38	0.74
Sheep Gulch	Large Flood	2.80	0.52	40.00	3.30	1.18	208.79	0.35	0.78
Sheep Creek	Moderate Fan	7.62	0.68	17.10	7.80	1.02	172.87	0.33	0.13
Tributary A	Moderate Fan	4.64	0.59	25.00	3.50	0.75	400.81	0.27	0.87
Black Hollow	Major Fan	17.26	0.56	14.50	9.70	0.56	159.17	0.22	0.91

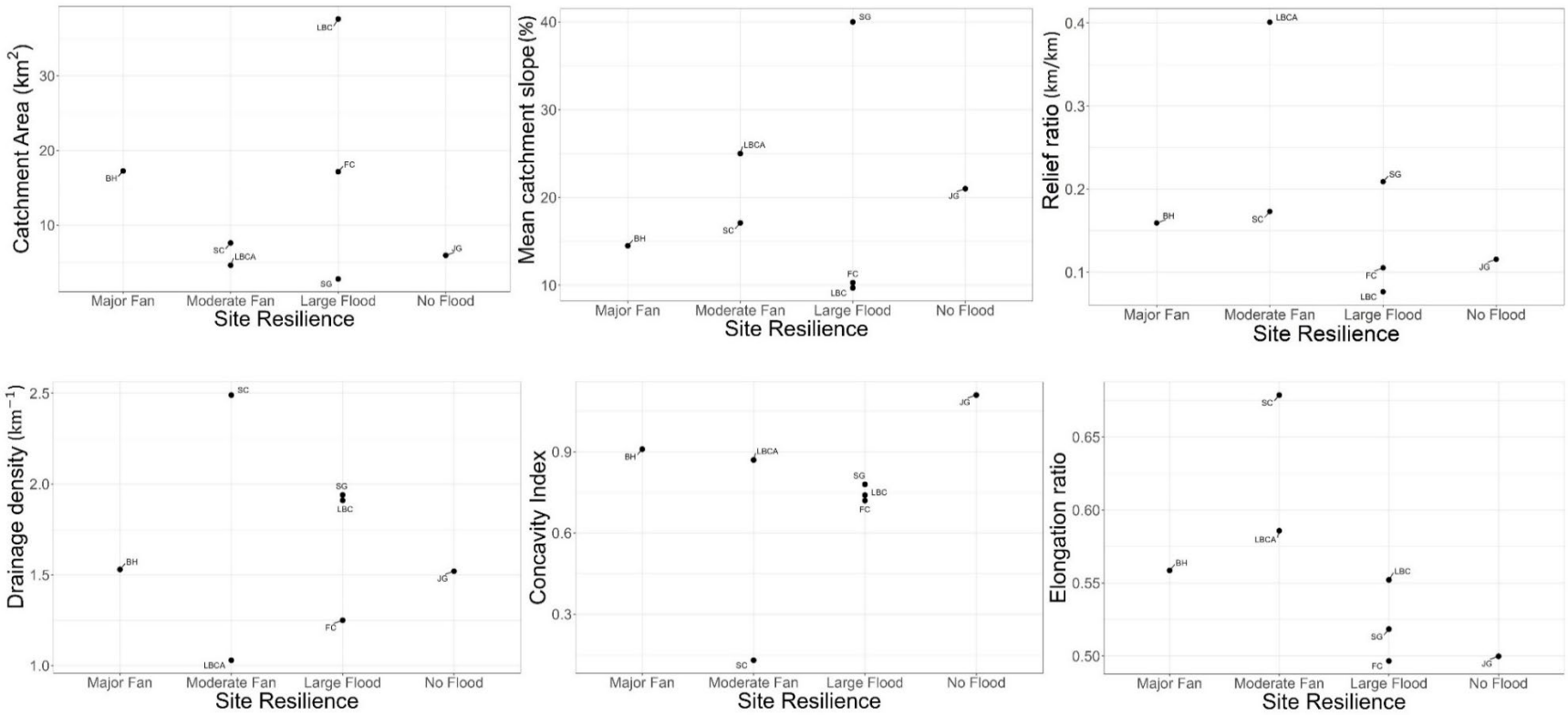

Figure 8: Catchment-scale geomorphic characteristics plotted against categorical site resilience ranking.

3.2.2 Burn characteristics

The mean burn extent was 93.2% and ranged from 77.1% at Tributary A to 99.9% at Sheep Gulch (Table 4). There are no apparent trends in burn extent and severity among the study catchments. The burn extent of each catchment varied between source layers when compared using publicly available data (Appendix II).

Table 4: The burn extent and severity of each catchment. Burn extent is the percent of the total catchment area burned and the burn severity is the percent of the total catchment area burned at moderate-high to high severity. The burn characteristics were calculated using dNBR data and U.S. Geological Survey burn severity classification.

Site	Resilience	Burn extent	Burn severity
Jack's Gulch	No Flood	96.25	48.26
Fish Creek	Large Flood	90.1	52.7
Little Beaver Creek	Large Flood	89.6	59.8
Sheep Gulch	Large Flood	99.92	38.99
Sheep Creek	Moderate Fan	99.8	27.6
Tributary A (LBC)	Moderate Fan	77.12	57.87
Black Hollow	Major Fan	99.8	49.5

3.2.3 Precipitation

Precipitation events over the study catchments were identified as beginning on 20 July 2021 at 1200 UTC at Black Hollow, Sheep Creek, and Sheep Gulch, or 15 July 2022 at 1700 UTC at Little Beaver Creek Tributary A, Fish Creek, Little Beaver Creek, and Jack's Gulch (Table 5). Across each of the seven catchments, maximum 15-minute precipitation rates over the 24-hour period ranged from 45.92 mm/h at Sheep Gulch to 148.86 mm/h Tributary A within Little Beaver Creek. The mean across the catchment 24-hour maximum values ranged from 23.90 mm/h at Sheep Creek to 91.87 mm/h at Tributary A. Across

the spatial area, the mean 15-minute precipitation rate summarizing the median over 24 hours ranged from 1.75 mm/h at Jack's Gulch to 2.89 mm/h at Sheep Gulch.

Table 5: The precipitation intensities calculated from the MRMS QPEs. The 24-hour maximums and medians are temporal summaries of each pixel within a catchment over the 24-hour period capturing the storm. The spatial means and medians are a single value summarizing those pixels over the area of each catchment.

	15-minute precipitation intensity (mm/h)				
	24-hour maximum		24-hour median		
Site	**Spatial mean**	**Spatial median**	**Spatial mean**	**Spatial median**	Start of 24-hour period (UTC)
Jack's Gulch	40.65	40.85	1.75	1.84	17:00 15 July 2022
Fish Creek	31.93	24.93	1.85	2.04	17:00 15 July 2022
LBC	55.63	60.21	1.95	1.98	17:00 15 July 2022
Sheep Gulch	32.34	35.95	2.89	2.93	12:00 20 July 2021
Sheep Creek	23.90	20.93	2.70	2.84	12:00 20 July 2021
Tributary A	91.87	81.36	2.47	2.53	17:00 15 July 2022
Black Hollow	49.18	46.51	2.73	2.78	12:00 20 July 2021

There is a negative relationship between the spatial median of the 15-minute median precipitation intensity over 24 hours and the resilience of the catchments (Figure 9). The outlier to this trend is Sheep Gulch, which was ranked as having a "Large Flood" and had the highest median 15-minute intensity of 2.93 mm/hr.

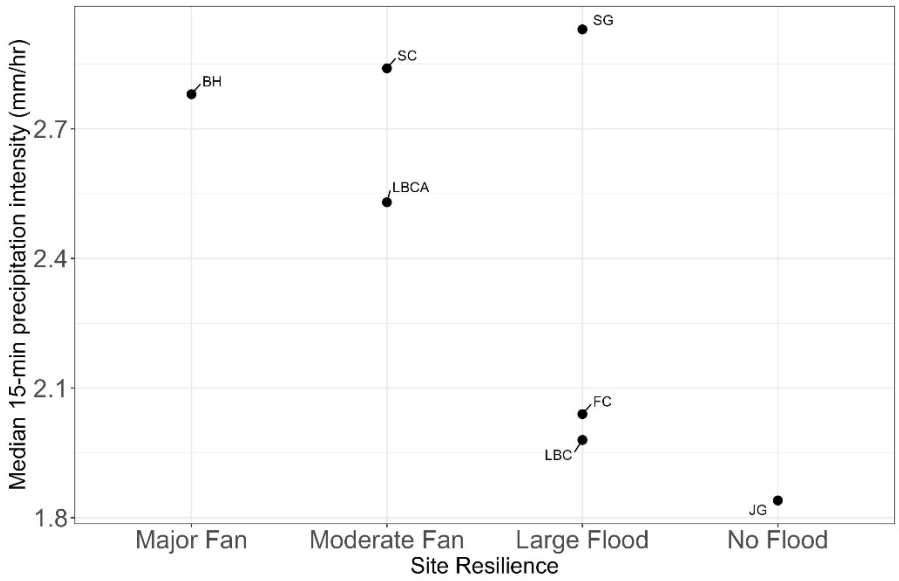

Figure 9: Catchment-scale precipitation plotted against categorical site resilience ranking. Precipitation was quantified as the temporal median of each pixel over a 24-hour period and then summarized for each catchment as a spatial median across the entire catchment, plotted here.

3.2.4 Vegetation

NDVI and NBR values decreased across all catchments between pre- and post-fire measures (Appendix II). NDVI values across catchments have begun to recover at all sites between 2021 and 2023 (Figure 10). The mean NDVI value over the entire catchment-scale fluctuates over the years (Figure 10). The values at all study catchments remained around 0.20 in the years preceding the fire and then dropped dramatically between 2020 and 2021. Over the years following the fire, the mean NDVI values across all study catchments increased between 2021 and 2023. The mean NDVI in a particular year did not vary substantially between catchments.

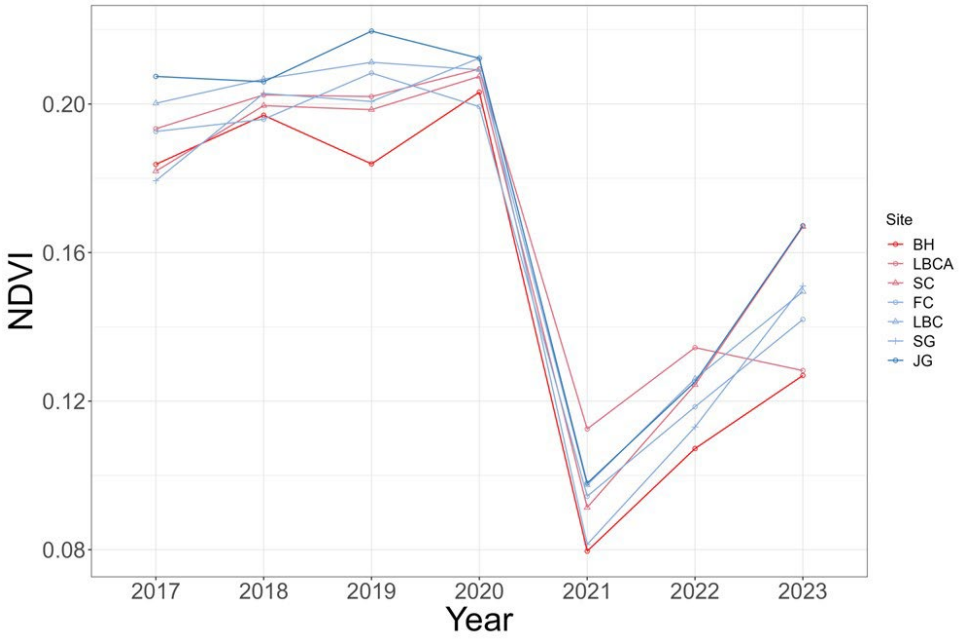

Figure 10: Mean Normalized Difference Vegetation Index (NDVI) of each catchment over three years pre-fire (2017-2019) and three years post-fire (2021-2023). Mean NDVI values did not differ between catchments.

3.4 Reach scale

Several of the variables were correlated because they quantify similar characteristics of each reach (Figure 11). The vegetation metrics measured remotely are all calculated using NDVI and had strong positive correlations between pre-fire, 2023, and 2023 recovery NDVI values. Moderate-high burn severity was correlated negatively with NDVI pre-fire, 2023, and recovery 2023 (corr = -0.6, -0.6, -0.5). Burn severity metrics were positively correlated (corr = 0.7). Geomorphic characteristics were correlated where one metric was used to calculate another including reach area and relative floodplain width with floodplain width. Distance downstream was negatively correlated with reach slope (corr = -0.6). Within each model, I selected only one variable amongst multiple correlated variables.

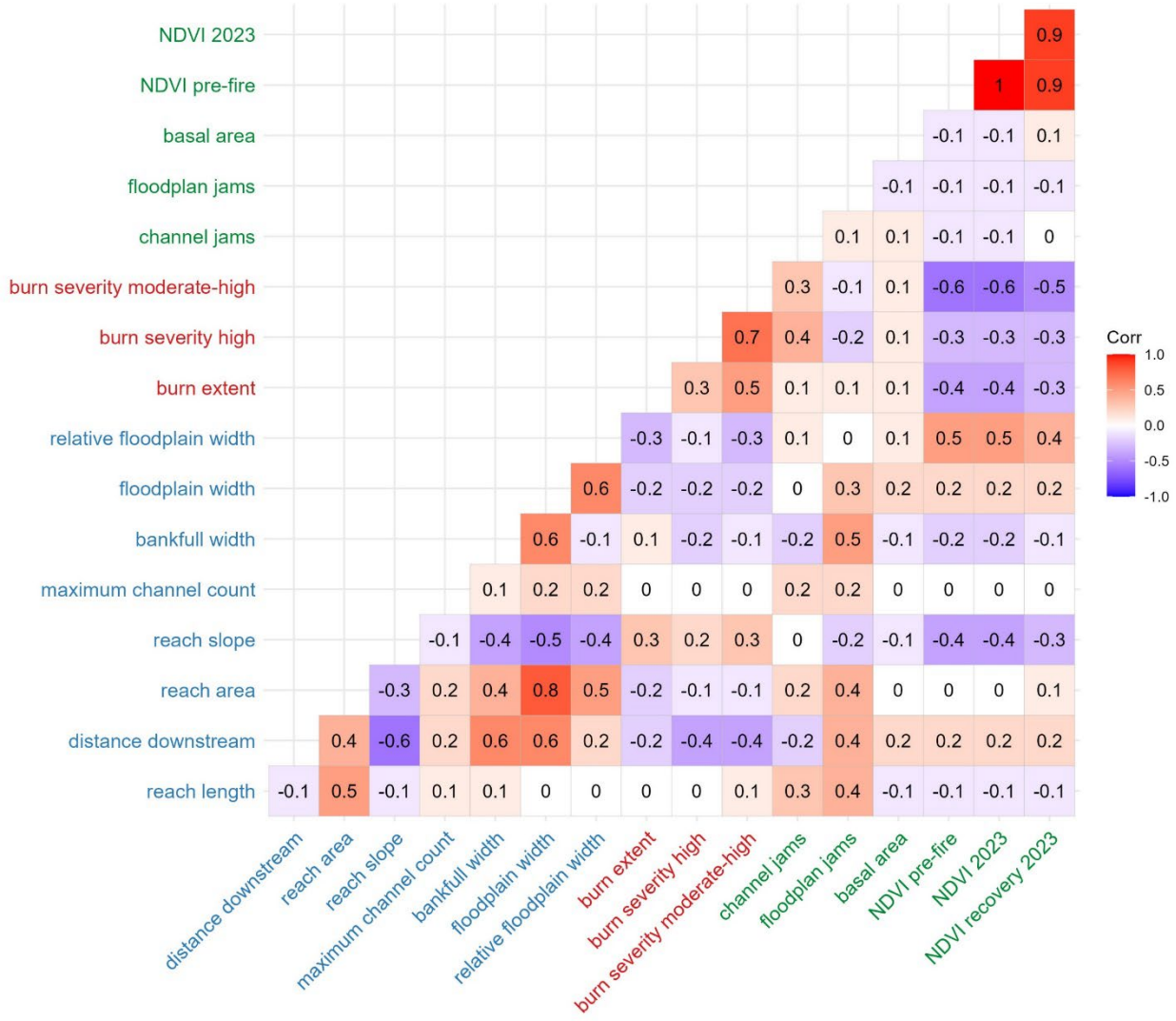

Figure 11: Correlogram of numerical variables considered in data analysis of the reach scale. The color of the square indicates the direction of the relationship between two variables where blue is negative, and red is positive correlation. Stronger correlations are darker in color and weaker correlations are lighter or white. The axes label colors indicate the category of each variable where blue indicates geomorphic, red indicates fire characteristics, and green is vegetation. Variables with correlations greater than 0.8 or less than -0.8 were considered highly correlated.

3.3.1 Geomorphic characteristics

The mean maximum channel count among reaches did not vary significantly between catchments. Reach slope varied between catchments ($p < 0.001$) (Figure 12). The mean of the reach slopes at Black Hollow is significantly greater than the means of Fish Creek, Jack's Gulch, and Little Beaver Creek (p-value table, but $p = 0.06, 0.006$). The mean of reach slopes at Fish Creek is greater than at Little Beaver Creek ($p = 0.001$) and smaller than at Little Beaver Creek Tributary A and Sheep Gulch ($p = 0.02$, $p = 0.0003$). Jack's Gulch has a lower mean of reach slopes than Little Beaver Creek Tributary A, Sheep Creek, and Sheep Gulch ($p = 0.0036$, $p = 0.0093$, $p < 0.001$). Little Beaver Creek has a lower reach slope mean than Little Beaver Creek Tributary A, Sheep Creek, and Sheep Gulch ($p < 0.0001$, $p < 0.001$, $p< 0.0001$).

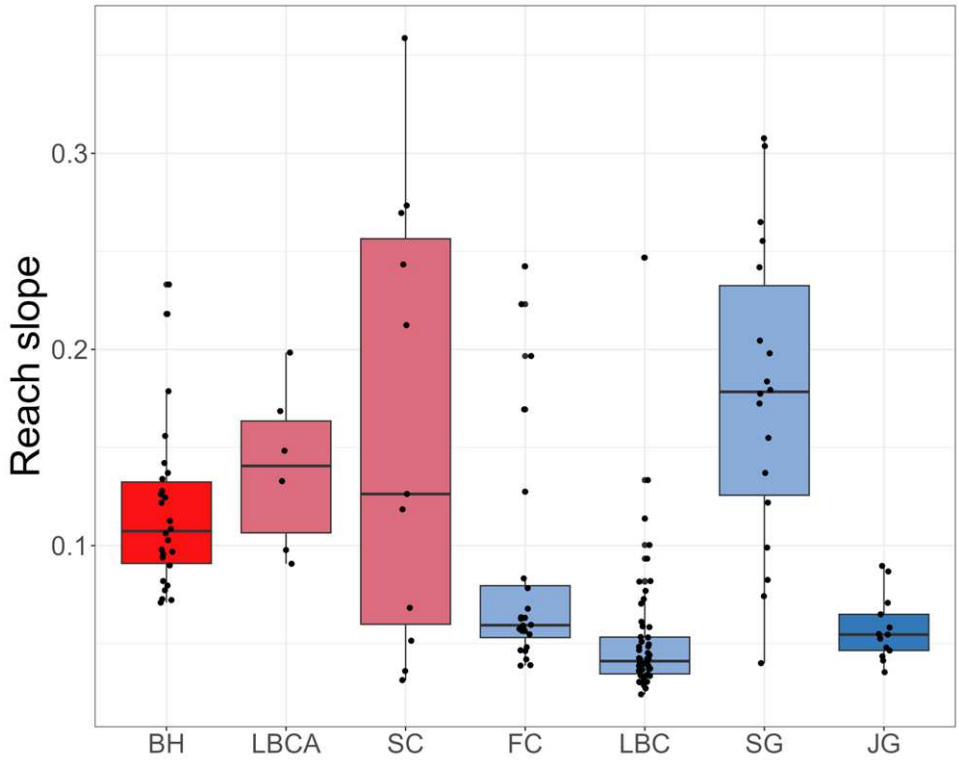

Figure 12: Interquartile distributions of reach-scale slope within each study site ordered from least resilient in dark red on the left (BH) to most resilient in dark blue on the right (JG). Reach slope varied between catchments ($p < 0.001$).

The distribution of relative floodplain width among reaches varied between catchments ($p < 0.001$) (Figure 13). The mean of the relative floodplain widths at Jack's Gulch is significantly greater than the relative floodplain widths at Sheep Gulch, Black Hollow, and Sheep Creek ($p < 0.001$, $p < 0.001$, $p = 0.02$). The mean of the relative floodplain widths at Little Beaver Creek is significantly greater than that of the relative floodplain widths at Black Hollow, Sheep Gulch, and Sheep Creek ($p < 0.001$, $p < 0.001$, $p = 0.003$). The mean of the relative floodplain widths is significantly greater at Fish Creek than at Sheep Gulch ($p = 0.02$). Jack's Gulch, Sheep Gulch, and Little Beaver Creek have 0.22, 0.43, and 0.17 km of reach stream length, respectively, that have a floodplain to channel width ratio greater than 15. Jack's Gulch, Sheep Gulch, Little Beaver Creek, Fish Creek, and Little Beaver Creek Tributary A have 0.37, 0.43, 0.3, 0.46, and 0.8 km of stream length, respectively, with a floodplain to channel width ratio greater than 10. There is a positive trend between floodplain to channel width ratio and resilience ranking where catchments with greater resilience are made up of reaches with greater floodplain to channel width ratios. The outlier to this trend is Sheep Gulch, which has the lowest mean floodplain to channel width ratio of all the sites but is ranked as having only a large flood.

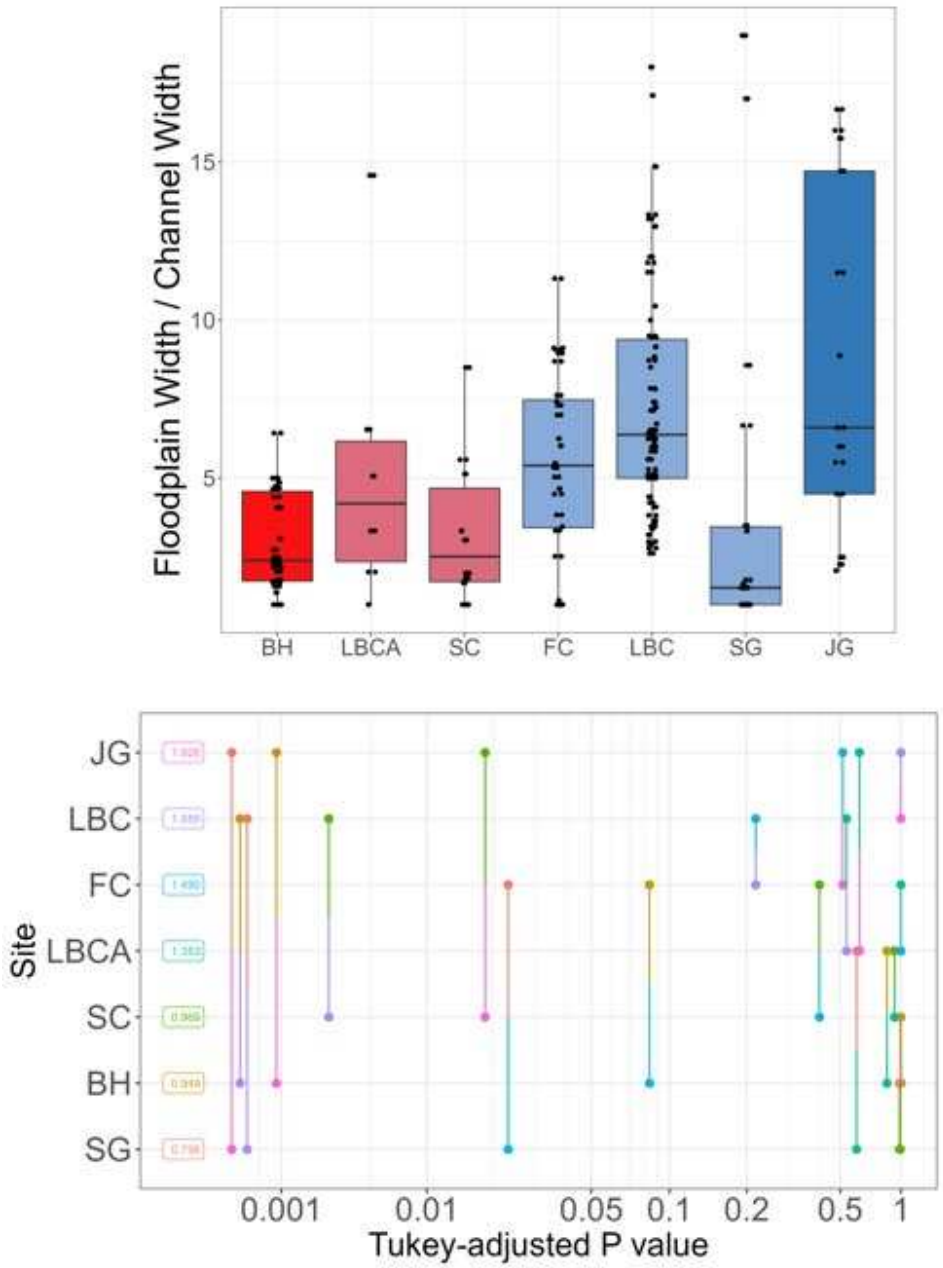

Figure 13: a) Interquartile distributions of floodplain to channel width ratio within each study site ordered from least resilient in dark red on the left (BH) to most resilient in dark blue on the right (JG). Floodplain to channel width ratio varied between catchments ($p < 0.001$). b) Pairwise p-value plot illustrating the results of pairwise contrasts of estimated marginal means between each site. Vertical lines connecting two sites show the p-value of each contrast on the horizontal scale.

The variance of floodplain to channel width ratio differed between sites ($p = 0.03$). Little Beaver Creek had greater floodplain to channel width ratio variance than Black Hollow ($p < 0.001$), and lower

variance than Sheep Gulch (p = 0.04) (Figure 14). Black Hollow had lower variance than Sheep Gulch, Little Beaver Creek Tributary A, Fish Creek, Jack's Gulch (p < 0.001 for all). Sheep Gulch had greater variance than Fish Creek (p = 0.01). Sheep Creek and Fish Creek had lower variance than Jack's Gulch (p = 0.02, p = 0.01).

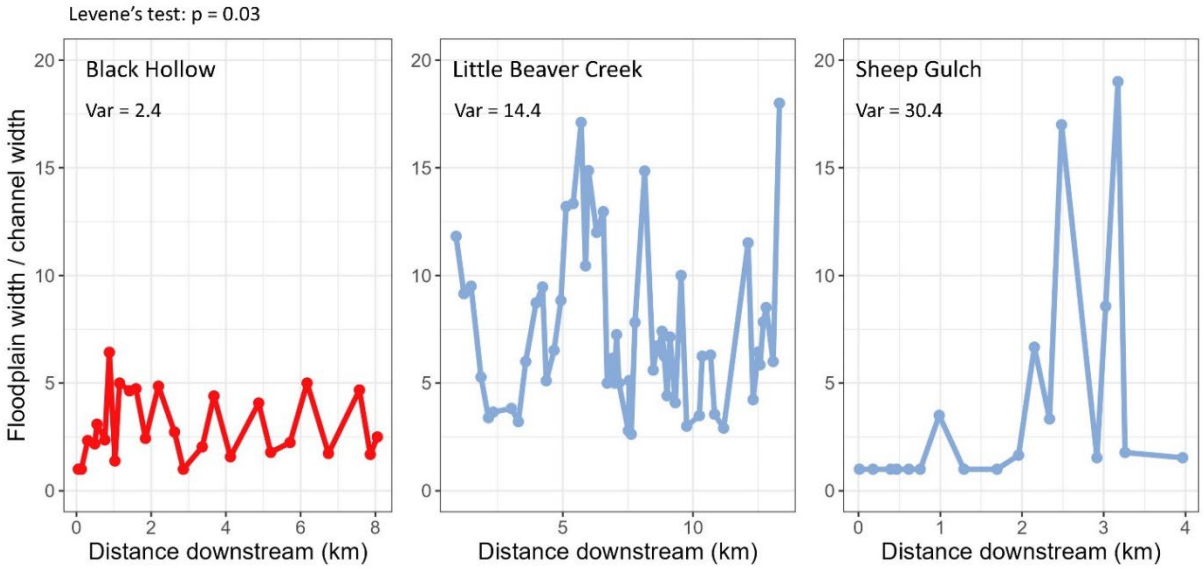

Figure 14: Floodplain to channel width ratios plotted against distance downstream at Black Hollow, Little Beaver Creek, and Sheep Gulch. Red indicates a less resilient catchment and blue indicates more resilient catchments.

Table 6: Results of multiple F tests comparing the equality of variances of the floodplain to channel width ratio at each site. Pairs with stars indicate a significant difference in variances the α = 0.05 level. The test statistic (F value), p-value, and ratio of variances are reported for each pair. The ratio of variances is the first site in the comparison divided by the variance of the second site in the comparison column. Values greater than 1 indicate that the first site in the comparison has a greater variance than the second. Values less than 1 indicate that the first site in the comparison has lower variance than the second.

Floodplain to channel width ratios			
Comparison	**F value**	**p-value**	**Ratio of variances**
LBC vs BH*	0.17	< 0.001	6.00
LBC vs SG*	0.47	0.04	0.47
LBC vs SC	0.41	0.15	
LBC vs LBCA	1.68	0.31	
LBC vs FC	0.60	0.18	
LBC vs JG	0.46	0.06	
BH vs SG*	0.08	< 0.001	0.08
BH vs SC	0.41	0.08	
BH vs LBCA*	0.10	< 0.001	0.10
BH vs FC*	0.28	0.00	0.28
BH vs JG*	0.08	< 0.001	0.08
SG vs SC*	0.19	0.02	5.20
SG vs LBCA	0.79	0.86	
SG vs FC*	0.28	0.01	3.53
SG vs JG	0.98	0.94	
SC vs LBCA	4.12	0.06	
SC vs FC	0.68	0.56	
SC vs JG*	0.19	0.02	0.19
LBCA vs FC	2.79	0.08	
LBCA vs JG	0.77	0.83	
FC vs JG*	0.28	0.01	0.28

Beaver berms were present in at least one reach of every catchment except Sheep Creek (Figure 15). Of the catchments with beaver berms present, the proportion of reaches with beaver berms present ranged from 0.12 at Black Hollow to 0.38 at Fish Creek and Jack's Gulch. Beaver meadows were

present in Little Beaver Creek, Sheep Gulch, and Jack's Gulch in 0.15, 0.06, and 0.31 of total reaches, respectively.

a)

Site	Beaver berm presence		
	No	Yes	Beaver meadow
BH	23	3	0
LBCA	3	3	0
SC	11	0	0
FC	15	9	0
LBC	26	20	8
SG	13	4	1
JG	4	5	4

b)

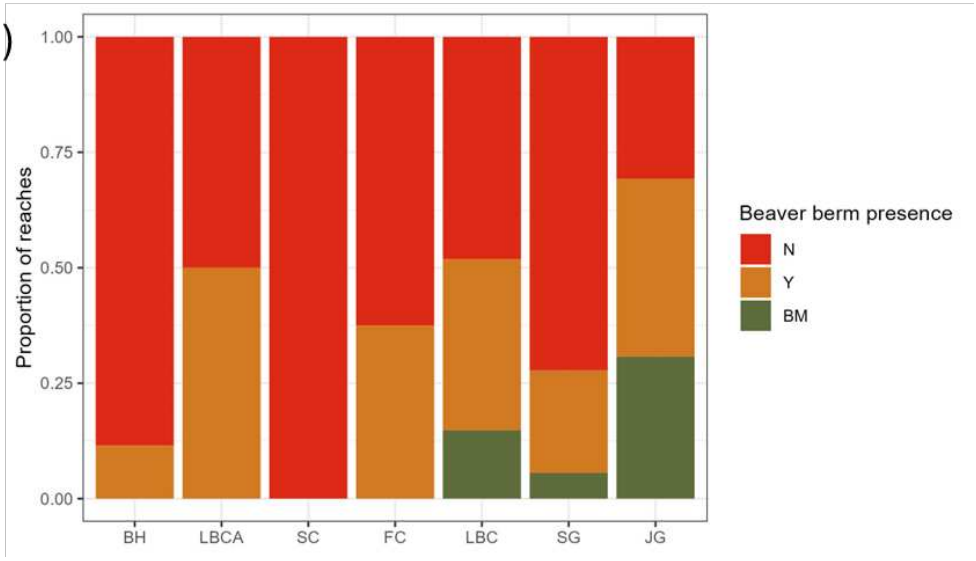

Figure 15: a) Table with the number of reaches with beaver presence. b) Stacked bar plot with the proportion of reaches with beaver berm presence at each of the sites. Red bars represent reaches that had no beaver berms. Orange bars represent reaches with at least one distinct beaver berm. Green bars represent reaches that were beaver meadows with many, possibly indistinct beaver berms.

3.3.2 Burn characteristics

In the field, the highest proportion of unburned reaches was at Little Beaver Creek at 0.26 followed by Sheep Gulch at 0.17 (Figure 16). Sheep Creek, Fish Creek, and Black Hollow had the highest proportion of reaches burned at 0.90, 0.89, and 0.88, respectively. The median remotely sensed dNBR-

derived burn extent of reaches was 100% among all catchments except at Jack's Gulch, where the median burn extent was 0.72.

a)

	Number of reaches		
Site	**Yes**	**Mixed**	**No**
BH	23	1	2
LBCA	4	2	0
SC	9	1	0
FC	18	2	4
LBC	28	12	14
SG	16	2	0
JG	8	4	1

b)

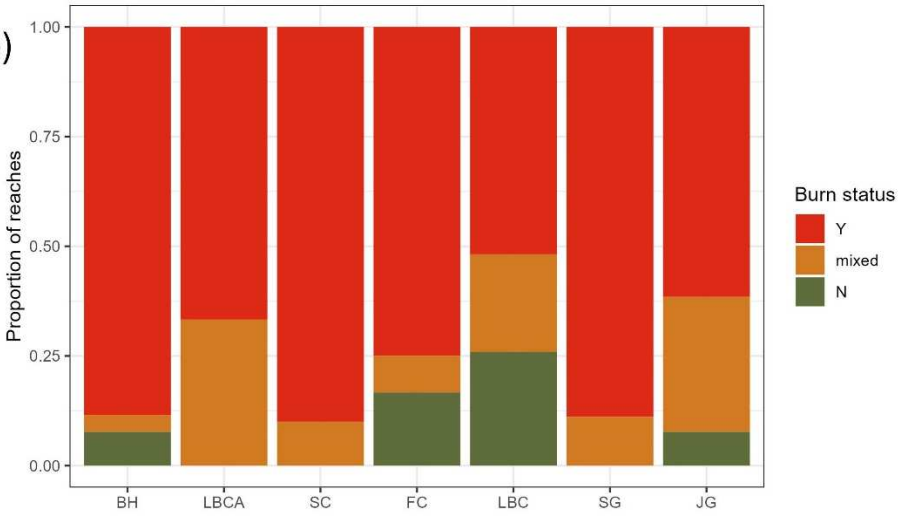

Figure 16: a) Table with the number of reaches with each burn status. b) Stacked bar plot with the proportion of reaches with each burn status at each of the sites. Red bars represent reaches that burned. Orange bars represent reaches with mixed burn. Green bars represent reaches that did not burn.

3.3.3 Vegetation

Fish Creek had the highest proportion of reaches with willow present at 0.63 (Figure 17). Black Hollow and Little Beaver Creek Tributary A had no reaches with willow present. Sheep Creek had the highest proportion of reaches with aspen but no willow at 0.80.

a)

Site	Number of reaches		
	Conifer	Aspen and conifer	Willow
BH	25	0	0
LBCA	3	3	0
SC	0	8	2
FC	5	4	15
LBC	28	0	22
SG	9	5	4
JG	4	6	3

b)

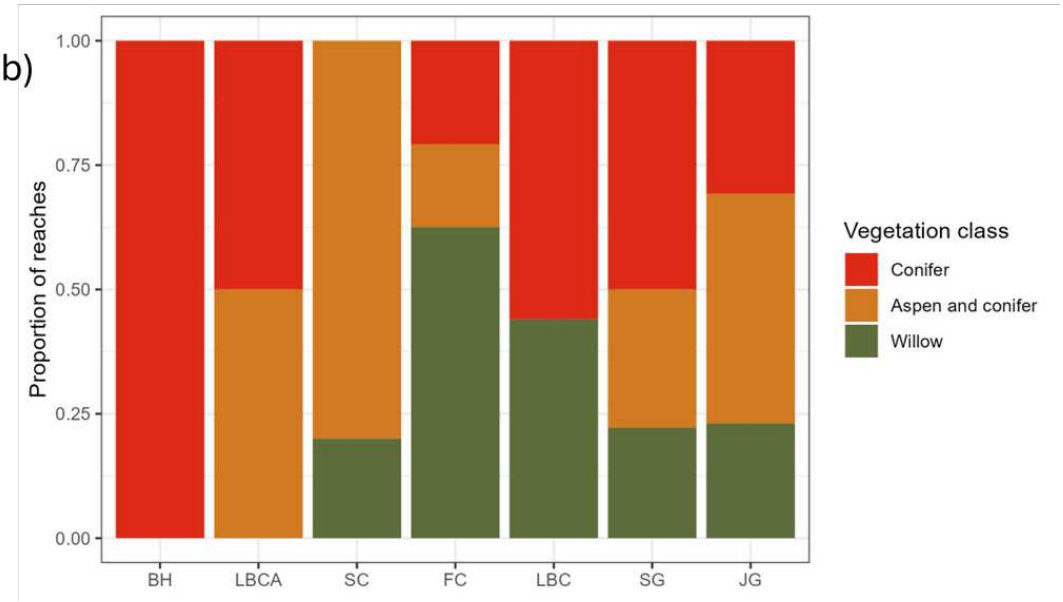

Figure 17: a) Table with number of reaches within each vegetation class amongst each site. b) Stacked bar plot with the proportion of reaches within each vegetation class at each of the sites. Red bars represent reaches with conifer and no other vegetation categories present. Orange bars represent reaches where aspen was present but not willow. Green bars represent reaches where willow was present in any combination with other vegetation categories.

NDVI recovery ratios among reaches differed between catchments over the three years following the fire (2021, 2022, 2023; $p < 0.001$ for all; Figure 18). In 2021, the reaches at Jack's Gulch had significantly higher recovery ratios than Black Hollow ($p < 0.001$), Little Beaver Creek Tributary A ($p < 0.001$), Sheep Creek ($p = 0.01$), and Sheep Gulch ($p < 0.001$). The reaches at Little Beaver Creek had significantly higher recovery ratios than Little Beaver Creek Tributary A ($p = 0.008$), Fish Creek ($p < 0.001$), Sheep Gulch, ($p < 0.001$), and Black Hollow ($p < 0.001$).

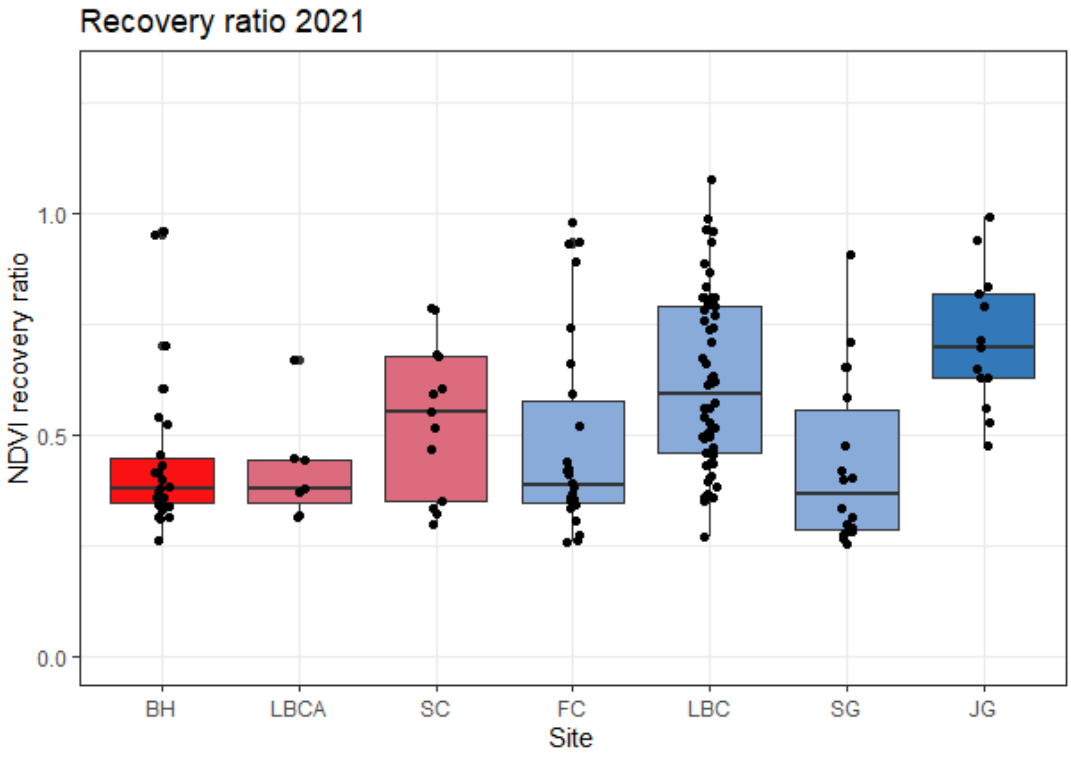

Figure 18: Mean normalized difference vegetation index (NDVI) recovery ratio of reaches within each study catchment in 2021, the first year following the Cameron Peak fire. NDVI recovery ratio is the ratio of the 2021 NDVI and the mean pre-fire NDVI form 2017, 2018, and 2019. NDVI recovery ratios among reaches differed between catchments ($p < 0.001$).

3.3.4 Logjams

The distribution of channel jam density values among reaches varied between catchments ($p < 0.001$) (Figure 19). Fish Creek had greater mean channel jam density than Little Beaver Creek, Sheep Creek, and Black Hollow ($p = 0.009$, $p = 0.01$, $p = 0.01$, $p = 0.02$, Figure 19b). Sheep Gulch had greater mean channel jam density than Sheep Creek and Little Beaver Creek ($p = 0.03$, $p = 0.04$).

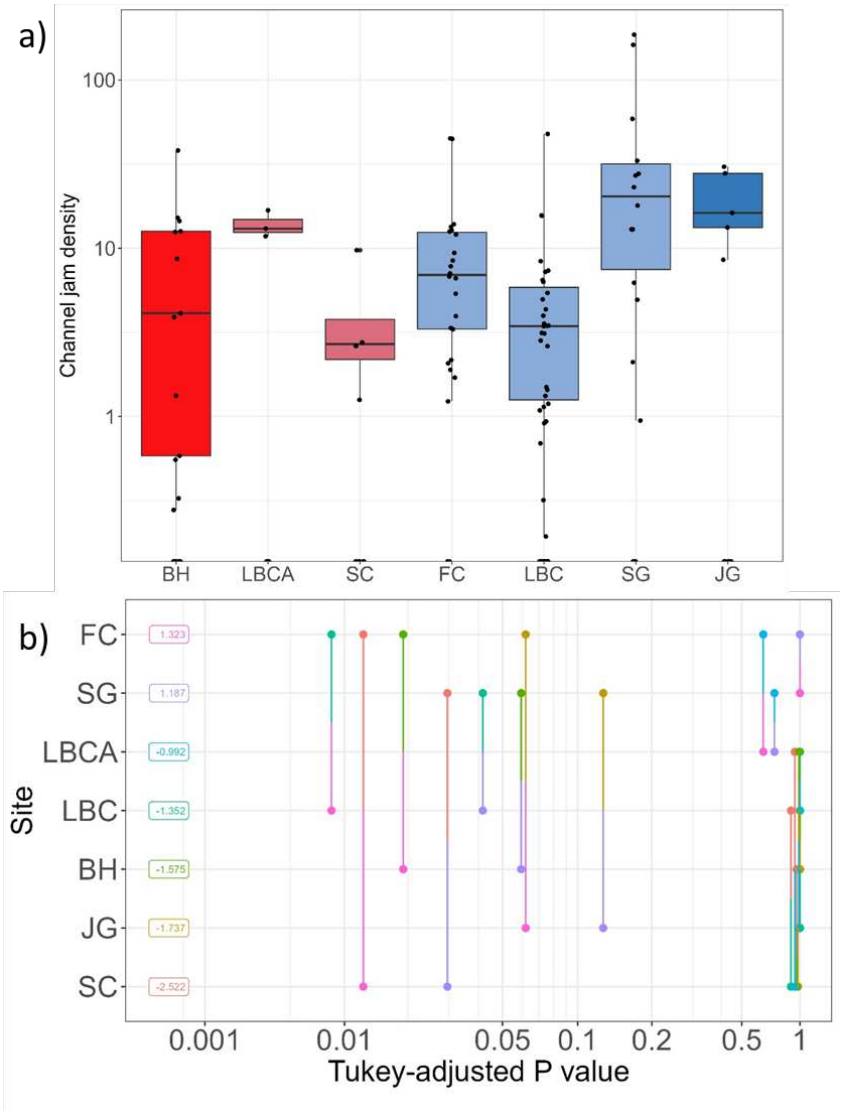

Figure 19: a) Interquartile distributions of channel jam density (channel jam count per channel area) within each study site ordered from least resilient in dark red on the left (BH) to most resilient in dark blue on the right (JG). Channel jam density varied between catchments ($p < 0.001$). b) Pairwise p-value plot illustrating the results of pairwise contrasts of estimated marginal means between each site. Vertical lines connecting two sites show the p-value of each contrast on the horizontal scale.

Of the six models tested using channel jams as the response variable, all models contained site as a predictor and bankfull channel area as an offset. All models tested had either reach slope, distance downstream, or both in the model. The top model had bankfull channel area as an offset with site, distance downstream, categorical floodplain vegetation, maximum channel count, bedform, and burn severity high as the best predictors (Table 7). The next best model had a delta AIC of 44.4, indicating that moderate-high values of burn severity, rather than high values of burn severity, was also a suitable predictor of the rate of channel jam formation. This indicates that burn characteristics, distance downstream, categorical floodplain vegetation, maximum channel count, bedform and burn severity were related to the rate of channel jams. The model with the best AIC score indicates a negative relationship between distance downstream and rate of channel jam presence among reaches in the study sites (Figure 20). This model also indicates a higher rate of channel jam presence among reaches in each of the other study sites when compared to Black Hollow. The likelihood-ratio test (LRT) on this model indicates that there are significant differences between channel jams at different sites, distances

downstream, with different floodplain vegetation, maximum channel counts, and proportions of high burn severity ($p < 0.001$ for all).

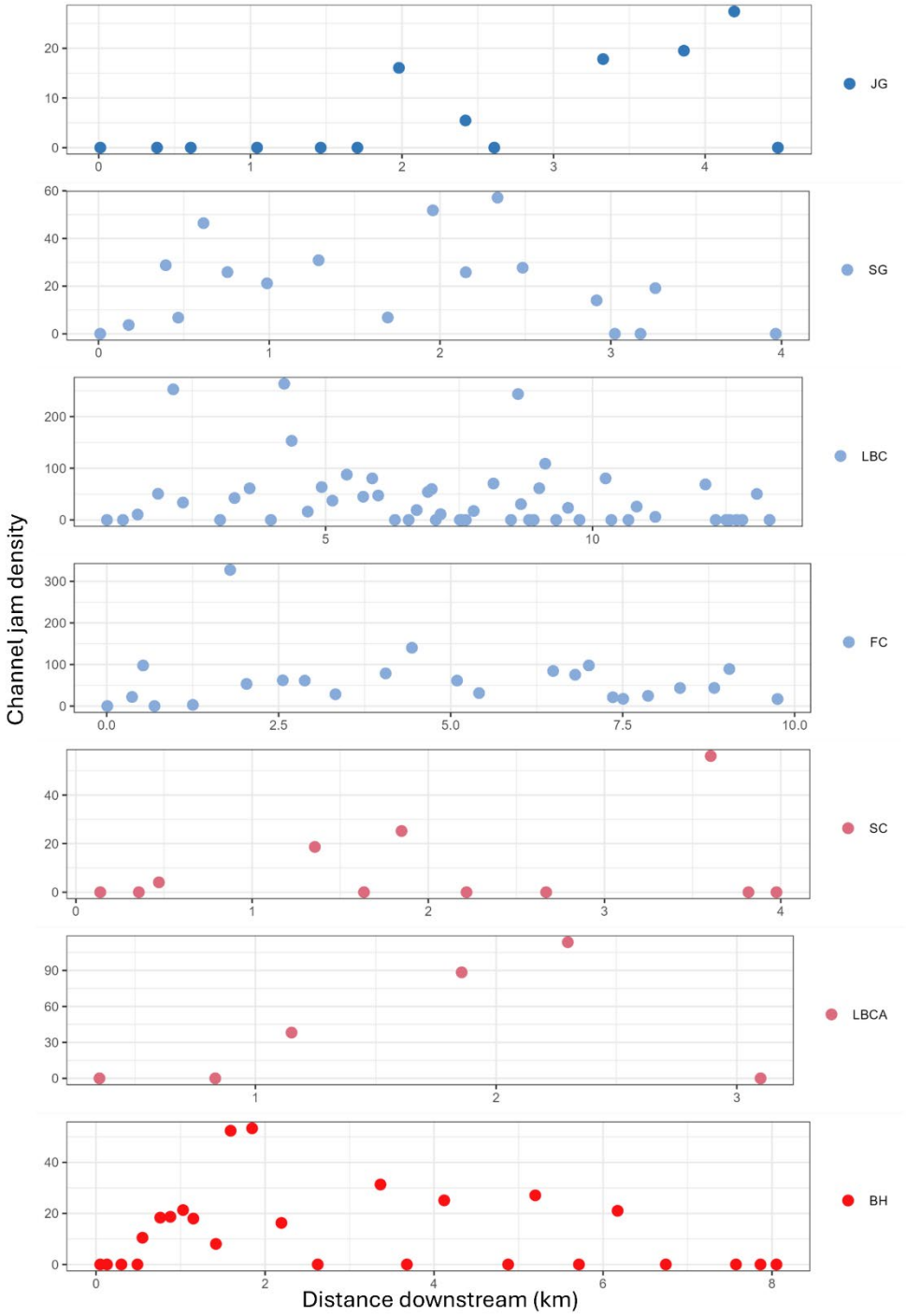

Figure 20: Longitudinal trends in channel jam density (channel jam count per channel area) amongst study sites. Channel jam density is the number of jams per reach area in km³.

Table 7: The predictors in the six Poisson models tested to describe channel jams as the outcome. The AIC and delta AIC relative to the best model were used to select the best models to describe channel jams. The model and associated metrics in bold was selected as the best performing model. Delta AIC values closer to zero indicate models that perform nearly as well as the best model.

Model	Predictors	AIC	Delta AIC
1	Site + offset(log(channel area)) + distance downstream	1013.29	156.48
2	Site + offset(log(channel area)) + reach slope	1101.89	245.08
3	Site + offset(log(channel area)) + reach slope + distance downstream + floodplain vegetation + maximum channel count + bedform	907.18	50.37
4	Site + offset(log(reach length * bankfull width)) + distance downstream + floodplain vegetation + maximum channel count + bedform + burn severity high	901.209	44.399
5	**Site + offset(log(channel area)) + distance downstream + floodplain vegetation + maximum channel count + bedform + burn severity high**	**856.81**	**0**
6	Site + offset(log(channel area)) + Reach_slope_13 + distance downstream + maximum channel count + bedform + burn severity high	908.67	51.86

Floodplain jam density differed between sites ($p < 0.001$, Figure 21). Jack's Gulch had lower floodplain jam density than Little Beaver Creek, Black Hollow, Fish Creek, and Sheep Gulch ($p < 0.001$, $p < 0.002$, $p < 0.001$, $p = 0.003$, Figure 21b).

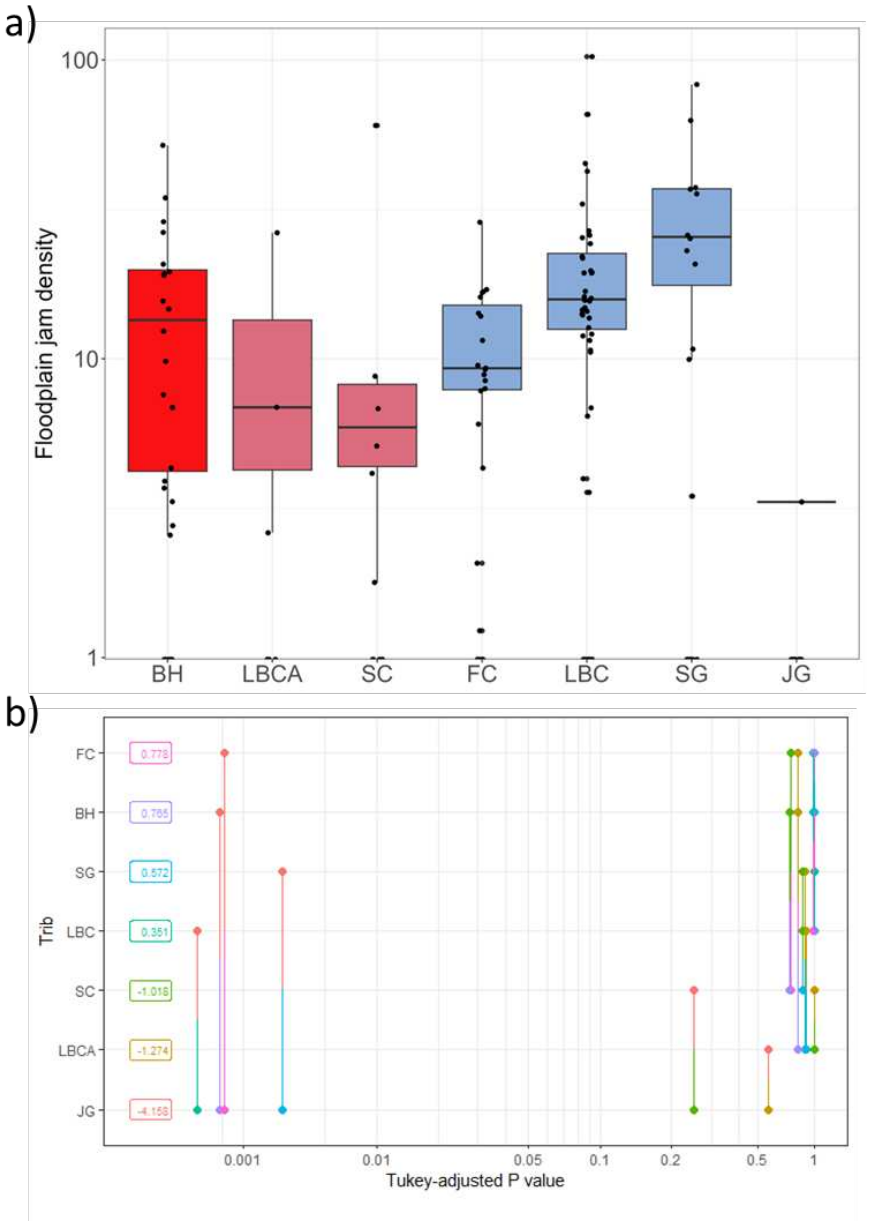

Figure 21: a) Interquartile distributions of floodplain jam density (floodplain jam count per reach area) within each study site ordered from least resilient in dark red on the left (BH) to most resilient in dark blue on the right (JG). Floodplain jam density varied between catchments ($p < 0.001$). b) Pairwise p-value plot illustrating the results of pairwise contrasts of estimated marginal means between each site. Vertical lines connecting two sites show the p-value of each contrast on the horizontal scale.

Of the six models tested with floodplain jams as the response variable, all models contained site and distance downstream as predictors and reach area as an offset (Table 8). The offset is a term in the Poisson regression model that represents the exposure time or area, in this case the log of the reach

area, to make the outcome a rate or density instead of a count. This allows for different areas between each observation reach. The top model had reach area as an offset with site, distance downstream, high burn severity, and categorical floodplain vegetation as predictors. The next models with substantial support had the same predictors with maximum channel count and basal area as additional predictors. These two models had delta AIC values under five indicating that models with maximum channel count and basal area as predictors were also suitable representations of floodplain jams. The LRT test on the model indicates that site, distance downstream, high burn severity, and categorical floodplain vegetation were related to the rate of floodplain jams ($p < 0.001$ for all). The model with the lowest and therefore best AIC score indicates a positive relationship between distance downstream and rate of floodplain jam presence among reaches in the study sites (Figure 22). This model also indicates a lower rate of floodplain jam presence among reaches in each of the study sites, apart from Sheep Gulch when compared to Black Hollow.

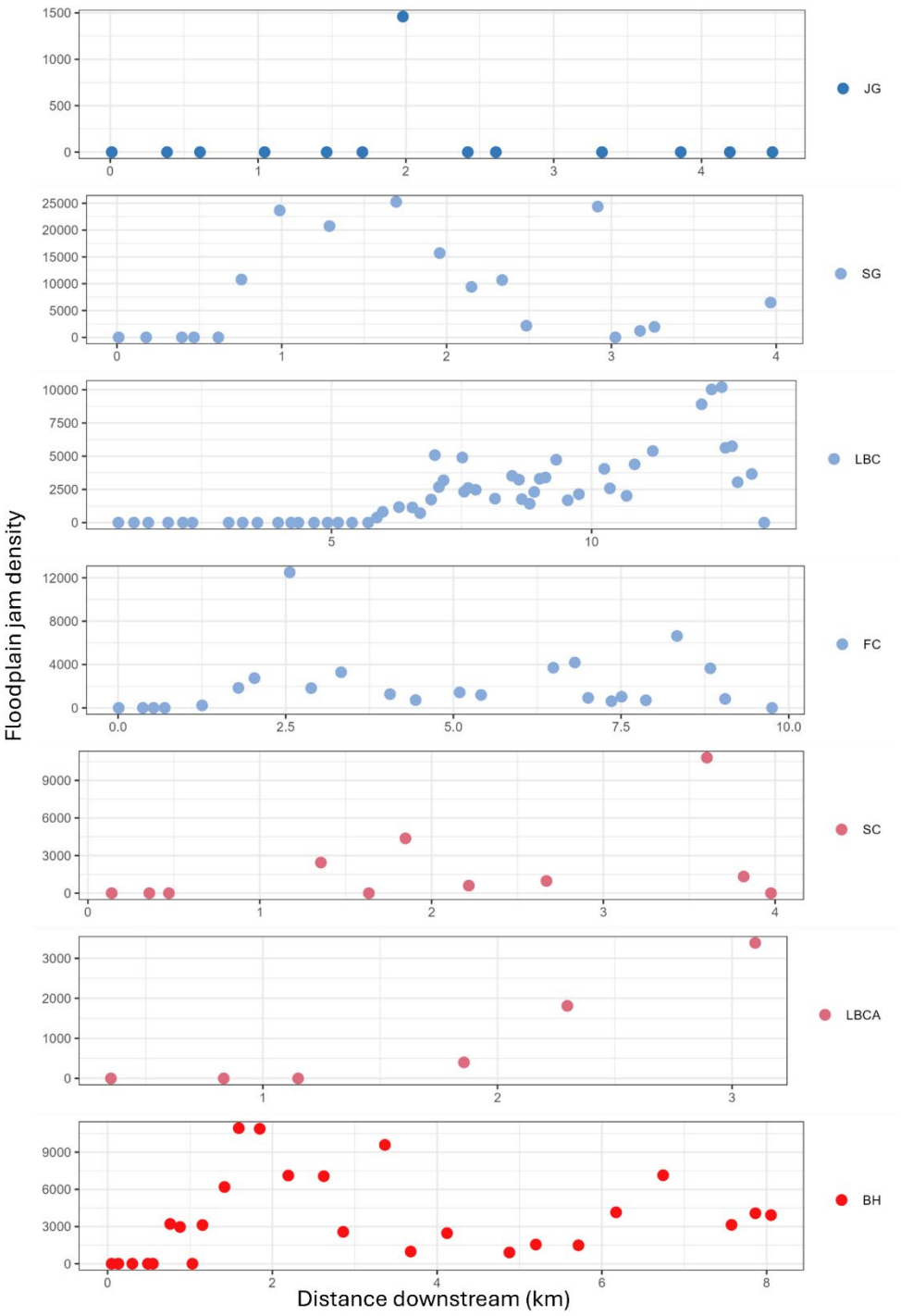

Figure 22: Longitudinal trends in floodplain jam density (floodplain jam count per reach area) amongst study sites. Floodplain jam density is the number of jams per reach area in km^3.

Table 8: The predictors in the six Poisson models tested to describe floodplain jams as the outcome. The AIC and delta AIC relative to the best model were used to select the best models to describe floodplain jams. The model and associated metrics in bold was selected as the best performing model. Delta AIC values closer to zero indicate models that perform nearly as well as the best model.

Model	Predictors	AIC	Delta AIC
1	offset(log(reach area)) + Site + distance downstream	2069.51	304.39
2	offset(log(reach area)) + Site + distance downstream + burn severity high	2061.52	296.4
3	offset(log(reach area)) + Site + distance downstream + burn severity high + basal area	2002.22	237.1
4	offset(log(reach area)) + Site **+ distance downstream + burn severity high + floodplain vegetation**	**1765.12**	**0**
5	offset(log(reach area)) + Site + distance downstream + burn severity high + maximum channel count + floodplain vegetation	1767.12	2
6	offset(log(reach area)) + Site + distance downstream + burn severity high + maximum channel count + floodplain vegetation + basal area	1769.03	3.91

4. DISCUSSION

I interpret and evaluate the observations and results of catchment and reach scale characteristics in relation to catchment resilience to address my research objectives and hypotheses. I discuss the results of this study in the context of these hypotheses and apply these interpretations to form a broad understanding of the impacts of the assessed characteristics on the fluvial response to wildfire. I interpret my results to identify the characteristics that are the most important in attenuating flood and debris flows after wildfire. Based on these interpretations, I discuss the implications of my findings for post-fire management strategies that aim to improve catchment resilience after wildfire.

4.1 Catchment

Hypothesis 1 was partially supported because resilience was not associated with individual geomorphic, burn, and vegetation catchment characteristics, but was associated with precipitation characteristics. There was a negative relationship between resilience and precipitation intensity, indicating that precipitation was driving response to disturbance. Although there was a relationship between resilience and precipitation, there was a range of precipitation intensities within resilience ranking categories, indicating that precipitation is one of many characteristics influencing resilience.

4.1.1 Geomorphic characteristics

Individual geomorphic characteristics at the catchment scale did not have clear trends with site resilience ranking, and therefore do not support Hypothesis 1. Other studies have found catchment morphology and lithology to describe instances of post-fire debris flows (Menitove, 1999; Cannon & Reneau, 2000), but these characteristics did not explain the trends in catchment response within the scope of this project where catchment response captured a spectrum of resilience. These catchments had many large-scale characteristics in common due to their physical proximity to each other. They do not differ in lithology or soil type, which simplifies the interactions between catchment scale

characteristics and eliminates the possibility that these characteristics are the reason for different responses as has been described in other settings (Cannon & Reneau, 2000). The catchments also burned at similar extents and severities in the Cameron Peak fire due to their spatial proximity. The catchments represent a range of sizes and mean catchment slopes for headwaters catchments. I found no trend in the resilience ranking and catchment area or slope, a conclusion that is supported by some but not all previous studies. Cannon & Reneau (2000) assessed three catchments that showed a range of responses after fire ranging from low runoff to debris flow. They found that the debris flow was generated at the catchment with the steepest hillslopes. Contrasting their findings, this study found that mean catchment slope was not an indicator of resilience amongst the study catchments. Likely the mean catchment slope calculated in this study does not capture the channel gradient where sediment is derived in this kind of debris flow. Meyer & Wells (1997) found that catchments less than 2 km^2 were likely to have debris flows and larger catchments were associated with sediment-laden floods rather debris flows. All study catchments in this project were greater than 2 km^2 and the catchment with the least resilience and largest debris flow was 17 km^2. Other studies have found that catchment area does not strongly influence post-wildfire response. Assessing 95 burned catchments in Colorado, New Mexico, and California, Cannon (2001) found that the catchments that produced debris flows could not be distinguished from those that did not produce debris flows by catchment area and slope.

Although the small number of study catchments limits the statistical analysis of multiple variable interactions, many of the characteristics that show no trends and outliers can be explained by other catchment variables. I expect steeper slopes to be a characteristic that drives response to disturbance that is associated with lower resilience, this is not true for all catchments. The major outliers are Sheep Gulch and Jack's Gulch. These two catchments are tributaries of other catchments included in the study, and therefore lower order, steeper catchments. Although the relationship between slope and longest flow path is described with relief ratio, there is no trend between resilience and relief ratio.

Sheep Creek stands out as the highest drainage density of the study catchments. This is a small catchment with a tributary almost equal in size to the main flow path. The other study catchments do not have tributaries nearly equal in size to their mainstems, suggesting that the total length of flow paths explains the high drainage density at Sheep Creek. Black Hollow and Jack's Gulch have nearly the same drainage densities despite being ranked as least and most resilient, respectively. Black Hollow is a catchment with a greater drainage area, but with many small tributaries that increase the drainage density. Jack's Gulch does not have many flow paths, but it is a relatively small basin. These results suggest that, amongst the seven study sites, there is no meaningful relationship between resilience and drainage density.

There is a trend between resilience and elongation ratio of each catchment where higher resilience is associated with lower elongation ratio. A lower elongation ratio is a catchment that is more "round" and less "long." The least resilient catchment, Black Hollow, has an elongation ratio very close to that of Little Beaver Creek, ranked as having only a large flood and therefore being more resilient. Despite the four catchments ranked as more resilient having lower elongation ratios than the less resilient catchments, this trend is likely not meaningful in these data. As with the other catchment-scale geomorphic characteristics, the sample size of seven is too small to statistically interpret a general trend from a single variable.

Although the vast majority of the catchment areas are above the 2300 m elevation threshold where floods caused by rainfall occur in Colorado (Jarrett, 1990), I observed flooding caused by summer convective storms in these catchments following the Cameron Peak fire (Figure 23). These catchments would typically have flood peaks caused by snowmelt rather than rainfall. Under normal conditions, rainfall intensity would not be sufficient to cause flooding of the magnitude observed. Post-fire, every flood and debris flow event I observed was caused by rainfall during summer convective storms. Because water is more efficiently conveyed from hillslope to channel on a burned landscape, rainfall

causes disproportionate flooding compared to unburned landscapes (Martin & Moody, 2001). The lower rates of precipitation that occur at higher elevations can therefore create flooding in a burned landscape. In the context of these study sites, this could be conceptualized as fire lifting the elevation threshold below which rainfall-induced flooding occurs in the Front Range. The lifting of a hydroclimatic boundary for rainfall-induced flooding is analogous to the elevation lift that decreased the mean drainage area above channel heads after a catchment burned (Wohl, 2013b). Much like the hydroclimatic boundary for rainfall-induced flooding, the location of channel heads within a catchment is a reflection of both climate and topography as the contributing drainage area must concentrate enough flow to create channel heads (Montgomery & Dietrich, 1989). In this same way, the rainfall-induced flood elevation threshold is reflective of the climate and topography (Jarrett, 1990). On a burned landscape, the removal of organic material as groundcover and associated increases in runoff and erosion relative to rainfall also seems to be manifesting as a shift in the elevation above which storms cause rainfall induced flooding at these sites.

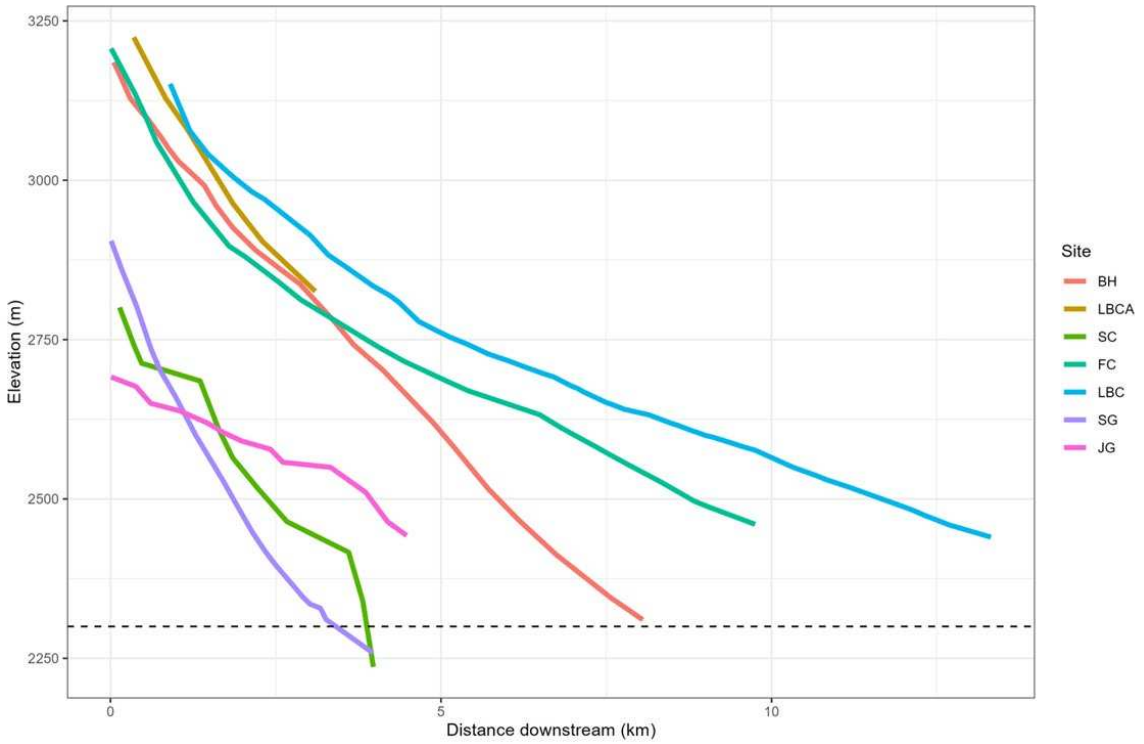

Figure 23: Elevation profiles of each of the study catchments in solid lines. The dashed horizontal line at 2300 m represents the elevation threshold above which floods in Colorado are typically caused by snowmelt instead of rainfall. Flooding at elevations above this threshold are typically produced by snowmelt.

4.1.2 Burn characteristics

Resilience was not associated with catchment scale burn characteristics, which I hypothesized as driving the magnitude of response to disturbance. All catchments in this study burned at high extents, with all except Little Beaver Creek Tributary A having almost 90% or greater of their total area burned. Burn severity also had a poor association with resilience ranking by site. The least resilient catchment, Black Hollow, and the most resilient catchment, Jack's Gulch, both had nearly the same burn severity of almost 50%.

Considering the combination of area burned at high and moderate severity, data published by Gartner et al. (2005) show that most debris flows were produced in catchments with greater than 65% of their area burned at high and moderate severity. Cannon et al. (2004) also found that burn severity was an effective way of statistically differentiating catchments where debris flows occurred compared to

a different response. Gartner et al. (2005) also found that despite the relationship between burn severity and debris flow occurrence, debris flows can be generated in basins that have little to no area burned at high severity. These findings are supported by studies assessing physical principles showing that of all other indicators for burn severity, the removal of organic material on the surface of catchments was most closely tied to increased rates of runoff and erosion (Agee, 1973) and (Neary et al., 1999). The results of my study indicate that, even among catchments with >50% area burned at high and moderate severity, proportion of catchment burned does not correlate with post-fire debris flow occurrence.

4.1.3 Precipitation

The negative trend between median precipitation intensity (mm/h) and resilience supports Hypothesis 1. Precipitation, a variable that I conceptualize as driving response to disturbance, decreases as resilience increases and increases as geomorphic response increases, suggesting that it is driving response to disturbance.

Although precipitation patterns are heterogeneous in the mountains especially (Lundquist et al., 2019), investigation into these relationships, including by the U.S. Geological Survey, relies on in-situ rain gauges that provide precipitation estimates at a single point (Staley et al., 2017). Therefore, the threshold values for precipitation intensity and duration to trigger debris flows are calculated using rain gauge measurements that are spatially explicit rather than the spatially continuous gridded data that I used to quantify precipitation in ungauged catchments. The median precipitation intensities across the Black Hollow catchment fall within the range of precipitation intensities over burned catchments that triggered debris flows; i.e., between 1.0 to 32.0 mm/h (Cannon et al., 2008). Precipitation can be quantified in many ways including a single value intensity or duration value or intensities for certain durations for a single storm. Typically, the storms that trigger debris flows in burned catchments are short in duration with storms lasting up to 3 hours and precipitation to trigger a debris flow occurring in

as little as 6 minutes (Cannon et al., 2008). There is commonly no initiation point and these can occur with little antecedent moisture (Cannon et al., 2008). The storms that trigger these debris flows in Colorado are typically short in duration, triggering debris flows within minutes to hours of rainfall, and high in intensity. Precipitation intensities to trigger debris flows in southwestern Colorado recorded by rain gauges are 3 mm/h for 3 hours. In California, Cannon et al. (2008) documented intensities recorded by rain gauges of 25 mm/h for 10 minutes and 5 mm/h for 20 h that triggered debris flows in the first season following fire. The mean and median precipitation characteristics across the catchments in my study agree with the literature and are within the same orders of magnitude as gauge-based estimates of precipitation.

Quantitative Precipitation Estimates (QPEs) are estimates of precipitation intended for use in locations where there are no in situ measurements, typically in the form of rain gauges. Radar-based precipitation estimates are expected to have high uncertainty in areas with less radar coverage (Maddox et al., 2002). Although the sites in this study are in the mountains of Colorado in remote locations relative to radar, White & Nelson (2024) found that MRMS data performed surprisingly well compared to prior estimates of error. MRMS had the least error compared to rain gauges in scenarios with longer storms that produced continuous rainfall. Despite these errors, MRMS provides a valuable alternative to traditional gauge-based measurements of intensity that do not capture the spatial variability convective storms and are often not available in remote locations (White et al., 2023).

The spatial distribution of the precipitation over a 24-hour period is different amongst catchments. Comparing Black Hollow and Little Beaver Creek, the highest median precipitation values are concentrated in only one upper part of the catchment at Little Beaver Creek (Figure 24). This aligns with the results when compared to resilience because the area with the highest precipitation intensities within Little Beaver Creek is centered over Little Beaver Tributary A, which was ranked with lower resilience than the mainstem. At Black Hollow, the 24-hour median precipitation intensities are

uniformly high across the entire catchment. This aligns with observations made of the debris flow resulting from the storm throughout the river corridor and beginning high in the drainage network. Evidence of scour beginning at the upper end of the catchment suggest that the 2021 flow continued to bulk up via erosion of the valley floor and grew in magnitude moving downstream.

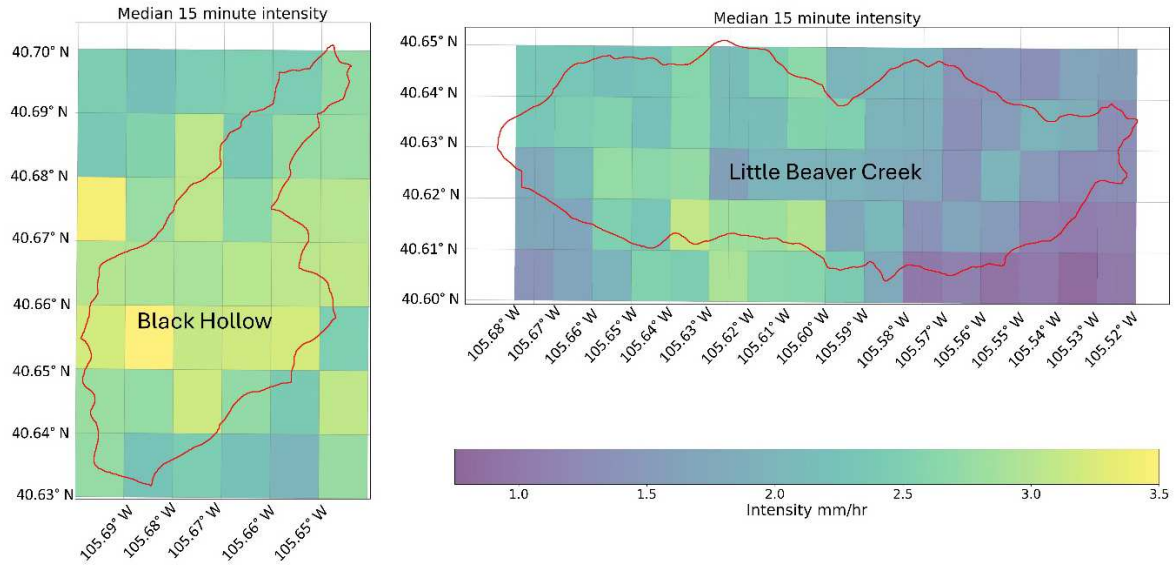

Figure 24: Spatial patterns of precipitation across Black Hollow and Little Beaver Creek with the catchment boundaries outlined in red. Each pixel is 1 x 1 km in dimensions. The pixel color represents the median 15-minute precipitation intensity (mm/h) over the 24 hours during which the storms occurred. These 24-hour periods began on 20 July 2021 at 12:00 UTC and 15 July 2022 at 17:00 UTC at Black Hollow and Little Beaver Creek, respectively.

4.1.4 Vegetation

The removal of vegetation via combustion is the primary reason for heightened flow and erosion after fire (Agee, 1973; Neary et al., 1999; Larsen et al., 2009). Because recovery of catchment-scale vegetation is related to the initiation of post-fire debris flows (Graber et al., 2023), I hypothesized that vegetation would be a characteristic that would resist response to disturbance after fire. My findings did not support this part of hypothesis 1, suggesting that catchment-scale vegetation cover and recovery is not associated with post-fire response. I propose three reasons that can explain why this part of hypothesis 1 is not supported. First, the vegetation on the hillslopes of the study catchments has not

recovered as much as the channel margins and floodplains, especially at higher elevations. The hillslopes make up the greatest portion of the catchments by area and are therefore predominantly reflected in the NDVI values for the entire catchment. During fieldwork three years after the Cameron Peak fire, some channels, floodplains, valley bottoms, and concavities that burned had aspen regrowing, along with grasses and herbaceous cover. Some hillslopes recovered similarly, but others had only sparse herbaceous vegetation and very few coniferous saplings establishing, leaving much of the hillslope dominated by exposed sediment, especially at high elevations (Figure 25). At lower elevations, there were commonly grassy hillslopes where there were trees before the fire. In many locations, the grass was dry and less green on the hillslope than on the valley floor by July.

Figure 25: Hillslopes at high elevations in Sheep Creek (July 2023) and Little Beaver Creek (June 2023). Sparse vegetation is present, but few if any trees have re-established in the three years since the Cameron Peak fire in 2020.

Second, the Landsat 8 imagery that I used to calculate NDVI has 30-m spatial resolution and 16-day temporal resolution. Although this is very effective as repeat imagery, there may be relatively few cloud-free pixels from the growing season to use in the composite image. Especially in the mountains, there are likely many images that have cloud cover and are therefore not usable to calculate median NDVI. This can introduce error by weighting certain years more heavily towards one part of the growing season in the final raster. Third, a combination of the scale of recovery and the resolution of the imagery could be responsible for the lack of support at the catchment scale. Vegetation recovery may be more spatially complex and have patterns on a smaller scale than the Landsat imagery is able to quantify with 30 m spatial resolution. This suggests that reach-scale vegetation metrics may be better suited to explain the different responses observed at each site and associated resilience.

4.1.5 Assumptions

This project is limited to assessing single catchment characteristics in isolation because of the small sample size. The site characteristics cover a wide range of areas and slopes for headwater systems, but this sample size was not sufficient to understand the interactions and associations between the catchment-scale characteristics. These analyses were performed as described, assuming that any characteristic can be assessed individually.

Black Hollow was mulched after the Cameron Peak fire in the summer of 2021. Mulch was applied to the upper part of the catchment at Black Hollow via helicopter. Mulch was not applied to the other study catchments. This study assumes that the impacts of mulching the hillslopes minimally affected the resilience response compared to the characteristics measured in this study.

Precipitation intensity over the catchment scale quantified using MRMS QPEs has numerous sources of error caused by different states of precipitation, high relief topography, and highly variable precipitation over small areas (Boodoo et al., 2015; Zhang et al., 2016). Comparing precipitation

estimates between gauges and MRMS, there are high and variable amounts of error in the magnitude and timing of precipitation (White & Nelson, 2024). To absorb the error likely introduced by MRMS, I used a 24-hour period to capture the storm. I presented summary statistics over space and time to produce an estimate of precipitation over the catchment that takes intensity and duration into account while absorbing the error.

I used the dNBR rather than the NBR that is published by the USFS as publicly available data. dNBR uses a baseline NBR value to quantify change induced by fire and is therefore standardized to different starting values that may be present amongst catchments. The publicly available dataset using NBR is already classified into four categories of unburned, low, moderate, and high severity. The dNBR derived layer can be classified into seven layers following the USGS guidance and therefore more closely resembles the continuous range of burn severity that can be observed in the field.

4.2 Reach Scale

There were trends between catchment resilience and reach characteristics. Reach characteristics that were conceptualized as resisting response to disturbance, including inter- and intra- reach heterogeneity elements, were associated with greater resilience. Reach-scale characteristics that were conceptualized as driving response to disturbance were associated with lesser resilience. These results support hypothesis 2. More resilient catchments had more reaches with wide floodplains, low channel gradient, multiple channels, beaver-modified topography, and multi-stem deciduous vegetation including willow.

Amongst many characteristics on the reach scale, Sheep Gulch did not align with many of the trends observed. Although it was ranked as having only a large flood, many of its traits aligned more closely to those measured at Sheep Creek to which it is a tributary almost equal in size. In the upper part of the catchment, there were similarities between Sheep Gulch and Sheep Creek on the reach scale.

There were patterns of erosion and deposition within the channel that showed evidence of a large flood in both catchments (Figure 26).

Figure 26: Patterns of erosion and deposition at Sheep Creek. White arrows indicate flow direction. a) Upper reach with confined channel and no floodplain. b) Early evidence of scouring within the channel. c) Deposition at a local low gradient section d) More erosion and incision in greater magnitudes further downstream.

Farther downstream in both catchments, the amounts of erosion and evidence of flood magnitude also grew larger. In Sheep Creek, this pattern continued to the outlet of the catchment

where the channel shifted and incised, and then deposited a large amount of sediment into the Poudre River. In Sheep Gulch, the patten of erosion and deposition related to the flood continued for about two thirds of the length of the catchment. At this point in the catchment, there was a series of reaches that were wider, lower gradient, and less incised. There was evidence of relict beaver dams, willow, and aspen recovering from the fire. The floodplain was wet, and the vegetation was healthy during fieldwork at the end of July, indicating a well-connected channel and floodplain (Figure 27). Below the wide reaches, there was no evidence of the major flood that had been bulking up as it moved downstream in the upper part of the catchment. In other words, the wide and hydraulically rough reaches at the downstream end of Sheep Gulch appear to have effectively attenuated the water and sediment fluxes coming downstream after the fire.

Figure 27: Sheep Gulch river corridor downstream progression. a) Upper Sheep Gulch with a confined channel and no floodplain. Dashed yellow lines outline the river corridor. b) Channel and bank scouring in Sheep Gulch in the upper part of the catchment. c) Wide floodplain two-thirds of the way downstream in Sheep Gulch. Dashed yellow lines outline the floodplain with a yellow box around a person for scale. d) A reach below the wide floodplain reach. There is less incision and erosion of banks.

4.2.1 Driving and resisting characteristics

Burn extent, measured in the field categorically and hypothesized to be a characteristic that drives response to disturbance, was greater at less resilient catchments, supporting hypothesis 2. Black Hollow had a higher proportion of unburned reaches than the other sites with low resilience, but these reaches were the upstream-most in the catchment. These headwaters reaches were upstream of the evidence of flooding and likely did not influence the magnitude of response at Black Hollow. Although some studies have found that high fire severities create a hydrophobic soil layer, Benavides-Solorio &

MacDonald (2001) found that there were no substantial differences in runoff proportional to rainfall between different burn severities. Larsen et al. (2009) found that post-fire runoff was influenced more by ground cover than water repellency. These studies support the use of a categorical indicator of burns status being an adequate proxy for the local impacts of fire and agree with the results of this study. Compared to the burn characteristics on the catchment-scale, these results on the reach scale indicate that the impacts of fire on the river corridor have a disproportionate effect on the post-fire response compared to the impacts of fire on the hillslope.

Slope amongst reaches showed a trend of decreasing mean slope as resilience of the catchment increased. This supports hypothesis 2 because slope is a driving characteristic towards response magnitude. Greater slopes are associated with greater energy and therefore less attenuation. Of the four catchments ranked as moderate flood or no flood, all but Sheep Gulch had lower mean reach slopes than any of the catchments ranked as having a major or moderate fan. Sheep Gulch was an outlier in the otherwise ubiquitous trend of lower mean reach slopes associated with greater resilience. This aligns with other studies that found that the average channel gradient within a catchment was a key parameter in debris flow generation in burned catchments (Cannon & Reneau, 2000).

The ratio of the floodplain to channel width of reaches was hypothesized as a resisting characteristic to disturbance response. The floodplain to channel width ratios were greater at the sites that were ranked as more resilient compared to the three catchments that were ranked as less resilient, except for Sheep Gulch. At Black Hollow, the floodplain to channel width ratio is low because, although the floodplains are wide, the channels were also relatively wide. The floodplain to channel width ratio at Sheep Creek was also low. At this site, the channels were narrow but there was also a narrow floodplain. This was the same reason for the low floodplain to channel width ratio at Little Beaver Creek Tributary A. At Little Beaver Creek, a site ranked high in resilience, the distribution of the floodplain to channel ratios was high because there were many reaches with wide floodplains. This was true amongst the

other catchments ranked as more resilient, except for Sheep Gulch. Sheep Gulch was an outlier with a low mean because most of the reaches that make up the catchment are confined with narrow floodplains, much like Sheep Creek.

Flood attenuation is promoted in low areas of floodplains (Dunne & Leopold, 1978). Once accessed during a flood, floodplains that are longer, wider, and have more hydraulic roughness increase attenuation of peak discharge during floods by slowing flows (O'Sullivan et al., 2012; Lininger & Latrubesse, 2016). Valley characteristics including floodplain size, stream gradient, and roughness influence peak discharge and can substantially moderate floods (Woltemade & Potter, 1994). Longitudinal changes in reach slope can be understood through the lens of stream power where specific stream power is the available power to do work, or transport sediment, on the banks and bed of a channel per unit channel width (Bagnold, 1966). The equation for specific stream power is:

$$\omega = \frac{\rho g Q S}{b}$$

where ω is the specific stream power, ρ is the density of water (1000 kg/m^3), g is acceleration due to gravity (9.8 m/s^2), Q is discharge (m^3/s), S is slope, and b is channel width. As Q and S increase, stream power increases. This means that as slope increases, there is an increase in the amount of energy available to mobilize and transport sediment, which I saw in the field as evidence of erosion. Typically, as distance downstream increases, discharge increases, slope decreases, and channel width increases. Expanding the understanding of specific stream power, this also supports the finding that sites with a greater number of wide floodplain reaches promoted attenuation and were therefore more resilient. As overbank flow accesses the floodplain, the width of total flow increases and there is lower specific stream power, or less force per surface area than a narrow channel of the same total stream power.

In addition to the benefit of flood attenuation, floodplains are also ecologically diverse. Aquatic organisms access the floodplain during floods (Junk et al., 1989; Hurd et al., 2016; McInerney et al.,

2017). Choné & Biron (2016) found floodplain to channel width ratio to be a good predictor of habitat diversity.

4.2.2 Inter-reach heterogeneity

Of the floodplain to channel width ratios, the variances differed between the less resilient and more resilient catchments. Resilient catchments had greater variance in floodplain to channel width ratios, supporting hypothesis 2. Despite many of its reach and catchment scale characteristics having commonalities with less resilient catchments, Sheep Gulch had a higher variance than Little Beaver Creek and Fish Creek, which were ranked in the same resilience category as Sheep Gulch. This indicates that inter-reach heterogeneity performed well as a metric of resilience compared to other characteristics on the catchment and reach-scales that did not capture the capacity of Sheep Gulch to absorb the impacts of disturbance. These findings agree with the literature that has explored the features of beads that make them resilience to disturbance (Wohl et al., 2018). The wide floodplains present in beads provide temporary storage during floods that promotes attenuation (Fryirs et al., 2007). Higher water tables can be present in wider bead reaches, which can protect them from burning during a wildfire (Westbrook et al., 2006; Hood & Bayley, 2008). Wide floodplains are also associated with the formation of other heterogeneity elements. Beaver tend to build dams in wide reaches and enhance the processes of overbank flow, hyporheic exchange, multithread channel formation, and the growth of willow (Westbrook et al., 2006), and attenuate downstream fluxes of sediment (Dunn, 2023). The numerous impacts of beaver protect against drought, flood, and fire (Fairfax & Small, 2018; Fairfax & Whittle, 2020; Puttock et al., 2021).

Of the seven study sites, the sites that exhibited the greatest resilience had network configurations with beads at the downstream end of the catchments. Fish Creek, Little Beaver Creek, Sheep Gulch, and Jack's Gulch had large beads at the downstream end of the catchment that were able to attenuate the impacts of disturbance and limit sediment export from the catchment. Little Beaver

Creek and Fish Creek had beads distributed throughout their drainage networks, but Sheep Gulch had beads only at the downstream end of the catchment. Jack's Gulch, comparable in length to Sheep Gulch, had larger beads at the downstream end of the catchment. The reach configurations at Sheep Gulch and Jack's Gulch point to beads at the downstream end of the catchment contributing to greater resilience to disturbance.

4.2.3 Intra-reach heterogeneity

Sites that were more resilient had greater intra-reach heterogeneity than less resilient catchments, supporting hypothesis 2. Although the mean number of channels within reaches indicated predominantly a single channel planform, the more resilient catchments had substantially greater numbers of reaches with multiple channels. At more resilient catchments there were substantially greater proportions of reaches with beaver-modified topography, ranging from the presence of a single relict beaver berm to entire reaches dominated by beaver modifications. These heterogeneity elements likely contributed to the ability of the reaches to attenuate flood flows and absorb the impacts of disturbance.

Sites with greater resilience had a greater proportion of reaches with willow than less resilient sites. Willow and other multi-stem deciduous vegetation were conceptualized as heterogeneity elements that act to resist response to disturbance. Previous studies have found vegetation to be related to morphological characteristics of the channel and specifically that willow presence is associated with stable banks compared to reaches dominated by spruce (David et al., 2009). The findings of this study agree with the prior literature in that greater resilience was associated with multi-stem deciduous vegetation.

NDVI recovery ratios on the reach-scale differed amongst sites during the first summer after the Cameron Peak fire in 2021. These NDVI ratios represent the entire growing season, including pre- and

post-events at the catchments that had floods in July 2021 -- Black Hollow, Sheep Creek, and Sheep Gulch. The results of this study indicate that vegetation coverage recovered more quickly at resilient catchments and suggest that vegetation coverage within the river corridor is important to the resilience outcome. This agrees with the literature that has found vegetation to be an important factor in recovery from wildfire. Vegetation recovery post-fire has been documented to decrease yields of runoff and sediment from the hillslope in the field (Moody et al., 2013; Graber et al., 2023). Hydraulic modeling supports these field observations by showing that channel and floodplain roughness are key characteristics in decreasing flood peaks (Sholtes & Doyle, 2011). By increasing roughness, riparian vegetation reduces shear along banks and therefore erosion (Thorne, 1990). Findings from this work on the reach scale add to a growing body of literature describing how interactions between vegetation and flow in the channel and floodplain influence large-scale processes (Gurnell, 2014).

There were significantly different floodplain and channel jam densities amongst the study catchments. The negative trend between distance downstream and channel jams and the positive relationship between distance downstream and floodplain jams indicates a transition from transport-limited to supply-limited from headwaters to outlet (Marcus et al., 2002). Focusing on channel jams, the transport limited reaches occur at the upstream-most headwaters where there is capacity for wood recruitment from the banks, but there is no capacity to move this wood into a jam. Moving downstream, the transport capacity increases and is balanced with the supply capacity. This is where the maximum channel jam densities are expected. Farther downstream, the transport capacity increases with increasing contributing drainage area and becomes greater than the supply capacity, decreasing jam density at the downstream end of the catchment. The longitudinal trends in channel jam density align with previous studies (Wohl & Jaeger, 2009). The positive relationship between distance downstream and floodplain jam density indicates that the transport capacity for floodplain jams was lower than the supply within the length of the catchments. In other words, the downstream limit of the system that I

observed only captured the transport-limited and maximum jam portions of the catchment. Based on these results, it is likely that the fire and flood disturbances shifted the distribution of channel and floodplain jams with respect to locations for transport- and supply-limited thresholds of logjams (Wohl et al., 2024a).

4.2.4 Assumptions

The observations made in the field are of a snapshot in time. Field data are not representative of changes in vegetation, particularly post-fire, and do not directly capture changes that happened during the floods and debris flows. I am assuming that the changes, particularly at less resilient catchments where there were greater magnitudes of change, are representative of the characteristics of the catchment pre-event.

4.3 Geomorphic changes

Field data were collected during the summer of 2023 following the fire and floods at each study site. At the time of these analyses, there were repeat lidar-derived DEM data at Black Hollow, Sheep Creek, and Sheep Gulch capturing pre- and post-event surfaces. I differenced the DEMs to quantify the total sediment erosion in the catchment. The total sediment erosion within the active channel and floodplain at Black Hollow was 130,000 m^3, excluding values ranging from -0.25 to 0.25 m to account for error in the DEM alignment. The total deposition within the active river corridor was 29,000 m^3. The net erosion was 100,000 m^3., or 5780 m^3 per km^2 catchment area. The debris fan at the outlet of the catchment was 14,000 m^3 of deposition, or greater than 800 m^3 of sediment per km^2 of catchment area. These large values of sediment export support the assessment of lack of resilience for this catchment.

Geomorphic characteristics measured at the reach-scale in this study were all measured post-event. These measurements therefore reflect the resilience of the river corridor after the impacts of fire and flood have been absorbed or caused a shift to another state. Where data were available reflecting

the state of the river corridor prior to the fire, I performed a sensitivity analysis. At Little Beaver Creek, Ader et al. (2021) measured bankfull channel width and valley width at Little Beaver Creek overlapping with four of the reaches designated in this study at the lower end of the catchment (LBC 49, LBC 51, LBC 55, and LBC 56). The values from 2021 reflect average across the reaches ranging from 50 to 360 m in stream length. A paired t-test shows that the bankfull channel widths increased between 2018 and 2023 (Figure 28; $p = 0.002$). The valley-bottom widths and associated floodplain widths did not change between the years of this study.

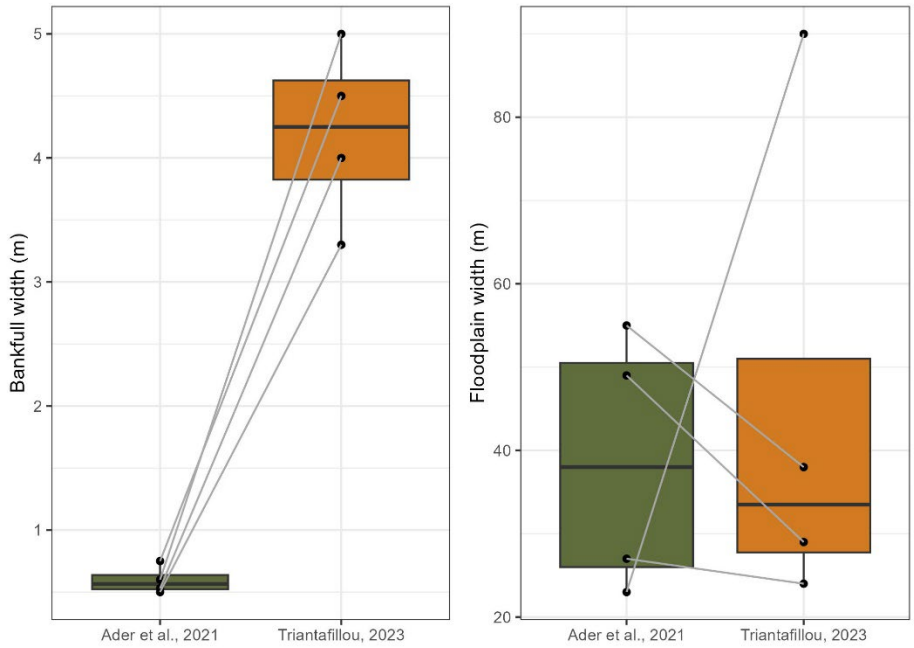

Figure 28: Bankfull channel and floodplain widths measured in the same reaches within Little Beaver Creek by Ader et al. (2021) compared to measurements in this study, post-fire and flood, in the summer of 2023. Measurements from Ader et al. (2021) represent average values over a reach defined for a separate study that are within reaches defined in this study. Bankfull channel widths changed (paired t-test, p =0.002), but floodplain widths did not change.

Data to assess pre-event channel and floodplain geometry at Black Hollow are available as a DEM from 2020. Rengers (2024) measured the pre- and post-event channel widths and valley width at 50 m intervals down the channel. These measurements exist where there is DEM coverage and overlap with some of the reaches defined in this study (BH_13 through BH_27). I averaged the pre- and post-

event measurements from the DEM over the reaches defined in this study to do a pairwise comparison. Comparing field-measured channel and floodplain widths at Black Hollow to pre-event channel and valley widths measured from a DEM, the channel widths measured using field and remote methods did not statistically differ despite the observed changes to form (Figure 29). This is likely due to the difference in methods to measure channel width but reflects how the field-measurements captured the identity of the system, not simply the post-disturbance form. The floodplain widths measured in the field were different than the valley widths measured using the pre-event DEM ($p = 0.03$). Because bankfull channel widths were measured based on evidence of the most recent peak snowmelt flow, the channel widths measured at Black Hollow in 2023 are likely representative of pre-event channel geometry. This is supported by the comparison of field measured data post-event and remotely measured data pre-event.

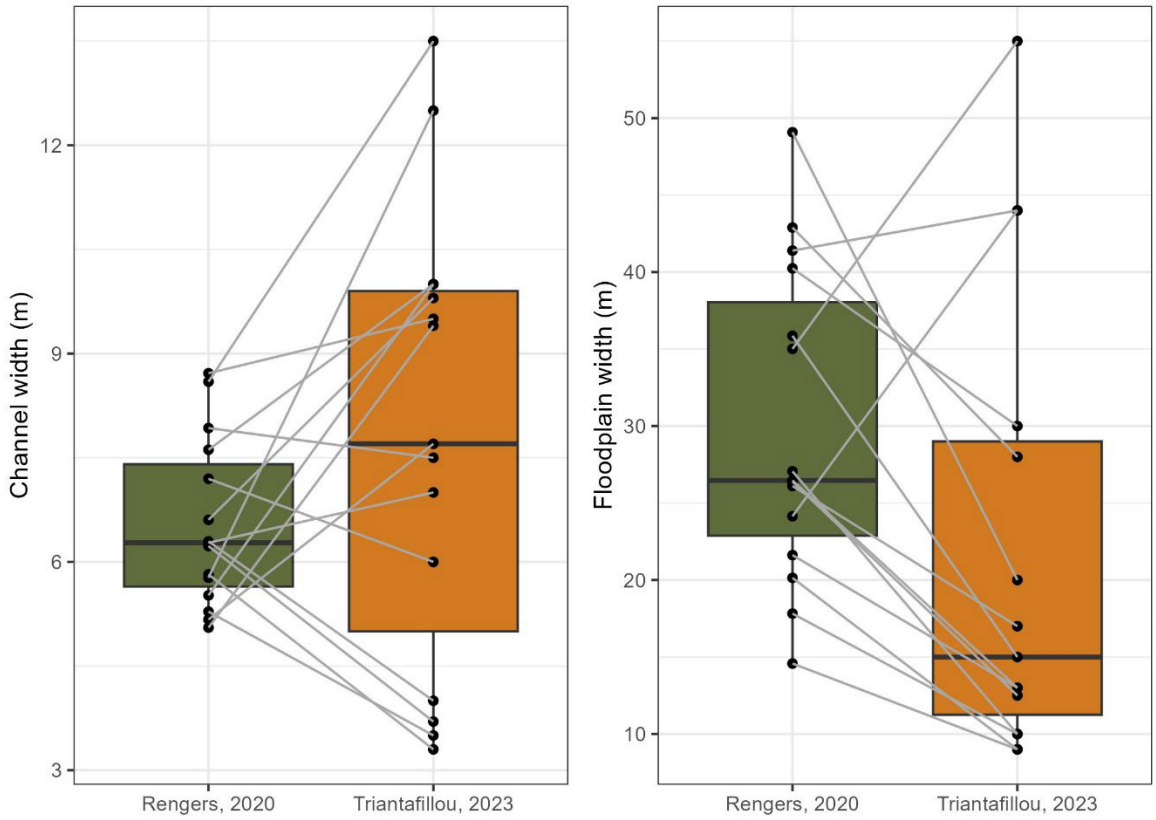

Figure 29: Channel and floodplain widths measured in the same reaches within Black Hollow by Rengers (2024) compared to measurements in this study, post-fire and flood, in the summer of 2023. Measurements from Rengers (2024) represent average values over a reach defined for a separate study that are within reaches defined in this study. a) Channel widths measured pre-flood (Rengers, 2020) did not statistically vary from the values measured in the field in 2023. b) Measurements made by Rengers (2024) from 2020 DEMs was of valley width, which was different than the floodplain width measured in the field in 2023 (paired t-test, p = 0.03).

Although the field-measured channel widths post-flood at Black Hollow do not differ from the pre-flood remote measurements, the geometry of the channel undoubtedly changed in the flood. The channel measurements made from DEMs pre- and post-event were statistically different (Figure 30; $p < 0.001$).

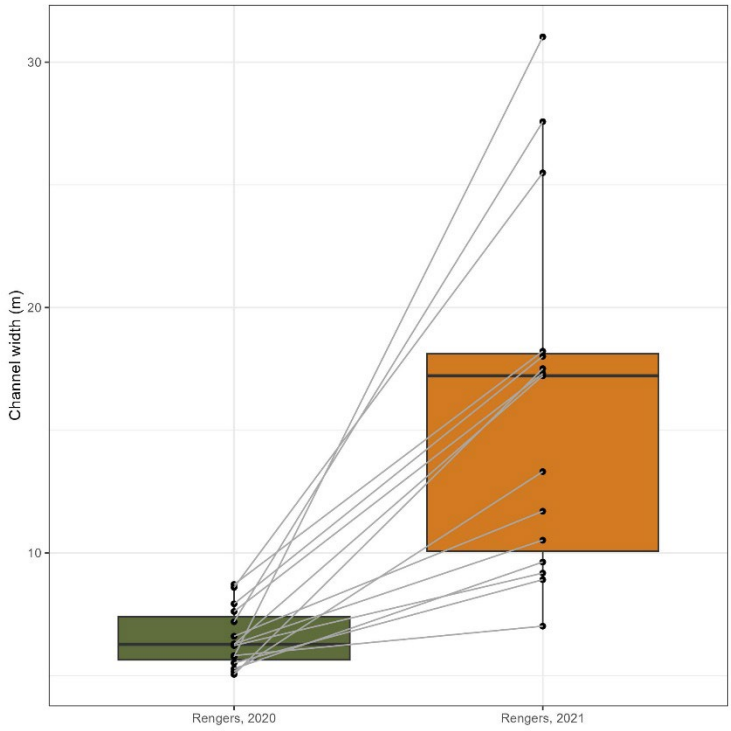

Figure 30: Average channel widths at Black Hollow measured by Rengers (2024) from DEMs from 2020 before the debris flow and 2021 after the debris flow. Measurements from Rengers (2024) represent values over a reach defined for a separate study that are averaged within reaches defined in this study. The channel widths differed between years (paired t-test, $p < 0.001$).

The assumption underpinning these observations is that the floods that caused geomorphic change at these sites activated the entire floodplain. Depending on the resilience of a site, the change in floodplain form may affect future floodplain function. At Black Hollow, the river incised to such a degree that even an event of the same magnitude would likely no longer activate the floodplain that I identified in the field. This will likely act as a terrace or very disconnected floodplain. Thus, the form and function of the river corridor has changed, and it is now in a different state. At Little Beaver Creek, a more resilient site, the floodplain identified in the field likely remains a functioning, connected floodplain in many reaches. Although the channel incised in some reaches and increased the stage at which the floodplain is inundated or prevented flood waters from accessing the floodplain at all, there are many reaches within the catchment that did not change in this way. This river corridor absorbed the impacts of the flood disturbance and maintained the same function. Although there was geomorphic change

within this river corridor, namely the channels widening, these changes did not fundamentally change the forms and processes that occur. For example, the multi-threaded reaches changed their primary flow path but remained multithreaded. The floodplains in some locations were reconfigured with the deposition of imbricated boulders and the formation of secondary floodplain channels, but their function in attenuating flows remained the same, perhaps enhanced by the heterogeneity elements (Figure 31).

Prior to the flood at Little Beaver Creek, nearly all the logjams were in the channel (Wohl, Marshall, Triantafillou, et al., 2024). The flood redistributed these logjams to the floodplain. Wohl et al. (2024) documented that the 91 channel-spanning jams that existed before the flood in the lower half of the catchment were redistributed, leaving only 42 after the flood. Within this part of the catchment, there were 700 floodplain logjams where there were very few before the flood. Many of these jams were pinned against standing trees in the floodplain and initiated secondary channel formation. Between the secondary channel formation and the transient inundation of the floodplain, these changes represent an increase in lateral connectivity.

Figure 31: Floodplain changes observed during the summer of 2023 at Little Beaver Creek following the flood in 2022. a) Imbricated boulders on a floodplain against standing trees. Flow direction of main channel is indicated with a white arrow. The red line is 0.5 m for scale. b) Secondary floodplain channel formation indicated by the yellow arrow. Flow direction of main channel is indicated with white arrows.

Spatial heterogeneity acts as a positive feedback that increases in response to disturbance. Studies have shown that spatial heterogeneity in the form of beaver-modified topography, sediment, and logjams create more heterogeneity in reaches with wide floodplains (Czuba & Foufoula-Georgiou, 2015; Wohl et al., 2022, 2024). In the context of these sites, beaver berms trap wood and create logjams. The logjams create backwaters that store water and sediment, promote overbank flow, and the formation of secondary channels. The wet floodplain promotes the growth of vegetation, which further increases spatial heterogeneity and the potential to trap wood and creates an environment that beaver are more likely to come back and maintain. In the context of logjams at Little Beaver Creek, the in-channel jams perpetuated spatial heterogeneity by forming floodplain jams. These floodplain jams created more spatial heterogeneity by creating secondary channels and will likely increase resilience by attenuating flows that access the floodplain. In Black Hollow, where the floodplains will likely not be accessed, the floodplain jams may still be enhancing resilience by attenuating flows from the unvegetated hillslopes. These cycles of self-enhancing heterogeneity illustrate how resilient systems undergo change to absorb the impacts of disturbance and reinforce the processes occurring to hold the system in a stable dynamic state.

4.4 Assumptions

All field-based analyses were measured post-event and are therefore reflecting the geomorphic response of the catchments in this study. The sensitivity analysis of geomorphic change indicates that even at the least resilient catchment, the field-measured bankfull channel widths are representative of pre-event geometry. At Little Beaver Creek, there is evidence to suggest that the channels did widen, but that the relative floodplain to channel width remains representative of the pre-event geometry. Because there are no data available pre-event at every study catchment, I am assuming that the sensitivity analyses performed at Black Hollow and Little Beaver Creek are representative of the pre- and post-event change at every site. These sensitivity analyses only capture the change in geomorphic

characteristics and do not reflect the change that likely occurred in vegetation communities within the river corridor, particularly at the less resilient catchments. At Black Hollow, so much incision and scour occurred that no evidence of pre-event vegetation remains. Aerial imagery shows that much of the channel and floodplain was not vegetated, but this is just a qualitative assessment of the entire river corridor.

There were sources of error due to spatial shifting of the pre- and post-event DEMs at Black Hollow. Based on an analysis of the elevation difference of the paved road, this error appears to be spatially discontinuous. Near the outlet of Black Hollow, the error is between -0.25 and 0.25 m. Calculations of total sediment volumes excluded pixels with values within this range to account for the error. Although the DEMs extend to include Sheep Creek and Sheep Gulch, the error near these catchments was greater, ranging from -0.50 to 0.50 on the paved road. Because of this, I did not include a quantification of sediment export from these catchments.

This study assumes that the time between fire and convective storm event had minimal impact on recovery. The difference between the first and second summer following the fire (2021 and 2022) likely had an impact on the resilience outcome of the catchments. Three catchments, Black Hollow, Sheep Creek, and Sheep Gulch were affected by a storm in 2021, the first summer following the fire, whereas the other four catchments were impacted by a large storm during the second summer following the fire. Time since the fire can be conceptualized as a characteristic that resists disturbance. This study also assumes that each catchment only experienced one geomorphic event in terms of storm and flood. This is well documented at Black Hollow and Little Beaver Creek, but there is less information available to confirm this assumption at the other catchments in the study.

4.5 Management implications

River restoration can increase the attenuation of flood pulses (Sholtes & Doyle, 2011). Post-fire management in the Poudre River catchment ranges from catchment-scale efforts like applying mulch, seeding hillslopes, and replanting trees to the reach-scale installation of in-channel structures. In-channel structures, commonly in the form of post-assisted log structures (PALS) or beaver dam analogues (BDAs), are typically placed in reaches where the channel is incised and disconnected from the floodplain. These installations are designed to allow flows to access the floodplain to slow down and deposit sediment. The results of this research support the use of reach-scale restoration as post-fire management. The resilient catchments in this study had more reaches with a capacity for attenuation, so reach-scale projects that focus on connecting the channel and floodplain where there is the potential to have a wide reach are likely an effective strategy. Sheep Gulch illustrated that the resilience outcome can be impacted by a small number of reaches with a capacity for attenuation, which further supports restoration efforts directed at the scale of individual reaches to address whole-catchment response to wildfire. Remote analysis can produce larger datasets that utilize the relationship between the floodplain to channel width ratio and resilience to identify reaches that should be prioritized to maximize attenuation.

5. CONCLUSIONS

The 2020 Cameron Peak fire initiated a cascade of disturbances resulting in floods and debris flows in river corridors. Post-fire precipitation events result in a much greater magnitude of response, evidenced as a disproportionate amount of flooding and erosion. The pulses of sediment and water that are transported throughout a burned landscape impact human life and property, water quality, and aquatic habitat. Wildfires and the associated cascade of impacts are becoming more frequent and severe due to decades of fire suppression and anthropogenic climate change (Williams et al., 2019). As the threat of wildfire grows, research and restoration in the context of resilience is more relevant than ever. Understanding the components of landscapes and river corridors that contribute to resilience to flood and debris flows after fire is necessary to manage and restore rivers most effectively.

In this study, I assessed the impacts of characteristics at the catchment and reach scales on the resilience response after wildfire. I ranked each of seven catchments on a scale of relative resilience based on the geomorphic evidence of sediment export. I used geospatial datasets to assess geomorphic, burn, vegetation, and precipitation characteristics associated with each catchment and the flood and debris flows that occurred. I assessed reach-scale characteristics by conducting longitudinal surveys of the river corridor and analyzing the population of characteristics for each catchment. Results indicate that resilience was most closely related to characteristics on the reach-scale that are associated with attenuation. Of the catchment characteristics assessed, greater resilience was associated with lower precipitation intensity. Greater resilience was associated with catchments made up of more reaches with wide floodplains, low channel gradient, multiple channels, beaver-modified topography, and multi-stem deciduous vegetation.

One catchment was ranked as more resilient compared to many other catchments, but it had high precipitation intensity and reach characteristics that aligned with the less resilient catchments. This

catchment had the steepest mean catchment slope and the highest precipitation intensity over the 24 hours that flooding occurred, but the outlet of the catchment showed no evidence of major sediment export. Although there was evidence of flooding and significant incision throughout much of the river corridor, a series of three wide reaches in the lower two-thirds of the catchment apparently attenuated the flood flows. These results suggest that resilient catchments may not need to have the capacity for attenuation evenly distributed throughout the river corridor. Additionally, multiple reaches with attenuation in succession may provide redundancy and attenuate flood flows even after they build up energy. Therefore, although many reaches with a capacity for attenuation create a resilient catchment, there are different configurations of reaches that make up river corridors with enhanced resilience.

5.1 Future research

There is a substantial body of research on debris flows, what triggers them, and thresholds for occurrence, but this project investigated the spectrum of responses to the wildfire disturbance cascade across catchments. There remains a gap in knowledge about how catchment-scale characteristics interact. Expanding on the current literature, this could be addressed by applying current knowledge of debris flows to a study focused on a spectrum of post-wildfire responses. This study ranked catchment resilience using field-based observations to infer the relative sediment export during post-fire precipitation events. These methods do not allow for the consideration of multiple precipitation events causing geomorphic change of different magnitudes. It also limited the sample size of catchments. Future research may use remote data to quantify total sediment export as a metric for resilience rather than using a qualitative, field-based ranking. Where there are available data, repeat lidar could be used to do this. Using these sediment export values and catchment-scale characteristics, this research could focus on building a descriptive multivariate regression model to further explore the role of multiple characteristics in combination in resilience outcomes. Assuming digital elevation data are available at sufficiently high spatial and temporal resolution, many of the reach-scale characteristics assessed in this

study could also be incorporated. Given a remote data set, this could be used to assess these relationships over a greater number of catchments and regions to understand the interactions between catchment-scale characteristics and how the relationship between fire and fluvial systems differs between regions.

Little Beaver Creek is an example of a catchment where reaches with wide floodplains distributed throughout the catchment were very effective at absorbing the impacts of disturbance. Sheep Gulch had very few reaches with wide floodplains, and they were in the lower third of the catchment. In this situation, these few reaches were effective in absorbing the impacts of the flood that was generated. Although this was true of the reach locations at Sheep Gulch, the Black Hollow event may have been too large to be absorbed at this point in the catchment. Although Sheep Gulch had similar trends of flood and debris flow bulking up downstream, Black Hollow had a much greater magnitude of event that started higher in the catchment based on qualitative assessment in the field. There was at least one location where it appears that a channel-spanning jam temporarily dammed the water and sediment during the event at Black Hollow. Evidence of this dam remains on the floodplain as logjams pinned against standing trees on both sides of the channel. It looks like this dam burst and released the water and sediment behind it in a large pulse. The evidence of this is scour throughout a steep reach downstream from this dam. Although there was no single location where the event at Black Hollow initiated, this location was one example of where the magnitude of the event became dramatically greater (F. K. Rengers, personal communication, 2023). By the time the debris flow reached the lower two thirds of the catchment, it is likely that the impacts of the flood were too large to be attenuated by only a small number of wide reaches like Sheep Gulch. These sites illustrate the need for more research to understand the factors at play on multiple scales that determine the most effective distribution of reaches with a capacity for attenuation. This question may be best addressed using

hydraulic modeling where similar scenarios can be modeled while controlling changes in the catchment and reach-scale characteristics.

Lastly, monitoring post-fire restoration strategies in collaboration with land managers would expand knowledge of attenuation on the reach-scale. Understanding capacity for individual reaches to attenuate fluxes while maintaining the same form and function and the thresholds of event magnitude that changes the system state would contribute to the growing body of research on resilience under different conditions.

REFERENCES

Ader, E., Wohl, E., McFadden, S., & Singha, K. (2021). *Logjams as a driver of transient storage in a mountain stream*. https://onlinelibrary.wiley.com/doi/full/10.1002/esp.5057

Agee, J. K. (1973). *Prescribed fire effects on physical and hydrologic properties of mixed-conifer forest floor and soil* (Contribution Report 143; p. 57). University of California Resources Center.

Bagnold, R. A. (1966). *An approach to the sediment transport problem from general physics* (Professional Paper 422). U.S. Geological Survey.

Battige, K. (2022). *Fish Survey and Management Information*. Colorado Parks and Wildlife.

Benavides-Solorio, J., & MacDonald, L. H. (2001). Post-fire runoff and erosion from simulated rainfall on small plots, Colorado Front Range. *Hydrological Processes*, *15*(15), 2931–2952. https://doi.org/10.1002/hyp.383

Benson, M. H., & Garmestani, A. S. (2011). Can We Manage for Resilience? The Integration of Resilience Thinking into Natural Resource Management in the United States. *Environmental Management*, *48*(3), 392–399. https://doi.org/10.1007/s00267-011-9693-5

Birkeland, P. W., Shroba, R. R., Burns, S. F., Price, A. B., & Tonkin, P. J. (2003). Integrating soils and geomorphology in mountains—An example from the Front Range of Colorado. *Geomorphology*, *55*(1–4), 329–344. https://doi.org/10.1016/S0169-555X(03)00148-X

Bladon, K. D., Emelko, M. B., Silins, U., & Stone, M. (2014). Wildfire and the Future of Water Supply. *Environmental Science & Technology*, *48*(16), Article 16. https://doi.org/10.1021/es500130g

Blodgett, D., & Johnson, M. (2023). *nhdplusTools: Tools for Accessing and Working with the NHDPlus* (0.6.2) [Computer software]. U.S. Geological Survey. https://doi.org/10.5066/P97AS8JD

Blount, K., Ruybal, C. J., Franz, K. J., & Hogue, T. S. (2020). Increased water yield and altered water partitioning follow wildfire in a forested catchment in the western United States. *Ecohydrology*, *13*(1), Article 1. https://doi.org/10.1002/eco.2170

Boodoo, S., Hudak, D., Ryzhkov, A., Zhang, P., Donaldson, N., Sills, D., & Reid, J. (2015). Quantitative Precipitation Estimation from a C-Band Dual-Polarized Radar for the 8 July 2013 Flood in Toronto, Canada. *Journal of Hydrometeorology*, *16*(5), 2027–2044. https://doi.org/10.1175/JHM-D-15-0003.1

Boulton, A. J. (2007). Hyporheic rehabilitation in rivers: Restoring vertical connectivity. *Freshwater Biology*, *52*(4), 632–650. https://doi.org/10.1111/j.1365-2427.2006.01710.x

Bowman, D. M. J. S., Balch, J. K., Artaxo, P., Bond, W. J., Carlson, J. M., Cochrane, M. A., D'Antonio, C. M., DeFries, R. S., Doyle, J. C., Harrison, S. P., Johnston, F. H., Keeley, J. E., Krawchuk, M. A., Kull, C.

A., Marston, J. B., Moritz, M. A., Prentice, I. C., Roos, C. I., Scott, A. C., Pyne, S. J. (2009). Fire in the Earth System. *Science*, *324*(5926), Article 5926. https://doi.org/10.1126/science.1163886

Bozek, M. A., & Young, M. K. (1994). Fish Mortality Resulting from Delayed Effects of Fire in the Greater Yellowstone Ecosystem. *Great Basin Naturalist*, *54*.

Brierley, G. J., Fryirs, K. A., Boulton, A., & Cullum, C. (2008). Working with change: The importance of evolutionary perspectives in framing the trajectory of river adjustment. In G. Brierley & K. A. Fryirs, *River Futures: An Integrative Scientific Approach to River Repair* (pp. 65–84). Island Press.

Brown, P. M., & Shepperd, W. D. (2001). Fire history and fire climatology along a 5 degree gradient in latitude in Colorado and Wyoming, USA. *Paleobotanist*, *50*(1), 133–140.

Brown, P. M., & Wu, R. (2005). Climate and disturbance forcing of episodic tree recruitment in a southwestern ponderosa pine landscape. *Ecology*, *86*(11), 3030–3038. https://doi.org/10.1890/05-0034

Burchsted, D., Daniels, M., Thorson, R., & Vokoun, J. (2010). The River Discontinuum: Applying Beaver Modifications to Baseline Conditions for Restoration of Forested Headwaters. *BioScience*, *60*(11), 908–922. https://doi.org/10.1525/bio.2010.60.11.7

Cannon, S. H. (2001). Debris-flow generation from recently burned watersheds. *Environmental and Engineering Geoscience*, *7*(4), 321–341. https://doi.org/10.2113/gseegeosci.7.4.321

Cannon, S. H., & Gartner, J. E. (2005). Wildfire-related debris fow from a hazards perspective. In *Chapter 15 in: Jakob, M. and Hungr, O. eds., Debris flow hazards and related phenomena* (pp. 363–385). Praxis, Springer, Berlin, Heidelberg.

Cannon, S. H., Gartner, J. E., Rupert, M. G., & Michael, J. A. (2004). *Emergency assessment of debris-flow hazards from basins burned by the Cedar and Paradise Fires of 2003, southern California* (Open-File Report) [Open-File Report 2004-1011]. U.S. Geological Survey.

Cannon, S. H., Gartner, J. E., Wilson, R. C., Bowers, J. C., & Laber, J. L. (2008). Storm rainfall conditions for floods and debris flows from recently burned areas in southwestern Colorado and southern California. *Geomorphology*, *96*(3–4), 250–269. https://doi.org/10.1016/j.geomorph.2007.03.019

Cannon, S. H., & Reneau, S. L. (2000). Conditions for generation of fire-related debris flows, Capulin Canyon, New Mexico. *Earth Surface Processes and Landforms*, *25*(10), 1103–1121. https://doi.org/10.1002/1096-9837(200009)25:10<1103::AID-ESP120>3.0.CO;2-H

Cenderelli, D. A., & Wohl, E. E. (2003). Flow hydraulics and geomorphic effects of glacial-lake outburst floods in the Mount Everest region, Nepal. *Earth Surface Processes and Landforms*, *28*(4), 385–407. https://doi.org/10.1002/esp.448

Chapman, S. S., Griffith, G. E., Omernik, J. M., Price, A. B., Freeof, J., & Schrupp, D. L. (2006). *Ecoregions of Colorado: U.S. Geological Survey Level IV Ecoregions 2 sided color poster with map, descriptive text, summary tables, and photographs*. http://www.ecologicalregions.info/data/co/co_front.pdf

Choné, G., & Biron, P. M. (2016). Assessing the Relationship Between River Mobility and Habitat: RELATIONSHIP BETWEEN MOBILITY AND HABITAT. *River Research and Applications*, *32*(4), 528–539. https://doi.org/10.1002/rra.2896

Collins, B. D., Montgomery, D. R., Fetherston, K. L., & Abbe, T. B. (2012). The floodplain large-wood cycle hypothesis: A mechanism for the physical and biotic structuring of temperate forested alluvial valleys in the North Pacific coastal ecoregion. *Geomorphology*, *139–140*, 460–470. https://doi.org/10.1016/j.geomorph.2011.11.011

Colorado State Forest Service. (2024). *Colorado's Forests in a Changing Climate*. Colorado State University. https://csfs.colostate.edu/colorados-forests-changing-climate/

Coombs, J. S., & Melack, J. M. (2013). Initial impacts of a wildfire on hydrology and suspended sediment and nutrient export in California chaparral watersheds. *Hydrological Processes*, *27*(26), 3842–3851. https://doi.org/10.1002/hyp.9508

Cooper, S. D., Klose, K., Herbst, D. B., White, J., Drenner, S. M., & Eliason, E. J. (2021). Wildfire and drying legacies and stream invertebrate assemblages. *Freshwater Science*, *40*(4), 659–680. https://doi.org/10.1086/717416

Cooper, S. D., Page, H. M., Wiseman, S. W., Klose, K., Bennett, D., Even, T., Sadro, S., Nelson, C. E., & Dudley, T. L. (2015). Physicochemical and biological responses of streams to wildfire severity in riparian zones. *Freshwater Biology*, *60*(12), 2600–2619. https://doi.org/10.1111/fwb.12523

Czuba, J. A., & Foufoula-Georgiou, E. (2015). Dynamic connectivity in a fluvial network for identifying hotspots of geomorphic change. *Water Resources Research*, *51*(3), 1401–1421. https://doi.org/10.1002/2014WR016139

Daly, C., Halbleib, M., Smith, J. I., Gibson, W. P., Doggett, M. K., Taylor, G. H., Curtis, J., & Pasteris, P. P. (2008). Physiographically sensitive mapping of climatological temperature and precipitation across the conterminous United States. *International Journal of Climatology*, *28*(15), 2031–2064. https://doi.org/10.1002/joc.1688

Daly, C., Neilson, R. P., & Phillips, D. L. (1994). A Statistical-Topographic Model for Mapping Climatological Precipitation over Mountainous Terrain. *Journal of Applied Meteorology*, *33*(2), 140–158. https://doi.org/10.1175/1520-0450(1994)033<0140:ASTMFM>2.0.CO;2

David, G. C. L., Bledsoe, B. P., Merritt, D. M., & Wohl, E. (2009). The impacts of ski slope development on stream channel morphology in the White River National Forest, Colorado, USA. *Geomorphology*, *103*(3), 375–388. https://doi.org/10.1016/j.geomorph.2008.07.003

Davis, W. M. (1898). The grading of mountain slope. *Science*, *7*(81).

De Girolamo, A. M., Cerdan, O., Grangeon, T., Ricci, G. F., Vandromme, R., & Lo Porto, A. (2022). Modelling effects of forest fire and post-fire management in a catchment prone to erosion: Impacts on sediment yield. *CATENA*, *212*, 106080. https://doi.org/10.1016/j.catena.2022.106080

DeBano, L. F. (2000). The role of fire and soil heating on water repellency in wildland environments: A review. *Journal of Hydrology*, *231–232*, 195–206. https://doi.org/10.1016/S0022-1694(00)00194-3

Dennison, P. E., Brewer, S. C., Arnold, J. D., & Moritz, M. A. (2014). Large wildfire trends in the western United States, 1984–2011. *Geophysical Research Letters*, *41*(8), Article 8. https://doi.org/10.1002/2014GL059576

Dethier, D. P., Ouimet, W. B., Murphy, S. F., Kotikian, M., Wicherski, W., & Samuels, R. M. (2018). Anthropocene Landscape Change and the Legacy of Nineteenth- and Twentieth-Century Mining in the Fourmile Catchment, Colorado Front Range. *Annals of the American Association of Geographers*, *108*(4), 917–937. https://doi.org/10.1080/24694452.2017.1406329

Doesken, N., Pielke, R. A., Sr., & Bliss, O. A. P. (2003). *Climatography of the United States No. 60: Colorado Climate Center*. Colorado Climate Center. https://climate.colostate.edu/climate_long.html

Donnegan, J. A., Veblen, T. T., & Sibold, J. S. (2001). Climatic and human influences on fire history in Pike National Forest, central Colorado. *Canadian Journal of Forest Research*, *31*(9), 1526–1539. https://doi.org/10.1139/x01-093

Downes, B. J., & Hindell, J. S. (2000). What's in a site? Variation in lotic macroinvertebrate density and diversity in a spatially replicated experiment. *Austral Ecology*, *25*(2), 128–139. https://doi.org/10.1046/j.1442-9993.2000.01019.x

Downing, J. (2012). Global abundance and size distribution of streams and rivers. *Inland Waters*, *2*(4), 229–236. https://doi.org/10.5268/IW-2.4.502

Dunn, O. J. (1964). *Multiple comparisons using rank sums*. Technometrics 6, 241–252.

Dunn, S. B. (2023). *Dammed Ponds! A Study of Post-Fire Sediment and Carbon Dynamics in Beaver Ponds and Their Contributions to Watershed Resilience* [M.S.]. Colorado State University.

Dunne, T., & Leopold, L. B. (1978). *Water in Environmental Planning*. W.H. Freeman and Company.

Duvall, A., Kirby, E., & Burbank, D. (2004). Tectonic and lithologic controls on bedrock channel profiles and processes in coastal California. *Journal of Geophysical Research: Earth Surface*, *109*(F3), 2003JF000086. https://doi.org/10.1029/2003JF000086

Ehlen, J., & Wohl, E. (2002). Joints and landform evolution in bedrock canyons. *Trans Jpn Geomorphol Union*, *23:237-255*.

Elliott, A. H., & Brooks, N. H. (1997). Transfer of nonsorbing solutes to a streambed with bed forms: Laboratory experiments. *Water Resources Research*, *33*(1), 137–151. https://doi.org/10.1029/96WR02783

Emelko, M. B., Stone, M., Silins, U., Allin, D., Collins, A. L., Williams, C. H. S., Martens, A. M., & Bladon, K. D. (2016). Sediment-phosphorus dynamics can shift aquatic ecology and cause downstream

legacy effects after wildfire in large river systems. *Global Change Biology*, *22*(3), 1168–1184. https://doi.org/10.1111/gcb.13073

Entwistle, N., Heritage, G., & Milan, D. (2018). Flood energy dissipation in anabranching channels: Flood energy dissipation in anabranching channels. *River Research and Applications*, *34*(7), 709–720. https://doi.org/10.1002/rra.3299

ESRI. (2023). *ArcGIS Pro* (3.1.2) [Computer software].

Fairfax, E., & Small, E. E. (2018). Using remote sensing to assess the impact of beaver damming on riparian evapotranspiration in an arid landscape. *Ecohydrology*, *11*(7), e1993. https://doi.org/10.1002/eco.1993

Fairfax, E., & Whittle, A. (2020). Smokey the Beaver: Beaver-dammed riparian corridors stay green during wildfire throughout the western United States. *Ecological Applications*.

Fox, J., & Weisberg, S. (2019). *An R Companion to Applied Regression* (Version 3) [R]. https://socialsciences.mcmaster.ca/jfox/Books/Companion/

Frings, R. M. (2008). Downstream fining in large sand-bed rivers. *Earth-Science Reviews*, *87*(1–2), 39–60. https://doi.org/10.1016/j.earscirev.2007.10.001

Fryirs, K. A., Brierley, G. J., & Erskine, W. D. (2012). Use of ergodic reasoning to reconstruct the historical range of variability and evolutionary trajectory of rivers. *Earth Surface Processes and Landforms*, *37*(7), 763–773. https://doi.org/10.1002/esp.3210

Fryirs, K. A., Brierley, G. J., Preston, N. J., & Kasai, M. (2007). Buffers, barriers and blankets: The (dis)connectivity of catchment-scale sediment cascades. *CATENA*, *70*(1), 49–67. https://doi.org/10.1016/j.catena.2006.07.007

Fuller, I. C., Gilvear, D. J., Thoms, M. C., & Death, R. G. (2019). Framing resilience for river geomorphology: Reinventing the wheel?: Framing resilience for river geomorphology. *River Research and Applications*, *35*(2), 91–106. https://doi.org/10.1002/rra.3384

Gannon, B. M., Wei, Y., Thompson, M. P., Scott, J. H., & Short, K. C. (2021). System Analysis of Wildfire-Water Supply Risk in Colorado, USA with Monte Carlo Wildfire and Rainfall Simulation. *Risk Analysis*, *n/a*(n/a), Article n/a. https://doi.org/10.1111/risa.13762

Gartner, J. E., Cannon, S. H., Bigio, E. R., Davis, N. K., McDonald, C., Pierce, K. L., & Rupert, M. G. (2005). *Compilation of data relating to the erosive response of 608 recently-burned basins in the western United States* (Open-File Report) [Open-File Report 2005-1218]. U.S. Geological Survey.

Gartner, M. H., Veblen, T. T., Sherriff, R. L., & Schoennagel, T. L. (2012). Proximity to grasslands influences fire frequency and sensitivity to climate variability in ponderosa pine forests of the Colorado Front Range. *International Journal of Wildland Fire*, *21*(5), 562. https://doi.org/10.1071/WF10103

Goldblum, D., & Veblen, T. T. (1992). Fire history of a ponderosa pine/douglas fir forest in the colorado front range. *Physical Geography*, *13*(2), 133–148. https://doi.org/10.1080/02723646.1992.10642449

Graber, A. P., Thomas, M. A., & Kean, J. W. (2023). How Long Do Runoff-Generated Debris-Flow Hazards Persist After Wildfire? *Geophysical Research Letters*, *50*(19), e2023GL105101. https://doi.org/10.1029/2023GL105101

Graham, R. T. (2003). *Hayman Fire Case Study* (RMRS-GTR-114; p. RMRS-GTR-114). U.S. Department of Agriculture, Forest Service, Rocky Mountain Research Station. https://doi.org/10.2737/RMRS-GTR-114

Green, G. N. (1992). *The digital geologic map of Colorado in ARC/INFO format* (92-507-D-O; Open-File Report). U.S. Geological Survey.

Gresswell, R. E. (1999). Fire and Aquatic Ecosystems in Forested Biomes of North America. *Transactions of the American Fisheries Society*, *128*(2), 193–221. https://doi.org/10.1577/1548-8659(1999)128<0193:FAAEIF>2.0.CO;2

Grimm, M. M., Wohl, E. E., & Jarrett, R. D. (1995). Coarse-sediment distribution as evidence of an elevation limit for flash flooding, Bear Creek, Colorado. *Geomorphology*, *14*(3), 199–210. https://doi.org/10.1016/0169-555X(95)00037-6

Gurnell, A. (2014). Plants as river system engineers. *Earth Surface Processes and Landforms*, *39*(1), 4–25. https://doi.org/10.1002/esp.3397

Gurnell, A. M., Piégay, H., Swanson, F. J., & Gregory, S. V. (2002). Large wood and fluvial processes. *Freshwater Biology*, *47*(4), 601–619. https://doi.org/10.1046/j.1365-2427.2002.00916.x

Hansen, W. R., Chronic, J., & Matelock, J. (1978). Climatography of the front range urban corridor and vicinity, colorado. *Geological Survey Professional Paper 1019*, *1019*.

Harrison, H. N., Hammond, J. C., Kampf, S., & Kiewiet, L. (2021). On the hydrological difference between catchments above and below the intermittent-persistent snow transition. *Hydrological Processes*, *35*(11), e14411. https://doi.org/10.1002/hyp.14411

Harvey, A. M. (1984). Geomorphological response to an extreme flood: A case from southeast Spain. *Earth Surface Processes and Landforms*, *9*(3), 267–279. https://doi.org/10.1002/esp.3290090306

Hauer, F. R., Locke, H., Dreitz, V. J., Hebblewhite, M., Lowe, W. H., Muhlfeld, C. C., Nelson, C. R., Proctor, M. F., & Rood, S. B. (2016). Gravel-bed river floodplains are the ecological nexus of glaciated mountain landscapes. *Science Advances*, *2*(6), e1600026. https://doi.org/10.1126/sciadv.1600026

Hernangómez, D. (2023). Using the {tidyverse} with {terra} objects: The {tidyterra} package. *Journal of Open Source Software*, *8*, 5751. https://doi.org/10.21105/joss.05751

Higuera, P. E., Cook, M. C., Balch, J. K., Stavros, E. N., Mahood, A. L., & St. Denis, L. A. (2023). Shifting social-ecological fire regimes explain increasing structure loss from Western wildfires. *PNAS Nexus*, *2*(3), pgad005. https://doi.org/10.1093/pnasnexus/pgad005

Hijmans, R. J. (2023). *terra: Spatial Data Analysis* (1.7-39) [Computer software]. https://CRAN.R-project.org/package=terra

Hislop, S., Jones, S., Soto-Berelov, M., Skidmore, A., Haywood, A., & Nguyen, T. (2018). Using Landsat Spectral Indices in Time-Series to Assess Wildfire Disturbance and Recovery. *Remote Sensing*, *10*(3), 460. https://doi.org/10.3390/rs10030460

Hohner, A. K., Cawley, K., Oropeza, J., Summers, R. S., & Rosario-Ortiz, F. L. (2016). Drinking water treatment response following a Colorado wildfire. *Water Research*, *105*, 187–198. https://doi.org/10.1016/j.watres.2016.08.034

Holling, C. S. (1973). Resilience and Stability of Ecological Systems. *Annual Review of Ecology and Systematics*, 1–23.

Hood, G. A., & Bayley, S. E. (2008). Beaver (Castor canadensis) mitigate the effects of climate on the area of open water in boreal wetlands in western Canada. *Biological Conservation*, *141*(2), 556–567. https://doi.org/10.1016/j.biocon.2007.12.003

Hoover, T. M., Richardson, J. S., & Yonemitsu, N. (2006). Flow-substrate interactions create and mediate leaf litter resource patches in streams. *Freshwater Biology*, *51*(3), 435–447. https://doi.org/10.1111/j.1365-2427.2005.01499.x

Horton, J. D. (2017). *The State Geologic Map Compilation (SGMC) Geodatabase of the Conterminous United States* [dataset]. https://doi.org/10.5066/F7WH2N65

Horton, R. E. (1932). Drainage-basin characteristics. *Eos, Transactions American Geophysical Union*, *13*(1), 350–361. https://doi.org/10.1029/TR013i001p00350

Hurd, L. E., Sousa, R. G. C., Siqueira-Souza, F. K., Cooper, G. J., Kahn, J. R., & Freitas, C. E. C. (2016). Amazon floodplain fish communities: Habitat connectivity and conservation in a rapidly deteriorating environment. *Biological Conservation*, *195*, 118–127. https://doi.org/10.1016/j.biocon.2016.01.005

Hynes, H. B. N. (1975). The stream and its valley. *Verb. Internat. Verein. Limnol.*, *19*, 1–15.

Jarrett, R. D. (1990). Paleohydrologic techniques used to define the spatial occurrence of floods. *Geomorphology*, *3*(2), 181–195. https://doi.org/10.1016/0169-555X(90)90044-Q

Jarrett, R. D. (1993). *Flood elevation limits in the rocky mountains*. American Society of Civil Engineers.

Johnson, N. (2021). *Cameron Peak Fire*. Colorado Encyclopedia. https://coloradoencyclopedia.org/article/cameron-peak-fire

Jonas, J. L., Berryman, E., Wolk, B., Morgan, P., & Robichaud, P. R. (2019). Post-fire wood mulch for reducing erosion potential increases tree seedlings with few impacts on understory plants and

soil nitrogen. *Forest Ecology and Management*, *453*, 117567. https://doi.org/10.1016/j.foreco.2019.117567

Jones, J. B., & Smock, L. A. (1991). Transport and Retention of Particulate Organic Matter in Two Low-Gradient Headwater Streams. *Journal of the North American Benthological Society*, *10*(2), 115–126. https://doi.org/10.2307/1467572

Junk, W., Bayley, P., & Sparks, R. (1989). The Flood Pulse Concept in River-Floodplain Systems. In *Can. Spec. Public Fish. Aquat. Sci.* (Vol. 106).

Kassambara, A. (2023). *ggcorrplot: Visualization of a Correlation Matrix using "ggplot2"* (01.4.1) [R]. https://CRAN.R-project.org/package=ggcorrplot

Keeley, J. E. (2009). Fire intensity, fire severity and burn severity: A brief review and suggested usage. *International Journal of Wildland Fire*, *18*(1), 116. https://doi.org/10.1071/WF07049

Knighton, A. D. (1999). Downstream variation in stream power. *Geomorphology*, *29*(3–4), 293–306. https://doi.org/10.1016/S0169-555X(99)00015-X

Kostelnik, J., Schmitt, R. G., Rengers, F. K., & Kean, J. W. (2022). *Cameron Peak Fire: Flooding and Debris Flows* [Story Map]. https://landslides.usgs.gov/storymap/cameronpeak/

Krebs, P., Pezzatti, G. B., Mazzoleni, S., Talbot, L. M., & Conedera, M. (2010). Fire regime: History and definition of a key concept in disturbance ecology. *Theory in Biosciences*, *129*(1), 53–69. https://doi.org/10.1007/s12064-010-0082-z

Larsen, I. J., MacDonald, L. H., Brown, E., Rough, D., Welsh, M. J., Pietraszek, J. H., Libohova, Z., Dios Benavides-Solorio, J., & Schaffrath, K. (2009). Causes of Post-Fire Runoff and Erosion: Water Repellency, Cover, or Soil Sealing? *Soil Science Society of America Journal*, *73*(4), 1393–1407. https://doi.org/10.2136/sssaj2007.0432

Lenth, R. V. (2023). *emmeans: Estimated Marginal Means, aka Least-Squares Means* (1.8.8) [R]. https://CRAN.R-project.org/package=emmeans

Lininger, K. B., & Latrubesse, E. M. (2016). Flooding hydrology and peak discharge attenuation along the middle Araguaia River in central Brazil. *CATENA*, *143*, 90–101. https://doi.org/10.1016/j.catena.2016.03.043

Livers, B., & Wohl, E. (2016). Sources and interpretation of channel complexity in forested subalpine streams of the Southern Rocky Mountains. *Water Resources Research*, *52*(5), 3910–3929. https://doi.org/10.1002/2015WR018306

Livers, B., Wohl, E., Jackson, K. J., & Sutfin, N. A. (2018). Historical land use as a driver of alternative states for stream form and function in forested mountain watersheds of the Southern Rocky Mountains. *Earth Surface Processes and Landforms*, *43*(3), 669–684. https://doi.org/10.1002/esp.4275

Lundquist, J., Hughes, M., Gutmann, E., & Kapnick, S. (2019). Our Skill in Modeling Mountain Rain and Snow is Bypassing the Skill of Our Observational Networks. *Bulletin of the American Meteorological Society*, *100*(12), 2473–2490. https://doi.org/10.1175/BAMS-D-19-0001.1

Madole, R. F., VanSistine, D. P., & Michael, J. A. (1998). *Pleistocene glaciation in the upper Platte River drainage basin, Colorado: IMAP*. https://doi.org/10.3133/i2644

Maiolo-Heath, M. (2021). *Aerial Mulching Operations to Resume in Cameron Peak Burn Area*. https://www.fcgov.com/utilities/news/view/8059

Malone, D., Rondeau, R., & Decker, K. (2019). *Rocky Mountain Subalpine-Montane Riparian Shrubland: Colorado Natural Heritage Program*. https://cnhp.colostate.edu/projects/ecological-systems-ofcolorado/

Marcus, W. A., Marston, R. A., Colvard, C. R., & Gray, R. D. (2002). Mapping the spatial and temporal distributions of woody debris in streams of the Greater Yellowstone Ecosystem, USA. *Geomorphology*, *44*(3–4), 323–335. https://doi.org/10.1016/S0169-555X(01)00181-7

Marshall, A., Iskin, E., & Wohl, E. (2021). Seasonal and diurnal fluctuations of coarse particulate organic matter transport in a snowmelt-dominated stream. *River Research and Applications*, *37*(6), 815–825. https://doi.org/10.1002/rra.3802

Martin, D. A., & Moody, J. A. (2001). Comparison of soil infiltration rates in burned and unburned mountainous watersheds. *Hydrological Processes*, *15*(15), Article 15. https://doi.org/10.1002/hyp.380

Mast, M. A., & Clow, D. W. (2008). Effects of 2003 wildfires on stream chemistry in Glacier National Park, Montana. *Hydrological Processes*, *22*(26), 5013–5023. https://doi.org/10.1002/hyp.7121

McDaniel, J. (2021, December). Forests, Fire, and Faucets: What We Are Learning About Lingering Water Quality Effects of High-Severity Wildfires. *Rocky Mountain Research Station: Science You Can Use Bulletin*, *51*, Article 51.

McInerney, P. J., Stoffels, R. J., Shackleton, M. E., & Davey, C. D. (2017). Flooding drives a macroinvertebrate biomass boom in ephemeral floodplain wetlands. *Freshwater Science*, *36*(4), 726–738. https://doi.org/10.1086/694905

McKinney, S. T. (2019). Systematic review and meta-analysis of fire regime research in ponderosa pine (Pinus ponderosa) ecosystems, Colorado, USA. *Fire Ecology*, *15*(1), 38. https://doi.org/10.1186/s42408-019-0056-6

Menitove, A. (1999). *Wildfire-related debris-flow susceptibility in the Santa Monica mountains, Los Angeles and Ventura Counties, California* [M.S.]. Department of Geology and Geological Engineering,Colorado School of Mines.

Meyer, G. A., & Wells, S. G. (1997). Fire-Related Sedimentation Events on Alluvial Fans, Yellowstone National Park, U.S.A. *SEPM Journal of Sedimentary Research*, *Vol. 67*. https://doi.org/10.1306/D426863A-2B26-11D7-8648000102C1865D

Minckley, T. A., Shriver, R. K., & Shuman, B. (2012). Resilience and regime change in a southern Rocky Mountain ecosystem during the past 17 000 years. *Ecological Monographs*, *82*(1), 49–68. https://doi.org/10.1890/11-0283.1

Minshall, G. W., Brock, J. T., & Varley, J. D. (1989). Wildfires and Yellowstone's Stream Ecosystems. *Bioscience*, *39*(10), Article 10. http://dx.doi.org/10.2307/1311002

Montgomery, D. R., & Buffington, J. M. (1997). Channel-reach morphology in mountain drainage basins. *Geological Society of America Bulletin*, *109*(5), 596–611. https://doi.org/10.1130/0016-7606(1997)109<0596:CRMIMD>2.3.CO;2

Montgomery, D. R., & Dietrich, W. E. (1989). Source areas, drainage density, and channel initiation. *Water Resources Research*, *25*(8), 1907–1918. https://doi.org/10.1029/WR025i008p01907

Moody, J. A. (2001). Sediment transport regimes after a wildfire in steep mountainous terrain. *Proceedings of the Seventh Federal Interagency Sedimentation Conference, Reno, NV*, X41–X48. http://pubs.usgs.gov/misc/FISC_1947-2006/pdf/1st-7thFISCs-CD/7thFISC/7Fisc-V2/7FSC2-10.pdf#page=43

Moody, J. A., & Martin, D. A. (2001a). Initial hydrologic and geomorphic response following a wildfire in the Colorado Front Range. *Earth Surface Processes and Landforms*, *26*(10), Article 10. https://doi.org/10.1002/esp.253

Moody, J. A., & Martin, D. A. (2001b). Initial hydrologic and geomorphic response following a wildfire in the Colorado Front Range. *Earth Surface Processes and Landforms*, *26*(10), 1049–1070. https://doi.org/10.1002/esp.253

Moody, J. A., Shakesby, R. A., Robichaud, P. R., Cannon, S. H., & Martin, D. A. (2013). Current research issues related to post-wildfire runoff and erosion processes. *Earth-Science Reviews*, *122*, 10–37. https://doi.org/10.1016/j.earscirev.2013.03.004

Naiman, R. J., Bechtold, J. S., Drake, D. C., Latterell, J. J., O'Keefe, T. C., & Balian, E. V. (2005). Origins, Patterns, and Importance of Heterogeneity in Riparian Systems. In G. M. Lovett, M. G. Turner, C. G. Jones, & K. C. Weathers (Eds.), *Ecosystem Function in Heterogeneous Landscapes* (pp. 279–309). Springer New York. https://doi.org/10.1007/0-387-24091-8_14

National Interagency Fire Center. (2022). *Inter Agency Fire Perimeter History*. https://data-nifc.opendata.arcgis.com/datasets/e02b85c0ea784ce7bd8add7ae3d293d0_0/explore

Neary, D. G., Klopatek, C. C., DeBano, L. F., & Ffolliott, P. F. (1999). Fire effects on belowground sustainability: A review and synthesis. *Forest Ecology and Management*, *122*(1–2), 51–71. https://doi.org/10.1016/S0378-1127(99)00032-8

Nolan, R. H., Collins, L., Leigh, A., Ooi, M. K. J., Curran, T. J., Fairman, T. A., Resco de Dios, V., & Bradstock, R. (2021). Limits to post-fire vegetation recovery under climate change. *Plant, Cell & Environment*, *44*(11), 3471–3489. https://doi.org/10.1111/pce.14176

O'Connor, J. E., Jones, M. A., & Haluska, T. L. (2003). Flood plain and channel dynamics of the Quinault and Queets Rivers, Washington, USA. *Geomorphology*, *51*(1–3), 31–59. https://doi.org/10.1016/S0169-555X(02)00324-0

O'Sullivan, J. J., Ahilan, S., & Bruen, M. (2012). A modified Muskingum routing approach for floodplain flows: Theory and practice. *Journal of Hydrology*, *470–471*, 239–254. https://doi.org/10.1016/j.jhydrol.2012.09.007

Overpeck, J. T., Rind, D., & Goldberg, R. (1990). Climate-induced changes in forest disturbance and vegetation. *Nature*, *343*(6253), 51–53. https://doi.org/10.1038/343051a0

Pang, B. (1998). River Flood Flow and Its Energy Loss. *Journal of Hydraulic Engineering*, *124*(2), 228–231. https://doi.org/10.1061/(ASCE)0733-9429(1998)124:2(228)

Parks, S. A., Holsinger, L. M., Miller, C., & Nelson, C. R. (2015). Wildland fire as a self-regulating mechanism: The role of previous burns and weather in limiting fire progression. *Ecological Applications*, *25*(6), 1478–1492. https://doi.org/10.1890/14-1430.1

Parrett, C. (1987). *Fire-related debris flows in the Beaver Creek drainage, Lewis and Clark County, Montana* (Water Supply Paper 2330; pp. 57–67). U.S. Geological Survey.

Parrett, C., Cannon, S. H., & Pierce, K. L. (2004). *Wildfire-Related Floods and Debris Flows in Montana in 2000 and 2001* (Water-Resources Investigations Report 03–4319). U.S. Geological Survey.

Parsons, M., & Thoms, M. C. (2018). From academic to applied: Operationalising resilience in river systems. *Geomorphology*, *305*, 242–251. https://doi.org/10.1016/j.geomorph.2017.08.040

Pebesma, E. (2018). Simple Features for R: Standardized Support for Spatial Vector Data. *The R Journal*, *10*(1), 439. https://doi.org/10.32614/RJ-2018-009

Pebesma, E. (2023). *lwgeom: Bindings to Selected "liblwgeom" Functions for Simple Features* (0.2-13) [R].

Pebesma, E., & Bivand, R. (2023). *Spatial Data Science: With Applications in R* (1st ed.). Chapman and Hall/CRC. https://doi.org/10.1201/9780429459016

Peek, R. A. (2021, December 2). *Snapping Points (USGS Gages) to Lines (Rivers) and Calculate Distances Along Lines*. Mapping in R. https://mapping-in-r-workshop.ryanpeek.org/03_vig_snapping_points_to_line

Platt, R. V., Schoennagel, T., Veblen, T. T., & Sherriff, R. L. (2011). Modeling wildfire potential in residential parcels: A case study of the north-central Colorado Front Range. *Landscape and Urban Planning*, *102*(2), 117–126. https://doi.org/10.1016/j.landurbplan.2011.03.015

Pollock, M. M., Beechie, T. J., & Jordan, C. E. (2007). Geomorphic changes upstream of beaver dams in Bridge Creek, an incised stream channel in the interior Columbia River basin, eastern Oregon. *Earth Surface Processes and Landforms*, *32*(8), 1174–1185. https://doi.org/10.1002/esp.1553

Polvi, L. E., & Wohl, E. (2013). Biotic Drivers of Stream Planform. *BioScience*, *63*(6), 439–452. https://doi.org/10.1525/bio.2013.63.6.6

Pusey, B. J., Kennard, M. J., & Arthington, A. H. (2000). Discharge variability and the development of predictive models relating stream fish assemblage structure to habitat in northeastern Australia. *Ecology of Freshwater Fish*, *9*(1–2), 30–50. https://doi.org/10.1034/j.1600-0633.2000.90105.x

Puttock, A., Graham, H. A., Ashe, J., Luscombe, D. J., & Brazier, R. E. (2021). Beaver dams attenuate flow: A multi-site study. *Hydrological Processes*, *35*(2), e14017. https://doi.org/10.1002/hyp.14017

R Core Team. (2022). *R: A language and environment for statistical computing* [Computer software]. R Foundation for Statistical Computing. https://www.R-project.org/

Rahel, F. J. (2002). Homogenization of Freshwater Faunas. *Annual Review of Ecology and Systematics*, *33*(1), 291–315. https://doi.org/10.1146/annurev.ecolsys.33.010802.150429

Rathburn, S. L., Shahverdian, S. M., & Ryan, S. E. (2018). Post-disturbance sediment recovery: Implications for watershed resilience. *Geomorphology*, *305*, 61–75. https://doi.org/10.1016/j.geomorph.2017.08.039

Rengers, F. K. (2023). *Pers. Comm.* [Personal communication].

Robichaud, P. R., Beyers, J. L., & Neary, D. G. (2000). *Evaluating the effectiveness of postfire rehabilitation treatments* (RMRS-GTR-63; p. RMRS-GTR-63). U.S. Department of Agriculture, Forest Service, Rocky Mountain Research Station. https://doi.org/10.2737/RMRS-GTR-63

Robichaud, P. R., Lewis, S. A., Wagenbrenner, J. W., Brown, R. E., & Pierson, F. B. (2020). Quantifying long-term post-fire sediment delivery and erosion mitigation effectiveness. *Earth Surface Processes and Landforms*, *45*(3), Article 3. https://doi.org/10.1002/esp.4755

Robichaud, P. R., Wagenbrenner, J. W., Brown, R. E., Wohlgemuth, P. M., & Beyers, J. L. (2008). Evaluating the effectiveness of contour-felled log erosion barriers as a post-fire runoff and erosion mitigation treatment in the western United States. *International Journal of Wildland Fire*, *17*(2), 255. https://doi.org/10.1071/WF07032

Rodman, K. C., Veblen, T. T., Saraceni, S., & Chapman, T. B. (2019). Wildfire activity and land use drove 20th-century changes in forest cover in the Colorado front range. *Ecosphere*, *10*(2), e02594. https://doi.org/10.1002/ecs2.2594

Ryan, S. E., Shobe, C. M., Rathburn, S. L., & Dixon, M. K. (2024). Suspended-sediment response to wildfire and a major post-fire flood on the Colorado Front Range. *River Research and Applications*, rra.4286. https://doi.org/10.1002/rra.4286

Santi, P. M., deWolfe, V. G., Higgins, J. D., Cannon, S. H., & Gartner, J. E. (2008). Sources of debris flow material in burned areas. *Geomorphology*, *96*(3–4), 310–321. https://doi.org/10.1016/j.geomorph.2007.02.022

Schmeer, S. R., Kampf, S. K., MacDonald, L. H., Hewitt, J., & Wilson, C. (2018). Empirical models of annual post-fire erosion on mulched and unmulched hillslopes. *CATENA*, *163*, 276–287. https://doi.org/10.1016/j.catena.2017.12.029

Schumm, S. A. (1956). Evolution of drainage systems and slopes in badlands at perth amboy, new jersey. *Geological Society of America Bulletin*, *67*(5), 597. https://doi.org/10.1130/0016-7606(1956)67[597:EODSAS]2.0.CO;2

Schumm, S. A. (1979). Geomorphic Thresholds: The Concept and Its Applications. *Transactions of the Institute of British Geographers*, *4*(4), 485. https://doi.org/10.2307/622211

Sear, D. A., Millington, C. E., Kitts, D. R., & Jeffries, R. (2010). Logjam controls on channel:floodplain interactions in wooded catchments and their role in the formation of multi-channel patterns. *Geomorphology*, *116*(3–4), 305–319. https://doi.org/10.1016/j.geomorph.2009.11.022

Searle, S. R., Speed, F. M., & Milliken, G. A. (1980). Population Marginal Means in the Linear Model: An Alternative to Least Squares Means. *The American Statistician*, *34*(4), 216–221. https://doi.org/10.1080/00031305.1980.10483031

Shakesby, R. A., & Doerr, S. H. (2006). Wildfire as a hydrological and geomorphological agent. *Earth-Science Reviews*, *74*(3), Article 3. https://doi.org/10.1016/j.earscirev.2005.10.006

Sherriff, R. L., Platt, R. V., Veblen, T. T., Schoennagel, T. L., & Gartner, M. H. (2014). Historical, Observed, and Modeled Wildfire Severity in Montane Forests of the Colorado Front Range. *PLoS ONE*, *9*(9), e106971. https://doi.org/10.1371/journal.pone.0106971

Sherriff, R. L., & Veblen, T. T. (2006). Ecological effects of changes in fire regimes in *Pinus ponderosa* ecosystems in the Colorado Front Range. *Journal of Vegetation Science*, *17*(6), 705–718. https://doi.org/10.1111/j.1654-1103.2006.tb02494.x

Sherriff, R. L., & Veblen, T. T. (2007). A Spatially-Explicit Reconstruction of Historical Fire Occurrence in the Ponderosa Pine Zone of the Colorado Front Range. *Ecosystems*, *10*(2), 311–323. https://doi.org/10.1007/s10021-007-9022-2

Sholtes, J. S., & Doyle, M. W. (2011). Effect of Channel Restoration on Flood Wave Attenuation. *Journal of Hydraulic Engineering*, *137*(2), 196–208. https://doi.org/10.1061/(ASCE)HY.1943-7900.0000294

Silins, U., Bladon, K. D., Kelly, E. N., Esch, E., Spence, J. R., Stone, M., Emelko, M. B., Boon, S., Wagner, M. J., Williams, C. H. S., & Tichkowsky, I. (2014). Five-year legacy of wildfire and salvage logging impacts on nutrient runoff and aquatic plant, invertebrate, and fish productivity. *Ecohydrology*, *7*(6), 1508–1523. https://doi.org/10.1002/eco.1474

Smith, H., Sheridan, G., Lane, P., Nyman, P., & Haydon, S. (2011). Wildfire effects on water quality in forest catchments: A review with implications for water supply. *Journal of Hydrology*, *396*, 170–192.

Staley, D. M., Negri, J. A., Kean, J. W., Laber, J. L., Tillery, A. C., & Youberg, A. M. (2017). Prediction of spatially explicit rainfall intensity–duration thresholds for post-fire debris-flow generation in the

western United States. *Geomorphology*, *278*, 149–162. https://doi.org/10.1016/j.geomorph.2016.10.019

Stanford, J. A., Ward, J. V., Liss, W. J., Frissell, C. A., Williams, R. N., Lichatowich, J. A., & Coutant, C. C. (1996). A General Protocol for Restoration of Regulated Rivers. *Regulated Rivers: Research & Management*, *12*(4–5), 391–413. https://doi.org/10.1002/(SICI)1099-1646(199607)12:4/5<391::AID-RRR436>3.0.CO;2-4

Thoms, M. C., Delong, M. D., Flotemersch, J. E., & Collins, S. E. (2017). Physical heterogeneity and aquatic community function in river networks: A case study from the Kanawha River Basin, USA. *Geomorphology*, *290*, 277–287. https://doi.org/10.1016/j.geomorph.2017.02.027

Thoms, M. C., Meitzen, K. M., Julian, J. P., & Butler, D. R. (2018). Bio-geomorphology and resilience thinking: Common ground and challenges. *Geomorphology*, *305*, 1–7. https://doi.org/10.1016/j.geomorph.2018.01.021

Thoms, M. C., Piégay, H., & Parsons, M. (2018). What do you mean, 'resilient geomorphic systems'? *Geomorphology*, *305*, 8–19. https://doi.org/10.1016/j.geomorph.2017.09.003

Thorn, C. E., & Welford, M. R. (1994). The Equilibrium Concept in Geomorphology. *Annals of the Association of American Geographers*, *84*(4), 666–696. https://doi.org/10.1111/j.1467-8306.1994.tb01882.x

Thorne, C. R. (1990). Effects of Vegetation on Riverbank Erosion and Stability. In *Vegetation and Erosion* (pp. 125–144). Wiley.

Tiedemann, A. R., Conrad, C. E., Dieterich, J. H., Hornbeck, J. W., Megahan, W. F., Viereck, L. A., & Wade, D. D. (1979). Effects of Fire on Water. *USDA Forest Service*, General Technical Report WO-10.

Tuckett, Q. M., & Koetsier, P. (2018). Post-fire debris flows delay recovery and create novel headwater stream macroinvertebrate communities. *Hydrobiologia*, *814*(1), 161–174. https://doi.org/10.1007/s10750-018-3534-y

U.S. Geological Survey. (2022). *Normalized Burn Ratio (NBR)*. https://www.un-spider.org/advisory-support/recommended-practices/recommended-practice-burn-severity/in-detail/normalized-burn-ratio

USACE Hydrologic Engineering Center. (2023). *Basin Characteristics*. HEC-HMS Users Manual. https://www.hec.usace.army.mil/confluence/hmsdocs/hmsum/4.8/geographic-information/basin-characteristics

USDA Forest Service. (2020). *Soil Burn Severity Dataset for the CAMERON PEAK Fire occurring on the Arapaho & Roosevelt National Forests/Pawnee National Grassland National Forest: USDS Forest Service raster digital data* (USDA Forest Service, Geospatial Technology and Applications Center, BAER Imagery Support Program). https://fsapps.nwcg.gov/afm/baer/download.php

Veblen, T. T., & Donnegan, J. A. (2005). Historical Range of Variability for Forest Vegetation of the National Forests of the Colorado Front Range. *USDA Forest Service*.

Veblen, T. T., Kitzberger, T., & Donnegan, J. (2000). *Climatic and Human Influences on Fire Regimes in Ponderosa Pine Forests in the Colorado Front Range*.

Veblen, T. T., & Lorenz, D. C. (1986). Anthropogenic disturbance and recovery patterns in montane forests, colorado front range. *Physical Geography*, *7*(1), 1–24. https://doi.org/10.1080/02723646.1986.10642278

Vorster, A. G., Stevens-Rumann, C., Young, N., Woodward, B., Choi, C. T. H., Chambers, M. E., Cheng, A. S., Caggiano, M., Schultz, C., Thompson, M., Greiner, M., Aplet, G., Addington, R. N., Battaglia, M. A., Bowker, D., Bucholz, E., Buma, B., Evangelista, P., Huffman, D., … West Fordham, A. (2023). Metrics and Considerations for Evaluating How Forest Treatments Alter Wildfire Behavior and Effects. *Journal of Forestry*, *122*(1), 13–30. https://doi.org/10.1093/jofore/fvad036

Walker, B., Holling, C. S., Carpenter, S. R., & Kinzig, A. P. (2004). Resilience, Adaptability and Transformability in Social-ecological Systems. *Ecology and Society*, *9*(2), art5. https://doi.org/10.5751/ES-00650-090205

Westbrook, C. J., Cooper, D. J., & Baker, B. W. (2006). Beaver dams and overbank floods influence groundwater–surface water interactions of a Rocky Mountain riparian area. *Water Resources Research*, *42*(6), 2005WR004560. https://doi.org/10.1029/2005WR004560

Westerling, A. L., Hidalgo, H. G., Cayan, D. R., & Swetnam, T. W. (2006). Warming and Earlier Spring Increase Western U.S. Forest Wildfire Activity. *Science*, *313*(5789), 940–943. https://doi.org/10.1126/science.1128834

White, D. C., Morrison, R. R., & Wohl, E. (2022). Fire and ice: Winter flooding in a Southern Rocky Mountain stream after a wildfire. *Geomorphology*, *413*, 108370. https://doi.org/10.1016/j.geomorph.2022.108370

White, P., & Nelson, P. A. (2024). *Evaluation of sub-hourly MRMS quantitative precipitation estimates in mountainous terrain using machine learning*. https://doi.org/10.22541/essoar.171052553.36909541/v1

White, P., Rengers, F. K., Barnhart, K. R., & Nelson, P. (2023, May 8). *Exploring the Applicability of Radar-Based Quantitative Precipitation Estimates for Emergency Assessment of Post-Wildfire Debris Flow Hazards in Colorado*. Sedimentation and Hydrologic Modeling Conference, St. Louis, Missouri, USA.

Williams, A. P., Abatzoglou, J. T., Gershunov, A., Guzman-Morales, J., Bishop, D. A., Balch, J. K., & Lettenmaier, D. P. (2019). Observed Impacts of Anthropogenic Climate Change on Wildfire in California. *Earth's Future*, *7*(8), Article 8. https://doi.org/10.1029/2019EF001210

Wohl, E. (2001). *Virtual Rivers*. Yale University Press.

Wohl, E. (2011). Threshold-induced complex behavior of wood in mountain streams. *Geology*, *39*(6), 587–590. https://doi.org/10.1130/G32105.1

Wohl, E. (2013a). Landscape-scale carbon storage associated with beaver dams. *Geophysical Research Letters*, *40*(14), 3631–3636. https://doi.org/10.1002/grl.50710

Wohl, E. (2013b). Migration of channel heads following wildfire in the Colorado Front Range, USA. *Earth Surface Processes and Landforms*, *38*(9), 1049–1053. https://doi.org/10.1002/esp.3429

Wohl, E. (2016). Spatial heterogeneity as a component of river geomorphic complexity. *Progress in Physical Geography: Earth and Environment*, *40*(4), 598–615. https://doi.org/10.1177/0309133316658615

Wohl, E. (2018). Geomorphic context in rivers. *Progress in Physical Geography: Earth and Environment*, *42*(6), 841–857. https://doi.org/10.1177/0309133318776488

Wohl, E., Greenbaum, N., Schick, A. P., & Baker, V. R. (1994). Controls on bedrock channel incision along nahal paran, Israel. *Earth Surface Processes and Landforms*, *19*(1), 1–13. https://doi.org/10.1002/esp.3290190102

Wohl, E., & Jaeger, K. (2009). A conceptual model for the longitudinal distribution of wood in mountain streams. *Earth Surface Processes and Landforms*, *34*(3), 329–344. https://doi.org/10.1002/esp.1722

Wohl, E., Lininger, K. B., & Scott, D. N. (2018). River beads as a conceptual framework for building carbon storage and resilience to extreme climate events into river management. *Biogeochemistry*, *141*(3), 365–383. https://doi.org/10.1007/s10533-017-0397-7

Wohl, E., Marshall, A. E., Scamardo, J., White, D., & Morrison, R. R. (2022). Biogeomorphic influences on river corridor resilience to wildfire disturbances in a mountain stream of the Southern Rockies, USA. *Science of The Total Environment*, 153321. https://doi.org/10.1016/j.scitotenv.2022.153321

Wohl, E., Marshall, A. E., Triantafillou, S., Mobley, M., Means-Brous, M., & Morrison, R. R. (2024). Distribution of logjams in relation to lateral connectivity in the River Corridor. *Geomorphology*, *451*, 109100. https://doi.org/10.1016/j.geomorph.2024.109100

Wohl, E., Marshall, A., Scamardo*, J., & Rathburn, S. (2024). Biogeomorphic processes, spatial heterogeneity, and river corridor resilience to stand-killing wildfire. In J. L. Florsheim, A. P. O'Dowd, & A. Chin, *Biogeomorphic Responses to Wildfire in Fluvial Ecosystems* (pp. 153–176). Geological Society of America. https://doi.org/10.1130/2024.2562(08)

Wohl, E., Rathburn, S., Chignell, S., Garrett, K., Laurel, D., Livers, B., Patton, A., Records, R., Richards, M., Schook, D. M., Sutfin, N. A., & Wegener, P. (2017). Mapping longitudinal stream connectivity in the North St. Vrain Creek watershed of Colorado. *Geomorphology*, *277*, 171–181. https://doi.org/10.1016/j.geomorph.2016.05.004

Woltemade, C. J., & Potter, K. W. (1994). A watershed modeling analysis of fluvial geomorphologic influences on flood peak attenuation. *Water Resources Research*, *30*(6), 1933–1942. https://doi.org/10.1029/94WR00323

Woodward, B., & Vorster, A. G. (2022). *Cameron Peak burn severity dNBR* [Unpublished data].

Zhang, J., Howard, K., Langston, C., Kaney, B., Qi, Y., Tang, L., Grams, H., Wang, Y., Cocks, S., Martinaitis, S., Arthur, A., Cooper, K., Brogden, J., & Kitzmiller, D. (2016). Multi-Radar Multi-Sensor (MRMS)

Quantitative Precipitation Estimation: Initial Operating Capabilities. *Bulletin of the American Meteorological Society*, *97*(4), 621–638. https://doi.org/10.1175/BAMS-D-14-00174.1

APPENDICES

Appendix I – Data tables

Reach data: doi:10.5061/dryad.qfttdz0r3

Table of floodplain to channel width ratio variance

Site	Variance
Jack's Gulch	31.1
Sheep Gulch	30.4
Little Beaver Creek	14.4
Fish Creek	8.6
Sheep Creek	5.9
Little Beaver Creek Tributary A	24.1
Black Hollow	2.4

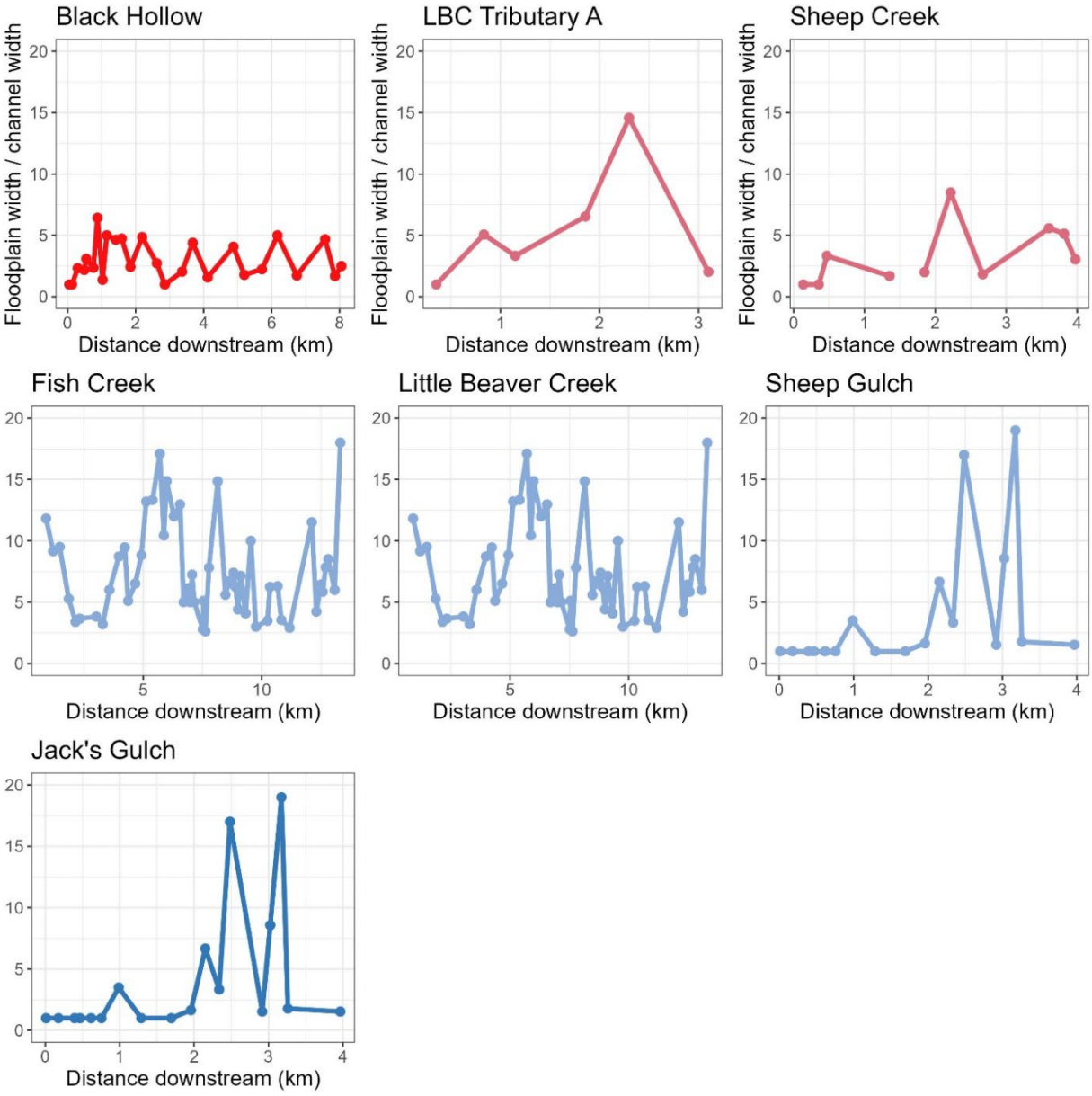
Black Hollow
LBC Tributary A
Sheep Creek
Fish Creek
Little Beaver Creek
Sheep Gulch
Jack's Gulch
Floodplain width / channel width
Distance downstream (km)

Reach variable descriptions

Category	Variable Name	Units	Description	Format
Geomorphic	reach length	km	Length of NHD flowline bounded by reach start and end points	Numerical
	distance downstream	km	Length of NHD flowline from the channel head to the upstream reach boundary	Numerical
	reach area	km^2	Floodplain width multiplied by reach length	Numerical
	reach slope		Difference in elevation between upstream and downstream reach boundaries over the reach length	Numerical
	planform		Single or multi-thread	Categorical
	bedform		Step-pool, pool-riffle, etc.	Categorical
	maximum channel count		Number of channels present	Numerical (count)
	bankfull channel width	m	Channel width based on high water marks from spring snowmelt at the beginning of field season	Numerical
	floodplain width	m	Based on high water marks from the largest flood	Numerical
	floodplain to channel ratio		Ratio of floodplain and channel width to create relative floodplain width	Numerical
	berms		Presence of beaver berms, or beaver meadow when a reach is dominated by beaver modified topography	Categorical
Fire	burn extent	%	Percent of area burned	Numerical
	burn severity high	%	Percent of area burned at high severity	Numerical
	burn severity moderate high	%	Percent of area burned at high and moderate-high severity	Numerical
	burn status		Burn status determined in the field as yes, no, or mixed	Categorical
Vegetation	channel jams		Count of channel jams	Numerical (count)
	floodplain jams		Count of floodplain jams	Numerical (count)
	floodplain vegetation		Categorical floodplain vegetation determined in the field	Categorical
	basal area		Metric for area of standing trees measured with Panama Angle Gauge	Numerical (count)
	willow		Presence of willow	Categorical
	NDVI pre-fire		Median NDVI of the years 2017, 2018, and 2019	Numerical
	NDVI 2023		Median NDVI in the 2023 growing season	Numerical

	NDVI recovery 2023		Ratio of NDVI in 2023 to the pre-fire median NDVI	Numerical

Catchment characteristics

Site	Resilience	Area (km^2)	R_e	Mean basin slope (%)	Total stream length (km)	Drainage density	Relief ratio	Concavity Index
Jack's Gulch	No Flood	5.96	0.50	21.00	4.60	0.77	115.53	1.11
Fish Creek	Large Flood	17.16	0.50	10.30	9.20	0.54	105.02	0.72
Little Beaver Creek Mainstem	Large Flood	37.61	0.55	9.70	27.20	0.72	76.44	0.74
Sheep Gulch	Large Flood	2.80	0.52	40.00	3.30	1.18	208.79	0.78
Sheep Creek	Moderate Fan	7.62	0.68	17.10	7.80	1.02	172.87	0.13
Tributary A	Moderate Fan	4.64	0.59	25.00	3.50	0.75	400.81	0.87
Black Hollow	Major Fan	17.26	0.56	14.50	9.70	0.56	159.17	0.91

Appendix II – Burn metric comparisons

Comparison of dNBR and NBR data sources used to calculate burn characteristics

	Woodward and Vorster (dNBR)			USFS (NBR)	
	Burn extent	Burn severity moderate-high to high	Burn severity high	Burn extent	Burn severity high
Jack's Gulch	96.25	48.26	4.97	95.87	4.02
Fish Creek	90.1	52.7	21.00	81.03	9.46
Little Beaver Creek	89.6	59.8	20.86	86.26	16.76
Sheep Gulch	99.92	38.99	4.97	99.34	18.62
Sheep Creek	99.8	27.6	2.71	99.76	13.79
Tributary A (LBC)	77.12	57.87	29.18	64.71	15.06
Black Hollow	99.8	49.5	11.85	94.25	57.97

NDVI and NBR pixel value density plots

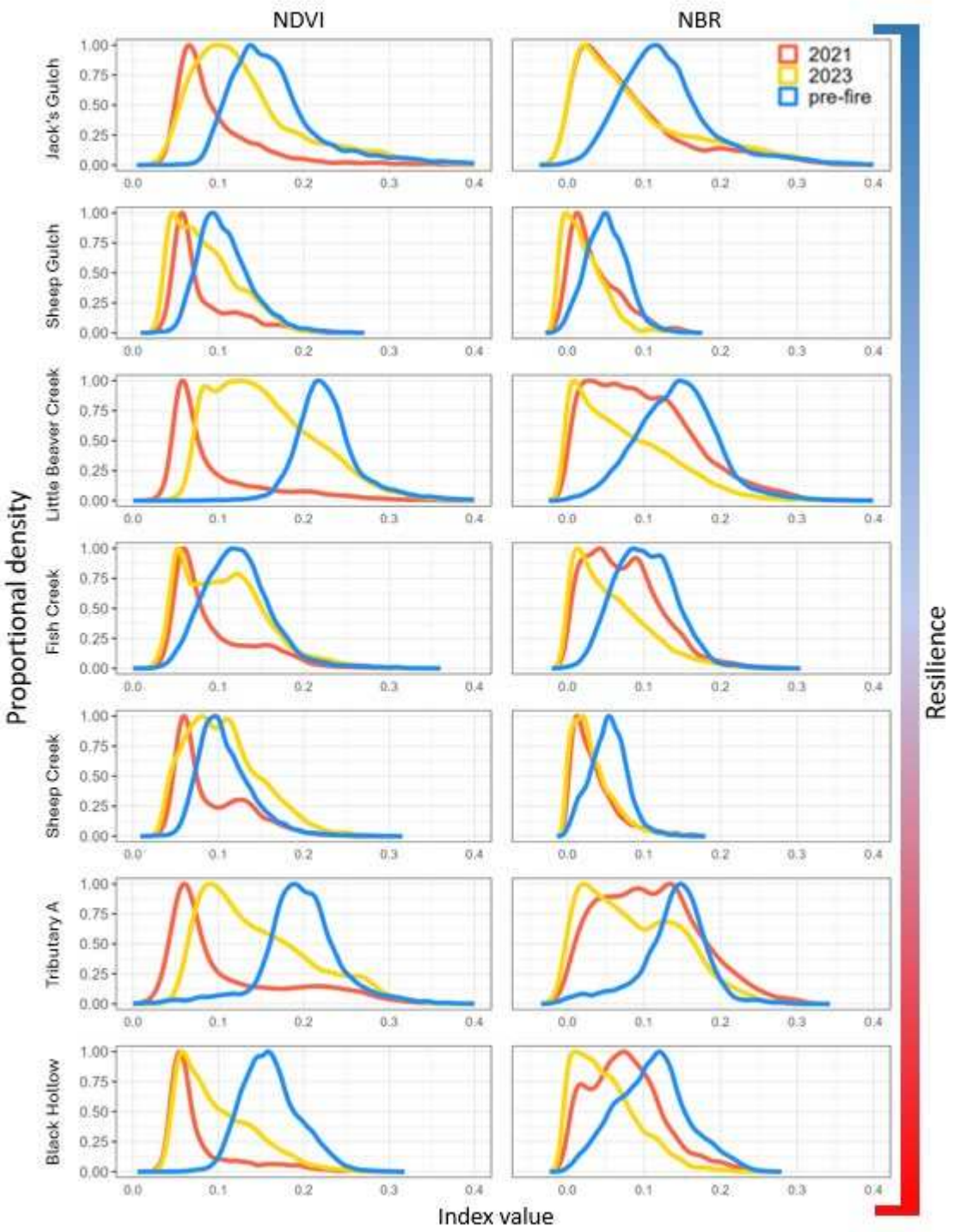

Appendix III – NDVI code

GEE NDVI code

```
/** Remote Sensing of the Earth System, Lab 4.3
 * Code below calculates the NDVI and area for watersheds in the Cameron Peak Fire burn area
 *
 * Code compiled by Bri Rick, February 2021; updated D. McGrath/L. Zeller, February 2023; updated S. Triantafillou, February 2024 ***/

// Zoom to a location.
Map.setCenter(-105.65955327884019,40.643662247514754, 9); // Center on LBC and BH

//Create a function to mask clouds based on the pixel_qa band of Landsat 8 SR data.
function cloudMaskL8(image) {
  // Bits 3 and 5 are cloud shadow and cloud, respectively.
  var cloudShadowBitMask = (1 << 3);
  var cloudsBitMask = (1 << 5);
  // Get the pixel QA band.
  var qa = image.select('QA_PIXEL');
  // Both flags should be set to zero, indicating clear conditions.
  var mask = qa.bitwiseAnd(cloudShadowBitMask).eq(0)
                 .and(qa.bitwiseAnd(cloudsBitMask).eq(0));
  return image.updateMask(mask);
}


// ----------------CREATING MOSAICS-------------------------------------------------------
/** Create an image for every year between 2017 and 2022
// Landsat 8 is available for 2013 - 2023, Landsat 5 available for 1984 - 2012
// For each year we call the image collection (Landsat 5 or 8 surface reflectance)
// Then we filter by date, choosing the likely snow-free months of each year of interest
// Then we apply the cloud mask -- finds all cloud-free pixels during the date range
// Takes the median value of all clear images for each pixel and creates one cloud-free mosaic
*/
var L8_2023 = ee.ImageCollection('LANDSAT/LC08/C02/T1_L2')  // Open the image collection of all Landsat 8 SR images
    .filterDate('2023-06-01', '2023-09-30')              // Filter by date for images in 2022
    .map(cloudMaskL8)                                    // Apply the cloud mask to only keep cloud-free pixels
    .median();                                   // Is this saying that its taking the median pixel value?

var L8_2022 = ee.ImageCollection('LANDSAT/LC08/C02/T1_L2')  // Open the image collection of all Landsat 8 SR images
    .filterDate('2022-06-01', '2022-09-30')              // Filter by date for images in 2022
    .map(cloudMaskL8)                                    // Apply the cloud mask to only keep cloud-free pixels
    .median();                                   // Is this saying that its taking the median pixel value?

var L8_2021 = ee.ImageCollection('LANDSAT/LC08/C02/T1_L2')  // Open the image collection of all Landsat 8 SR images
```

```
  .filterDate('2021-06-01', '2021-09-30')          // Filter by date for images in 2021
  .map(cloudMaskL8)                          // Apply the cloud mask to only keep cloud-free pixels
  .median();

var L8_2020 = ee.ImageCollection('LANDSAT/LC08/C02/T1_L2')  // Open the image collection of all
Landsat 8 SR images
  .filterDate('2020-06-01', '2020-09-30')          // Filter by date for images in 2020
  .map(cloudMaskL8)                          // Apply the cloud mask to only keep cloud-free pixels
  .median();                                // Take the median of all the cloud-free pixels to create one
image

var L8_2019 = ee.ImageCollection('LANDSAT/LC08/C02/T1_L2')  // Open the image collection of all
Landsat 8 SR images
  .filterDate('2019-06-01', '2019-09-30')          // Filter by date for images in 2022
  .map(cloudMaskL8)                          // Apply the cloud mask to only keep cloud-free pixels
  .median();

var L8_2018 = ee.ImageCollection('LANDSAT/LC08/C02/T1_L2')  // Open the image collection of all
Landsat 8 SR images
  .filterDate('2018-06-01', '2018-09-30')          // Filter by date for images in 2021
  .map(cloudMaskL8)                          // Apply the cloud mask to only keep cloud-free pixels
  .median();

var L8_2017 = ee.ImageCollection('LANDSAT/LC08/C02/T1_L2')  // Open the image collection of all
Landsat 8 SR images
  .filterDate('2017-06-01', '2017-09-30')          // Filter by date for images in 2020
  .map(cloudMaskL8)                          // Apply the cloud mask to only keep cloud-free pixels
  .median();

//----------------VISUALIZING & INDICIES-------------------------------------------------------------

// The following code adds the mosaics created in the previous steps to the map
// We identify which bands to display, using [B4, B3, B2] for a true color Landsat 8 image
// You can play around with which bands are displayed to create false-color images

// Create a visualization scheme for L8
var L8_RGBViz = {bands: ['SR_B4', 'SR_B3', 'SR_B2'], min: 5000, max: 25000, gamma: 1.3};

// Calculate the NDVI for each time step using the 'normalized difference' function
// NDWI is calculated using the NIR and red bands
// Create a new variable for each year, renaming the band 'NDVI'

var L8_2023_ndvi = L8_2023.normalizedDifference(['SR_B5', 'SR_B4']).rename('NDVI')
var L8_2022_ndvi = L8_2022.normalizedDifference(['SR_B5', 'SR_B4']).rename('NDVI')
var L8_2021_ndvi = L8_2021.normalizedDifference(['SR_B5', 'SR_B4']).rename('NDVI')
var L8_2020_ndvi = L8_2020.normalizedDifference(['SR_B5', 'SR_B4']).rename('NDVI')
var L8_2019_ndvi = L8_2019.normalizedDifference(['SR_B5', 'SR_B4']).rename('NDVI')
var L8_2018_ndvi = L8_2018.normalizedDifference(['SR_B5', 'SR_B4']).rename('NDVI')
```

```
var L8_2017_ndvi = L8_2017.normalizedDifference(['SR_B5', 'SR_B4']).rename('NDVI')


// Using the images created above,
// Mask the polygon.
var ndvi2023 = L8_2023_ndvi.updateMask(L8_2023_ndvi.clip(geometry));
var ndvi2022 = L8_2022_ndvi.updateMask(L8_2022_ndvi.clip(geometry));
var ndvi2021 = L8_2021_ndvi.updateMask(L8_2021_ndvi.clip(geometry));
var ndvi2020 = L8_2020_ndvi.updateMask(L8_2020_ndvi.clip(geometry));
var ndvi2019 = L8_2019_ndvi.updateMask(L8_2019_ndvi.clip(geometry));
var ndvi2018 = L8_2018_ndvi.updateMask(L8_2018_ndvi.clip(geometry));
var ndvi2017 = L8_2017_ndvi.updateMask(L8_2017_ndvi.clip(geometry));

// Create a function to calculate the percentage of missing pixels without changing the pixel values
function calculateMissingPercentage(image) {
  // Compute the count of masked pixels
  var maskedCount = image.mask().reduceRegion({
    reducer: ee.Reducer.count(),
    geometry: image.geometry(),
    scale: 30,
    maxPixels: 1e9,
  }).get('NDVI');

  // Compute the total count of pixels
  var totalCount = image.reduceRegion({
    reducer: ee.Reducer.count(),
    geometry: image.geometry(),
    scale: 30,
    maxPixels: 1e9,
  }).get('NDVI');

  // Calculate the percentage of missing pixels
  var missingPercentage = ee.Number(maskedCount).divide(totalCount).multiply(100);

  // Set the missing pixel percentage as a property of the image
  return image.set('system:missing_pixel_percentage', missingPercentage);
}

// Apply the calculateMissingPercentage function to each NDVI image
var calculated_L8_2023_ndvi = calculateMissingPercentage(L8_2023_ndvi);
var calculated_L8_2022_ndvi = calculateMissingPercentage(L8_2022_ndvi);
var calculated_L8_2021_ndvi = calculateMissingPercentage(L8_2021_ndvi);
var calculated_L8_2020_ndvi = calculateMissingPercentage(L8_2020_ndvi);
var calculated_L8_2019_ndvi = calculateMissingPercentage(L8_2019_ndvi);
var calculated_L8_2018_ndvi = calculateMissingPercentage(L8_2018_ndvi);
var calculated_L8_2017_ndvi = calculateMissingPercentage(L8_2017_ndvi);

// Export these as GeoTIFFs
```

```
Export.image.toDrive({
  image: ndvi2023,    // Name of image to export
  description: 'ndvi2023',   // Export name for file
  scale: 30,              // Define scale, in meters
  region: geometry,         // Define region to export
  fileFormat: 'GeoTIFF'})    // Define desired file format
  //crs: 'ESPG:3857'         // Define projection based on EPSG code. Default is WGS84
Export.image.toDrive({
  image: ndvi2022,
  description: 'ndvi2022',
  scale: 30,
  region: geometry,
  fileFormat: 'GeoTIFF'})
  //crs: 'ESPG:3857'
Export.image.toDrive({
  image: ndvi2021,
  description: 'ndvi2021',
  scale: 30,
  region: geometry,
  fileFormat: 'GeoTIFF'})
Export.image.toDrive({
  image: ndvi2020,
  description: 'ndvi2020',
  scale: 30,
  region: geometry,
  fileFormat: 'GeoTIFF'})
Export.image.toDrive({
  image: ndvi2019,
  description: 'ndvi2019',
  scale: 30,
  region: geometry,
  fileFormat: 'GeoTIFF'})
Export.image.toDrive({
  image: ndvi2018,
  description: 'ndvi2018',
  scale: 30,
  region: geometry,
  fileFormat: 'GeoTIFF'})
Export.image.toDrive({
  image: ndvi2017,
  description: 'ndvi2017',
  scale: 30,
  region: geometry,
  fileFormat: 'GeoTIFF'})
```

Appendix IV – NHD code

R NHD code

```
#Load packages
library(here)
library(tidyverse)
library(nhdplusTools)
library(ggthemes)
library(sp)
library(sf)
library(prettymapr)
library(rosm)
library(mapview)
# library(leaflet.extras)
# library(leaflet)

## Get stream lines, snap points (reach boundaries) and get distance along lines
#create a point at outlet of LBC (longitude, latitude)
LBC <- st_sfc(st_point(c(-105.524194, 40.623849)), crs = 4326)
#-105.537193,40.621729

#check class is "sfc" and "sfc_POINT"
class(LBC)

# now figure out the nearest stream segment ID to our point
LBC_comid <- discover_nhdplus_id(LBC)

# first make a list defining the sourcetype and ID
LBC_list <- list(featureSource="comid", featureID=LBC_comid)

# get upstream flowlines
LBC_us_flowlines <- navigate_nldi(nldi_feature = LBC_list,
                          mode="UT",
                          data_source = "",
                          distance_km = 200)

# get downstream mainstem only (from our starting segment):
# LBC_ds_flowlines <- navigate_nldi(nldi_feature = LBC_list,
#                       mode = "DM",
#                       distance_km = 50,
#                       data_source = "")
```

```
# make a list of all the comids we've identified:
all_comids_LBC <- c(LBC_us_flowlines[["UT_flowlines"]][["nhdplus_comid"]]) %>%
  as.numeric()

# download all data and create a geopackage with the comid list
LBC_gpkg <- subset_nhdplus(comids=all_comids_LBC,
                           simplified = TRUE,
                           overwrite = TRUE,
                           output_file = paste0(here::here(), "/LBC_nhdplus.gpkg"),
                           nhdplus_data = "download",
                           return_data = FALSE)

# check layers in database:
st_layers(paste0(here::here(), "/LBC_nhdplus.gpkg"))

# pull the flowlines back in
LBC_streams <- read_sf(paste0(here::here(), "/LBC_nhdplus.gpkg"), "NHDFlowline_Network")

# make a map

prettymapr::prettymap({
  rosm::osm.plot(project = FALSE,
                 bbox = matrix(st_bbox(LBC_streams), byrow = FALSE, ncol = 2,
                               dimnames = list(c("x", "y"), c("min", "max"))),
                 type = "cartolight", quiet = TRUE, progress = "none")
  plot(LBC_streams$geom, col = "steelblue", lwd = (LBC_streams$streamorde / 4), add=TRUE)
  plot(LBC, add=TRUE, pch=21, bg="orange", cex=1.5)
  prettymapr::addnortharrow()
})

# Iterate for each study site and bring merged site data in as a geopackage and reach boundaries in from
csv with coordinates.

# create function to snap points (reach boundaries) to the nearest line (flowline). This is a custom
function from Tim Salabim on Stack Overflow

st_snap_points <- function(x, y, namevar, max_dist = 1000) {

  # this evaluates the length of the data
  if (inherits(x, "sf")) n = nrow(x)
  if (inherits(x, "sfc")) n = length(x)

  # this part:
  # 1. loops through every piece of data (every point)
```

```
 # 2. snaps a point to the nearest line geometries
 # 3. calculates the distance from point to line geometries
 # 4. retains only the shortest distances and generates a point at that intersection
 out = do.call(c,
           lapply(seq(n), function(i) {
             nrst = st_nearest_points(st_geometry(x)[i], y)
             nrst_len = st_length(nrst)
             nrst_mn = which.min(nrst_len)
             if (as.vector(nrst_len[nrst_mn]) > max_dist) return(st_geometry(x)[i])
             return(st_cast(nrst[nrst_mn], "POINT")[2])
           })
 )
 # this part converts the data to a dataframe and adds a named column of your choice
 out_xy <- st_coordinates(out) %>% as.data.frame()
 out_xy <- out_xy %>%
   mutate({{namevar}} := x[[namevar]]) %>%
   st_as_sf(coords=c("X","Y"), crs=st_crs(x), remove=FALSE)

 return(out_xy)
}

# Snap Points to flowlines after running the above chunk to load function



# check for duplicates and correct number of reaches
reaches %>% distinct(ID) %>% nrow()

# use custom function to snap our reach boundaries to our flowline, using a buffer of 100 meters. We
need to project our data here for this to work correctly.

# first project
reach_boundaries_proj <- st_transform(reaches, crs = 26910)
# bring in shapefile of all flowlines that I merged in ArcGIS Pro
streams <-st_read("streams_merge.shp", crs = 4326)

streams_proj <- st_transform(streams, crs=26910)



# now snap points to the lines using a 500 meter buffer, select which ID column you want keep for
rejoining
boundaries_snapped <- st_snap_points(reach_boundaries_proj, streams_proj, namevar = "ID", max_dist
= 600)
st_write(boundaries_snapped, "boundaries_snapped.shp", append = FALSE)
```

```
mapview(boundaries_snapped, col.regions="cyan", layer.name="Snapped reach boundaries") +
  mapview(streams_proj, color="steelblue", layer.name="Flowlines") +
  mapview(reaches, col.regions="orange", layer.name="Field boundaries")

##Split segments by points

library(lwgeom)

# create a 1 meter buffer around snapped point
boundaries_snapped_buff <- st_buffer(boundaries_snapped, 1)

# now use lwgeom::st_split to split stream segments
seg <- st_collection_extract(lwgeom::st_split(streams_proj, boundaries_snapped_buff), "LINESTRING")
%>%
  tibble::rownames_to_column(var = "rowid") %>%
  mutate(rowid=as.integer(rowid))

st_write(seg, "seg.shp", append = TRUE)

#map
mapview(seg)  + mapview(seg, color="blue", lwd=0.3) +
  mapview(boundaries_snapped, col.regions="cyan", layer.name="Snapped Boundaries")

#Now we can calculate the distances between each point. Here we drop a few loose ends (segments on
either end of the most upstream/downstream gages), then we calculate the length of each line
segment, then arrange by the hydroseq (a sequential ID for stream flow), and use that to calculate a
cumulative distance from the upstream point to the downstream point!

seg_filt_dist <- seg %>%
  mutate(seg_len_m = units::drop_units(units::set_units(st_length(.), "m")),
         seg_len_km = seg_len_m/1000)
  arrange(desc(hydrosq)) %>%
  mutate(total_len_km = cumsum(seg_len_km)) %>%
  # filter to just cols of interest
  select(rowid, comid, gnis_id:reachcd, hydrosq, seg_len_km, total_len_km)

mapview(seg_filt_dist, zcol="total_len_km", layer.name="Cumulative Flowline<br> Distance (km)")  +
  mapview(boundaries_snapped, zcol="ID", layer.name="Reach Boundaries")
```

Appendix V – Precipitation code

Python precipitation code in Jupyter Notebook

```
# import required libraries
import eccodes
import cfgrib
import xarray as xr
import numpy as np
import pandas as pd
from datetime import datetime,timedelta
import os
import glob
from shapely.geometry import MultiPoint
import geopandas as gpd
import cartopy.crs as ccrs
import rioxarray as rxr
import matplotlib.pyplot as plt
import matplotlib.gridspec as gridspec
from matplotlib import colors
import matplotlib.animation as animation
from matplotlib.animation import ArtistAnimation
import cartopy.feature as cfeature
import shapefile as shp
import xarray

# open rate files
directory = r'filepath'
filenames_rate = glob.glob('*rate_CO.grib2')
rate = xr.open_mfdataset(filenames_rate, engine = "cfgrib",chunks={'time': '500MB'})

# missing values are negative, make nan
rate = rate.where(rate>=0)

# open multisensor 1hr QPE and apply multisensor correction

# open multisensor qpe for the correct year
mrms_multi = xr.open_dataset('2021_multiQPE_CO.grib2',engine = "cfgrib",chunks={'time': '500MB'})
mrms_multi = mrms_multi.where(mrms_multi>=0)
# open radar only qpe for the correct year
mrms_radar = xr.open_dataset('2021_radarQPE_CO.grib2',engine = "cfgrib",chunks={'time': '500MB'})
mrms_radar = mrms_radar.where(mrms_radar>=0)

correction = (mrms_multi/mrms_radar)
correction = correction.where(correction.unknown != np.inf).fillna(1)
```

```
# resample 1-hour to 2-min to apply to 2-min accumulation
correction = correction.resample(time='2min').pad()

rate = rate*correction

intensity = 15

import shapefile as shp

sf = shp.Reader("BH.shp")

for shape in sf.shapeRecords():
   shed_x = [i[0] for i in shape.shape.points[:]]
   shed_y = [i[1] for i in shape.shape.points[:]]

# define area of interest for mrms
# enter lat/lon ENTER SEQUENTIALLY
lat1 = np.min(shed_y)
lat2 = np.max(shed_y)
lon1 = np.min(shed_x)+360
lon2 = np.max(shed_x)+360

start = datetime(2021, 7, 20, 12, 0)
end = datetime(2021, 7, 21, 12, 0)

          # Multi sensor QPE over area of interest
ms_aoi =
mrms_multi.sel(time=slice(start,end),latitude=slice(lat1,lat2),longitude=slice(lon1,lon2),drop=True)
   # Create rate over area of interest
rate_aoi = rate.sel(time=slice(start,end),latitude=slice(lat1,lat2),longitude=slice(lon1,lon2),drop=True)

%%time
# calculate different intensity for entire aoi
rate_aoi_one = rate_aoi.resample(time='1Min').asfreq().fillna(0)
mrms_accum = rate_aoi_one*(2/60)
rate_15 = mrms_accum.rolling(time=intensity, min_periods=1).sum()*(60/intensity)

%%time
# calculate stats over time for each grid square - max
rate_15_pos = rate_15.where(rate_15.unknown>0) # only calculate max for positive values
rate_15_pos = rate_15_pos.to_dataframe().reset_index()
maximum = rate_15_pos.groupby(['latitude','longitude']).max()
maximum = maximum.to_xarray().unknown.fillna(0)
```

```
#Make a table to summarize stats over space (bounding box defined by watershed) over time
maximum_table = maximum.to_dataframe()
shed_max = maximum_table.agg((['idxmax', 'max', 'mean', 'median', 'std']))
shed_max

# Plot the maximum across the watershed
lon, lat = np.meshgrid(maximum.longitude,maximum.latitude)

fig = plt.figure(1, figsize=(20,16))
gs = gridspec.GridSpec(2, 1, height_ratios=[1, .02], bottom=.07, top=.99,
                       hspace=0.01, wspace=0.01)

plotcrs = ccrs.LambertConformal(central_latitude=38.5, central_longitude=-105)
ax = plt.subplot(1,1,1, projection=plotcrs)

plt.title('Maximum 15 minute intensity', fontsize=24)
mesh = ax.pcolormesh(lon,lat,maximum,transform=ccrs.PlateCarree(), alpha=0.6)
cb =fig.colorbar(mesh ,pad=0.01,ax=ax, orientation = 'horizontal')
cb.ax.tick_params(labelsize=20)
cb.set_label("Intensity mm/hr", fontsize=24)

ax.plot(shed_x,shed_y,color='red',transform=ccrs.PlateCarree()) # add shapefile of basin

plt.savefig('Max15minIntens.png', bbox_inches='tight', dpi=300)

%%time
# calculate stats over time for each grid square
median = rate_15_pos.groupby(['latitude','longitude']).median()
median = median.to_xarray().unknown.fillna(0)

#Make a table to summarize stats over space (watershed) over time (median)
median_table = median.to_dataframe()
shed_median_stats = median_table.agg((['idxmax', 'max', 'mean', 'median', 'std']))
shed_median_stats

# Visualize median over space
lon, lat = np.meshgrid(median.longitude, median.latitude)

fig = plt.figure(1, figsize=(20, 16))
gs = gridspec.GridSpec(2, 1, height_ratios=[1, .02], bottom=.07, top=.99,
                       hspace=0.01, wspace=0.01)

plotcrs = ccrs.LambertConformal(central_latitude=38.5, central_longitude=-105)
```

```
ax = plt.subplot(1, 1, 1, projection=plotcrs)

# Add latitude and longitude lines
gl = ax.gridlines(crs=ccrs.PlateCarree(), draw_labels=True, linestyle='-', color='gray', alpha=0.5)
gl.top_labels = True
gl.right_labels = False  # Disable latitude labels on the right
gl.xlabel_style = {'size': 20}  # Adjust label font size
gl.ylabel_style = {'size': 20}  # Adjust label font size

plt.title('Median 15 minute intensity', fontsize=24)
mesh = ax.pcolormesh(lon, lat, median, transform=ccrs.PlateCarree(), alpha=0.6, vmin=0.75, vmax=3.5)
cb = fig.colorbar(mesh, pad=0.01, ax=ax, orientation='horizontal')
cb.ax.tick_params(labelsize=20)
cb.set_label("Intensity mm/hr", fontsize=24)

ax.plot(shed_x, shed_y, color='red', transform=ccrs.PlateCarree())  # add shapefile of basin

plt.savefig('LBCMedian15minIntens.png', bbox_inches='tight', dpi=300)
```

Appendix VI – Statistical analysis

Reach variable summary for statistical tests between catchments.

Reach variable	Distribution	Transformation	Equal variance	Notes	Statistical tests	Results
Reach slope	Not normal	Log (ln)	No		Kruskal Wallis and Dunn test	Significant difference
Maximum channel count	Not normal	None	Yes		Kruskal Wallis	No significant differences
Floodplain to channel width ratio	Not normal	Log (ln)	Yes	added 0.01		
Basal area	Not normal	None	No		Kruskal Wallis and Dunn test	Significant difference
Channel jam density	Not normal	Log (ln)	Yes	added 0.01	Anova and emmeans pairs	Significant difference
Floodplain jam density	Not normal	Log (ln)	Yes	added 0.01	Anova and emmeans pairs	Significant difference